Chapter 2

HIGH TEMPERATURE ENGINEERING TEST REACTOR (HTTR) REACTOR PHYSICS BENCHMARKS

2.1. HTTR GENERAL INFORMATION

The High Temperature Engineering Test Reactor (HTTR) of the Japan Atomic Energy Research Institute (JAERI) is a graphite-moderated and helium gas cooled reactor with an outlet temperature of 950°C and a thermal output of 30 MW [2-1].

The major objectives of the HTTR are to establish and upgrade the technological basis for advanced high temperature gas-cooled reactors (HTGRs) and to conduct various irradiation tests for innovative high temperature basic researches.

The construction was completed on May 1996. The fuel loading of was started on July 1, 1998 from core periphery. The first criticality was attained in annular type core of 19 columns on Nov.10, 1998. The first full power operation with an average core outlet temperature of 850°C was completed on 7 December 2001, and operational licensing of the HTTR was approved on 6 March 2002.

2.1.1. Facility Description

2.1.1.1. Background

In June 1987, the Japanese Atomic Energy Commission (JAEC) issued a revised "Long Term Program for Development and Utilization of Nuclear Energy" stressing that Japan should proceed to develop more advanced reactor technologies in parallel with the upgrading of existing nuclear reactors. It was recognized in this programme that the HTGR was not to be incorporated into the present existing power plant system, but the benefits that could be derived, such as its inherent safety and production of high temperature heat, are remarkable and should be pursued. Therefore, the promotion of R&D on the HTGR in Japan is quite significant from the viewpoint of a new nuclear technology frontier.

Within this programme, the early construction of a test reactor in place of the experimental Very High Temperature Reactor (VHTR) was recommended based on the estimated length of time (~ 10 years) to construct the plant and perform associated testing. Based on the conclusions by a special committee investigating the HTGR R&D plan for the JAEC, demand of nuclear heat applications to ~ 1,000°C is expected to become strong in the early part of the 21st century. The committee requested that a test reactor making the most use of Japanese technology be designed and built to test and study advanced HTGRs for the future. Accordingly, the test reactor should have an in-core irradiation region equipped with the capability to test the threshold of fuel failure and for the irradiation of various materials.

The committee's report also stated that the reactor outlet coolant temperature should be 950°C, which is the highest temperature attainable considering the current technology level. For irradiation tests, a prismatic block type core structure was proposed, with a thermal power rating of 30MW for securing adequate regions for irradiation tests at high temperature [2-6, 2-7].

Based on these suggestions, JAERI suspended the previous programme where the experimental VHTR was defined as an initial step toward nuclear heat application development and proceed with the design and R&D specifically necessary to prepare the safety analysis report of the HTTR, with the objectives to:

- Establish and upgrade the technology base of the HTGR
- Perform innovative basic research in the field of high temperature engineering
- Demonstrate high temperature heat applications and utilization achieved from nuclear heat.

The Japanese government approved proceeding with the HTTR in its 1989 fiscal year budget. Construction began in March 1991 following submittal by JAERI of the HTTR safety analysis report and subsequent review by the Science and Technology Agency, and then, by the Nuclear Safety Commission.

2.1.1.2. General design features of the HTTR

The reactor core is designed to keep all specific safety features within the graphite blocks. The intermediate heat exchanger (IHX) is equipped to supply high temperature clean helium for process heat application systems, and the instrumentation and control system is designed to allow operations that simulate accidents and anticipated operational occurrences (AOOs). As the HTTR is the first HTGR in Japan and a test reactor with various purposes, it incorporates specific aspects regarding the safety design. JAERI established the following safety design principles for the HTTR in reference to the "Guidelines for Safety Design of LWR Power Plants", but taking into account the significant safety characteristics of the HTGR and the corresponding design requirements as a test reactor:

- Coated fuel particles shall not fail during normal operation and AOOs. To satisfy this principle, the maximum fuel temperature, including systematic and random uncertainties, shall not exceed 1600°C for any AOO.
- The reactor shall be shut down safely and reliably during operation using the control rod system. Furthermore, a reserved shutdown system (RSS) which is independent of the control rod system shall be provided.
- A severe accident resulting from control rod ejection must be avoided.
- The residual heat after reactor shutdown shall be removed safely and reliably for any AOO or accident.
- A containment vessel (C/V) shall be provided to prevent fission product release and excessive air ingress into the core in case of a depressurization accident.
- The pressure in the pressurized water cooling system (PWCS) shall be controlled so as to be lower than that of the primary helium gas to prevent a large water ingress into the core in case of rupture of a heat transfer tube in the primary pressurized water cooler (PPWC).
- The helium gas pressure in the secondary helium cooling system (SHCS) shall be controlled to be slightly higher than that of the primary helium gas to prevent fission product leakage from the primary cooling system (PCS) to the secondary due to a crack in a heat transfer tube in the IHX.
- The pressure and heat resisting functions of the structures, where the high pressure and high temperature coolant is contained, are separated to reduce mechanical loads on the high temperature metal structures [2-7].

Safe and reliable shutdown of the reactor from any operational condition is achieved with the control rod system. Furthermore, a reserved shutdown system composed of B_4C/C

pellets is provided. The power control and normal reactor shutdown of the HTTR are achieved with 16 pairs of control rods or 15 pairs when the center column of the core is used for an irradiation test. The control rod system can achieve subcriticality from any operational condition and maintain subcriticality under cold core conditions including the postulated event of a pair of control rods stuck in the operational position. The major design specifications of the HTTR are shown in Table 2.1. The reactor outlet coolant temperature at the full power is set at both 850° and 950°C. The reactor operational mode at 850°C is defined as "rated operation" and at 950°C is "high temperature test operation" because operation of the HTTR is not allowed at 950°C for full life of the initial core. Tests such as the safety demonstration tests and irradiation tests are allowed only in the rated operation mode. The high temperature nuclear process heat utilization system will be operated at the high temperature test operational mode. The design life of permanent structural components in the HTTR plant is based on 20 years with a load factor of 60 % of full power operation.

The HTGR has excellent safety capabilities with respect to the accidental release of fission products. Nevertheless, the HTTR is required to have a containment vessel to meet Japanese safety design guidelines for the light water nuclear power plants.

2.1.1.3. HTTR plant layout and cooling system

The HTTR is located on JAERI's Oarai Research Establishment site which is approximately 100 kilometers north of the Tokyo metropolitan area and is near the Pacific Ocean. The plant area is 200 m x 300 m in size. The shortest distance between the HTTR reactor core and site boundary is about 280 m in the southwest direction. As illustrated in Figure 2.1, the HTTR plant arrangement is comprised of the reactor building, spent fuel storage building, a machinery building, cooling towers, exhaust stack, a high temperature process heat utilization system and other auxiliary facilities. The reactor building of 48 m x 50 m in size is situated in the central area of the plant. The exhaust stack of 80 m in height is north of the reactor building for the air ventilated from the reactor building to be released to the atmosphere. The heat utilization system will be constructed south of the reactor building [2-8].
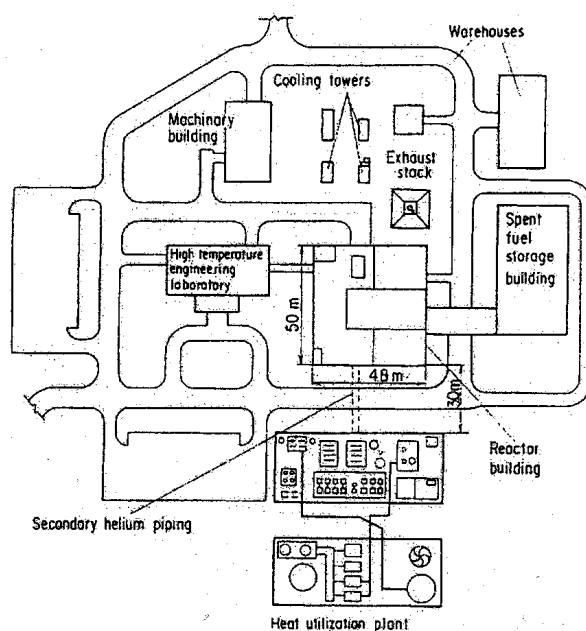

FIG. 2.1. HTTR plant arrangement.

The reactor building includes five levels with three floors underground (Figure 2.2). A steel reactor containment vessel of 18.5 m in diameter and 30 m in height is installed in the center of the reactor building. A refueling hatch is attached to the C/V above the reactor pressure vessel (RPV). Functions of the C/V are to:

1)   Contain fission products (FPs) as one of the multiple barriers against FP release into the atmosphere, and
2)   Limit the amount of air ingress into the core in a primary pipe rupture accident.

The reactor pressure vessel (RPV) is formed as a vertical cylinder, with a hemispherical top and bottom head closures and 31 standpipes. The top head closure is bolted to a flange of the vessel cylinder. The standpipes include "control rod (CR) stand-pipes", "irradiation stand-pipes", and standpipes for instrumentation. The irradiation standpipes are utilized to introduce specimens and experimental equipment into the core. A thermal shield is attached to the inner surface of the top head closure to prevent the closure from overheating in a depressurization accident such as a primary helium pipe rupture. The RPV is of 2-1/4Cr1Mo steel normalized and tempered.
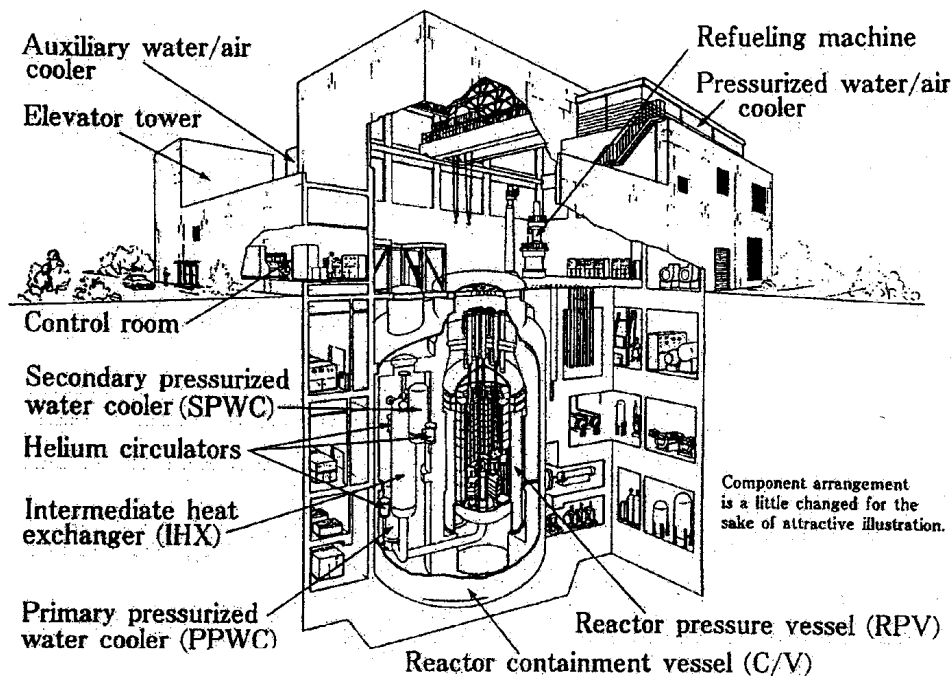

FIG. 2.2. HTTR reactor building.

The double containment concept (RPV + C/V) was applied to the HTTR, because the safety features of the HTGR have not been developed in Japan. The HTTR has multiple barriers to fission product release, namely, the fuel coatings, the RPV boundary, the C/V and the reactor building. Most HTGRs being designed in other countries also include these barriers except the C/V. Some compartments surrounding the C/V in the reactor building serve as confinement, or service area. The service area is maintained at a slightly negative pressure to atmosphere by a ventilation and an air conditioning system during normal operation and accident conditions. The barriers of the C/V and the service area significantly reduce the off-site radiation dose in an accident condition such as a primary helium pipe rupture. Major components such as primary cooling system components as well as the RPV (Figure 2.3) are contained within the C/V.
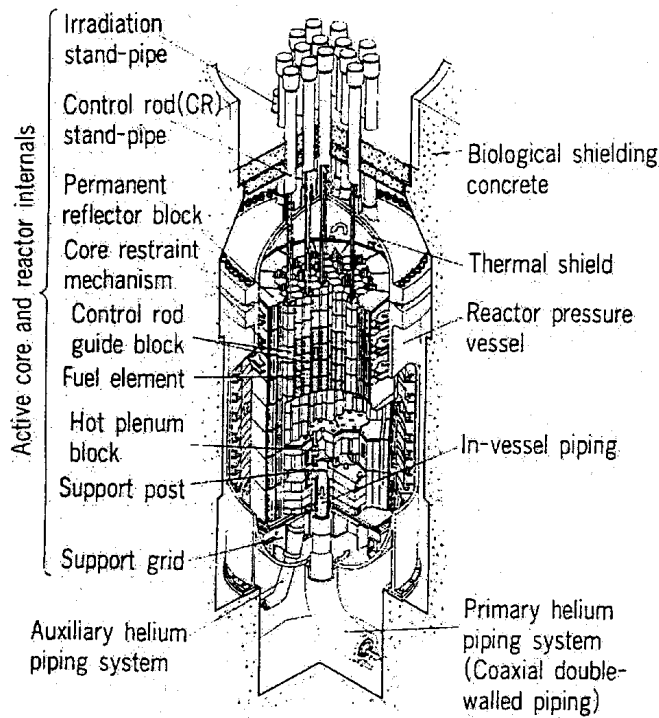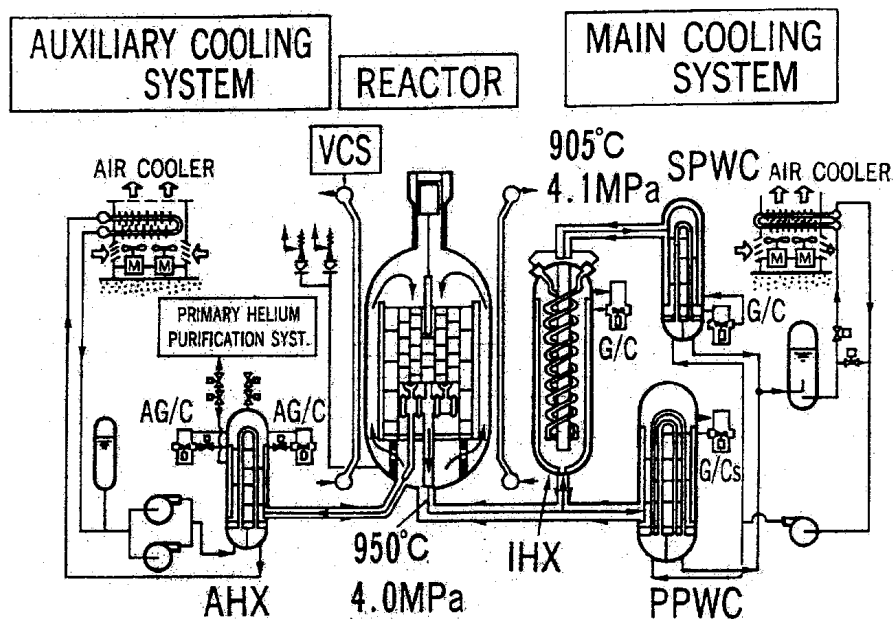
FIG.2.3. HTTR pressure vessel and internals.

FIG. 2.4. HTTR cooling system.

The flow diagram of the reactor cooling system is shown in Figure 2.4. This system is composed of a main cooling system (MCS), an auxiliary cooling system (ACS) and two reactor vessel cooling systems (VCSs). The MCS removes the heat energy from the reactor core during the normal operation, while the ACS and VCSs are functioned as engineered safety features and remove the residual heat energy after a reactor scram. As the core restraint mechanism requires protection against thermal damage from reactor heat during normal operation and anticipated operational occurrences, the ACS functions as protection by forced cooling the restraint mechanism.

During a reactor scram, gas circulators of the MCS are shut to protect the heat transfer tubes of the two pressurized water coolers against overheating. In an AOO and accident condition when forced cooling of the core is available, the ACS automatically starts in response to the reactor scram signal. The VCS functions as a residual heat removal system when forced circulation in the primary cooling system is no longer available due to a rupture of its piping system. It also operates during normal operation to cool the reactor shielding concrete wall.

The MCS consists of an IHX, a primary pressurized water cooler (PPWC), a secondary pressurized water cooler (SPWC) and pressurized water/air cooler. The MCS has two operational modes; "single loaded operation", and "parallel loaded operation". The PPWC functions to remove the reactor heat of 30 MW during the single loaded operation, while during parallel load operation the IHX removes 10MW and the PPWC removes 20MW. The SPWC serves the function of removing the heat from the IHX. The heat removed by the PPWC and the SPWC is transported through the pressurized water at 3.5MPa. The pressurized water is then cooled down by the air cooler. In the HTTR reactor plant, the reactor heat of 30 MW is eventually transferred to the atmosphere by the pressurized water and the air cooler. During normal operation, the pressure of the secondary helium is controlled to always be 0.1 MPa higher than that of the primary helium at the IHX heat transfer tubes in order to reduce the pressure load on the tubes and to protect for accidental leakage of radioactive materials into the secondary helium. The water pressure is controlled so that a large amount of water can not ingress into the core with a PPWC tube rupture accident.

The auxiliary helium transfers a small fraction of the reactor heat to pressurized water. Eventually, the reactor heat is dissipated to the atmosphere at the auxiliary water/air cooler. The ACS consists of an auxiliary heat exchanger (AHX), two auxiliary helium circulators and an air cooler. At the AHX, the auxiliary helium is cooled by water. During normal operation, a small flow of auxiliary helium (~ 200 kg/h) passes through the AHX to the primary helium purification system so as to remove impurities contained in the reactor coolant. With a reactor scram, while the reactor coolant pressure boundary remains intact, the auxiliary helium cooling system automatically starts and transfers the residual heat from the core to the auxiliary air cooler. The AHX has heat transfer capacity of approximately 3.5MW.

Two vessel cooling systems are provided as protection of the reactor core and the RPV against thermal damage by residual heat after a reactor scram when the ACS cannot, or fails to, cool the core. Each of these systems is capable of controlling temperatures of the core and RPV within safe limits and consists of water-cooled panels surrounding the RPV with two cooling water systems. Cooling tubes with fins form the panels and are arranged so that adjacent tubes do not belong to the same system and a tube failure will not danger the RPV and core. The heat removal rate from the RPV to the panels is designed as 0.6 MW so as to effectively remove heat to meet the requirement for the maximum allowable normal fuel temperature of 1495°C and also 0.3 MW or more with an accident condition where the reactor core is not cooled by the ACS. The VCS is also an engineered safety feature equipped with two independent complete sets which are backed up with an emergency power supply. It is operated even during normal operation in order to cool the biological shielding concrete wall.

The IHX is a helically coiled counter flow type heat exchanger. To minimize constraints of axial and radial thermal expansion of the helically coiled heat transfer tubes, a floating hot header with a combination of a central hot gas duct passes through the central space inside the helix bundle. An assembled tube support allows free thermal expansion of a

helix in the radial direction. The primary helium enters the IHX through the inner pipe of the primary concentric hot gas duct attached to the bottom of the IHX. It flows up outside the tubes thereby transferring nuclear heat of 10 MW to the secondary helium and flows back to the annular space between the inner and outer shells, The secondary helium flows down inside the heat transfer tubes and flows up through the center as hot gas. A double-walled shell with thermal insulation attached to the inside surface of the inner shell provides reliable separation of the heat resisting and pressure retaining functions. Cold helium flowing through the annulus brings uniform temperature distribution throughout the outer shell which serves the function of being the pressure retaining member.

2.1.1.4. HTTR core configuration

The annular core is one of the promising core types for future HTGRs because of high inherent safety characteristics for loss of coolant accidents [2-2, 2-3, 2-4]. The decay heat removal is enhanced by introduction of the annular core because the heat transfer pass will be shortened due to thinning of the fuel region. As a result, the fuel temperature on a loss of coolant accident can be maintained less than the fuel temperature limit of 1600°C by the vessel cooling system (VCS) surrounding the reactor pressure vessel. The decay heat will be transferred radially through the fuel regions, side reflector blocks and reactor pressure vessel to the cooling panel of the VCS by heat conduction, radiation and convection without any active cooling system.

Table 2-1. Specification of the HTTR

|	
Thermal power	30 MW
Outlet coolant temperature	950°C
Inlet coolant temperature	395°C
Primary coolant pressure	4 MPa
Core structure	Graphite
Equivalent core diameter	2.3 m
Effective core height	2.9 m
Average power density	2.5 W/cm^3
Fuel	UO$_2$
Uranium enrichment	3 to 10 wt%
Type of fuel	Pin-in-block
Burn-up period (efpd)	660 days
Coolant material	Helium gas
Flow direction in core	Downward
Reflector thickness	
Top	1.16 m
Side	0.99 m
Bottom	1.16 m
Number of fuel assemblies	150
Number of fuel columns	30
Number of pairs of control rods	
In core	7
In reflector	9
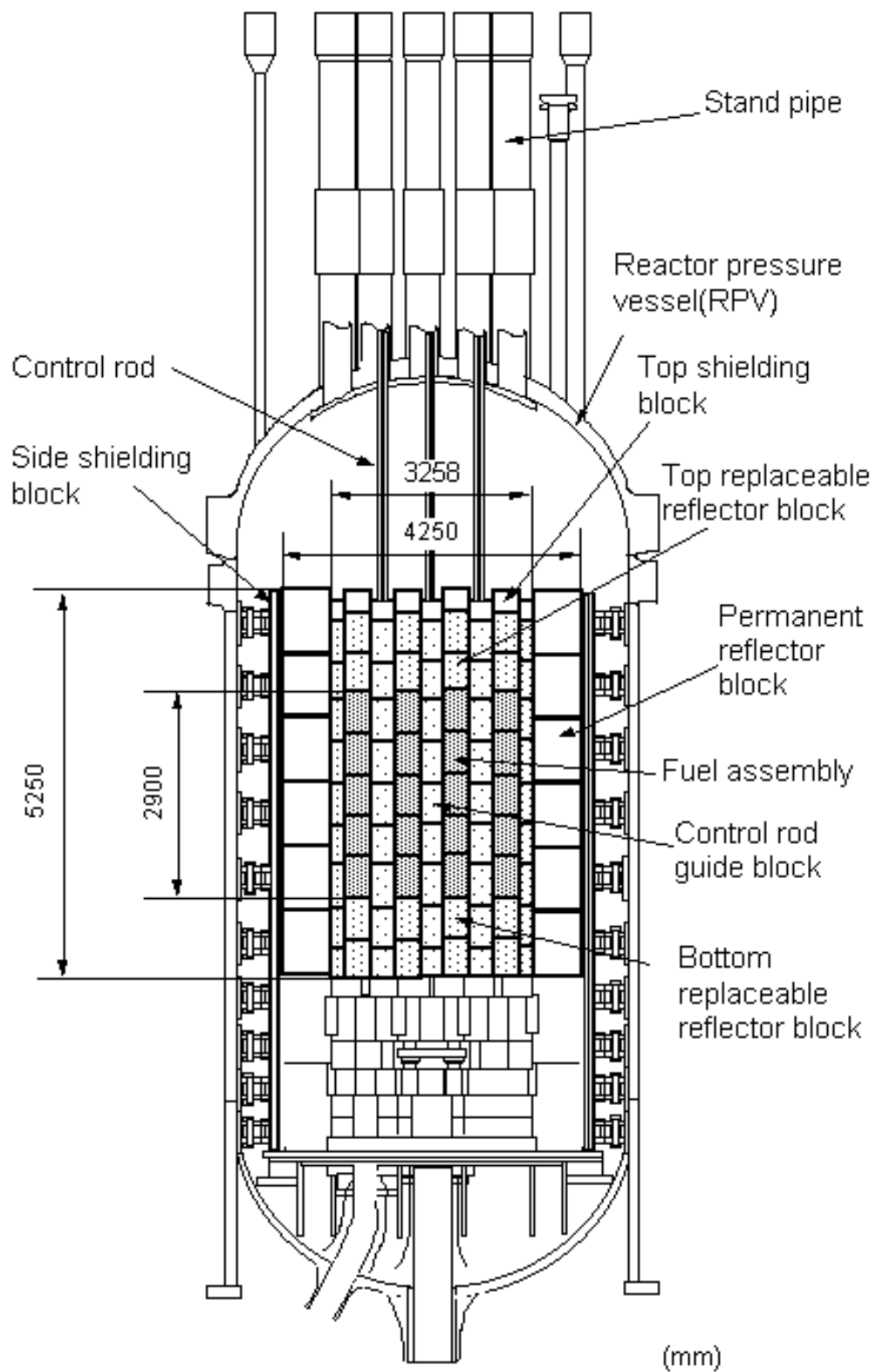
FIG.2.5. Vertical view of the HTTR.

Three different types of cores were formed during fuel loading for start-up core physics experiments; thin and thick annular cores were achieved at 18 and 24 fuel column loaded cores, respectively, and the fully-loaded core consists of 30 fuel columns. These three core types were proposed for benchmark problems within this CRP. The effective diameter and height of the HTTR are 230 and 290 cm, respectively. The core size of the HTTR corresponds to about one half of that of the future HTGRs [2-2, 2-3, 2-4]. Moreover, the high excess reactivity of the HTTR is similar to that of the future HTGRs because the large excess reactivity is necessary to compensate for power operation effects of temperature, xenon, burnup, etc.. Therefore, the benchmark problems of the HTTR's start-up core physics experiments are useful for verification of design codes of the future HTGRs.

The major specifications of the HTTR are given in Table 2-1 [2-1]. The reactor consists of core components and reactor internals. They are arranged in the reactor pressure vessel (RPV), which is 13.2m in height and 5.5m in diameter. Figure 2.5 shows the vertical cross section of the core and reactor internals structure. The core consists of core components which are prismatic hexagonal blocks 580mm in height and 360mm in width across the flats. These include fuel assembly blocks, control rod guide blocks, replaceable reflector blocks, and irradiation blocks. The core components are piled up cylindrically to form the core. The reactor internals consist of graphite and metallic core support structures and shielding blocks. They support and arrange the core components within the RPV.

The active core, 290cm in height and 230cm in effective diameter, consists of 30 columns and 7 control rod guide columns. Horizontal cross sections of the HTTR are shown in Figures 2.6 and 2.7. An additional 9 control rod columns are arranged among the adjacent reflector graphite columns. The replaceable reflector region adjacent to the active core consists of 9 control rod columns, 12 replaceable reflector columns, and 3 irradiation columns, which are surrounded by permanent reflector blocks. Each fuel column consists of 2 top reflector blocks, 5 fuel assemblies, and 2 bottom reflector blocks.
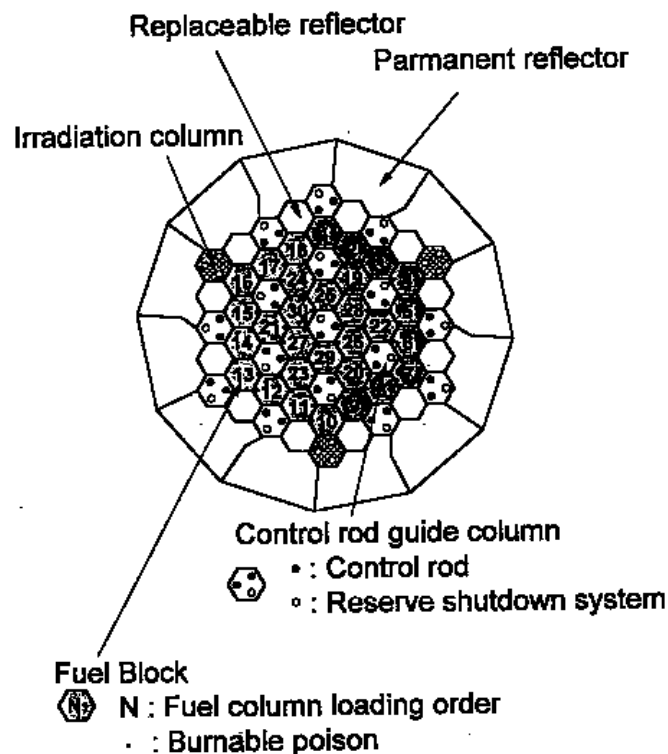

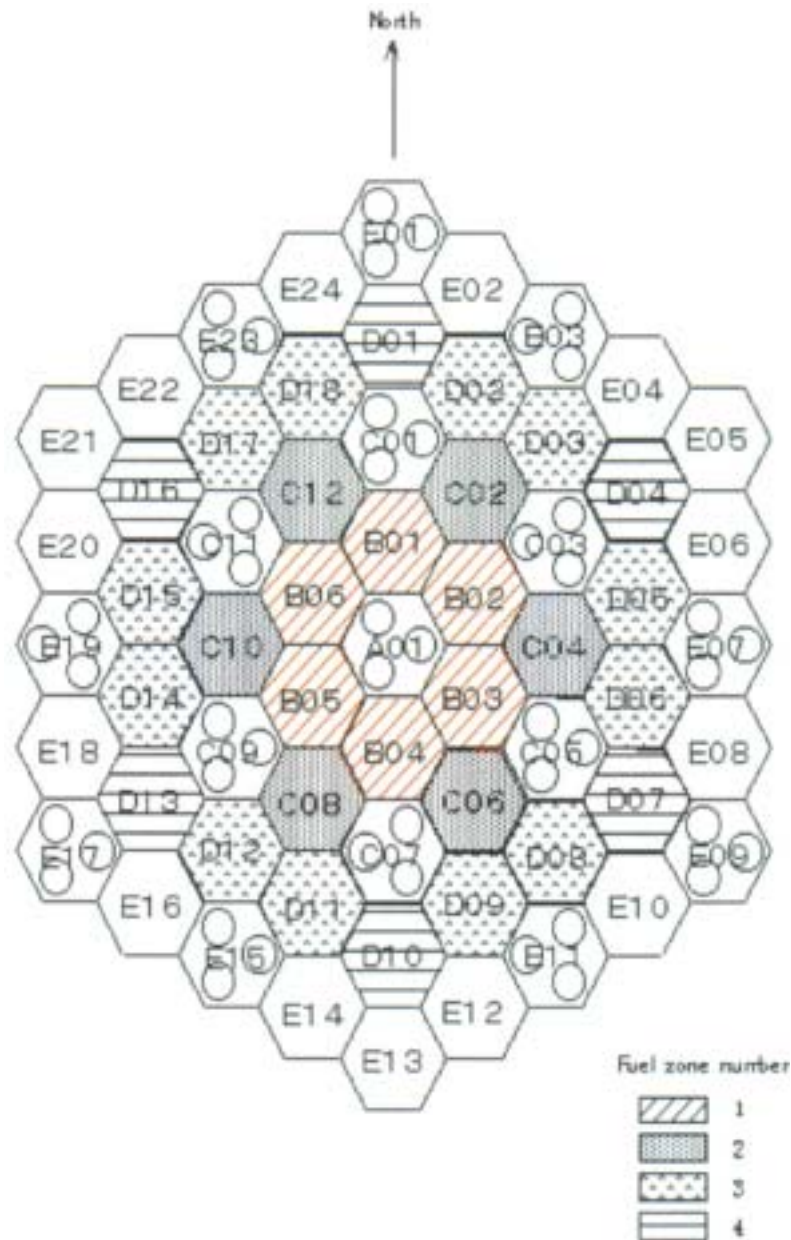*FIG. 2.6. Fuel column loading order and horizontal view of HTTR core.*

FIG. 2.7. HTTR fuel column name and zone number.

Figure 2.8 shows the structure of the pin-in-block type fuel. A fuel rod consists of a graphite sleeve containing 14 fuel compacts. The fuel rods are inserted into the coolant channels of the fuel graphite blocks. Each fuel compact contains about 13,000 coated fuel particles (CFPs) embedded in the graphite matrix. The number of uranium enrichments is 12. The highest and lowest enrichments are 9.9 and 3.4 wt%, respectively. Fuels of higher-enriched uranium are placed in the upper and outer core regions to reduce the maximum fuel temperature. Burnable poisons (BPs) made of boron carbide and carbon are inserted into two of three holes below the dowel pins in the fuel graphite block. The coolant gas flow is downward through annular channels formed by the graphite block and the fuel rod.
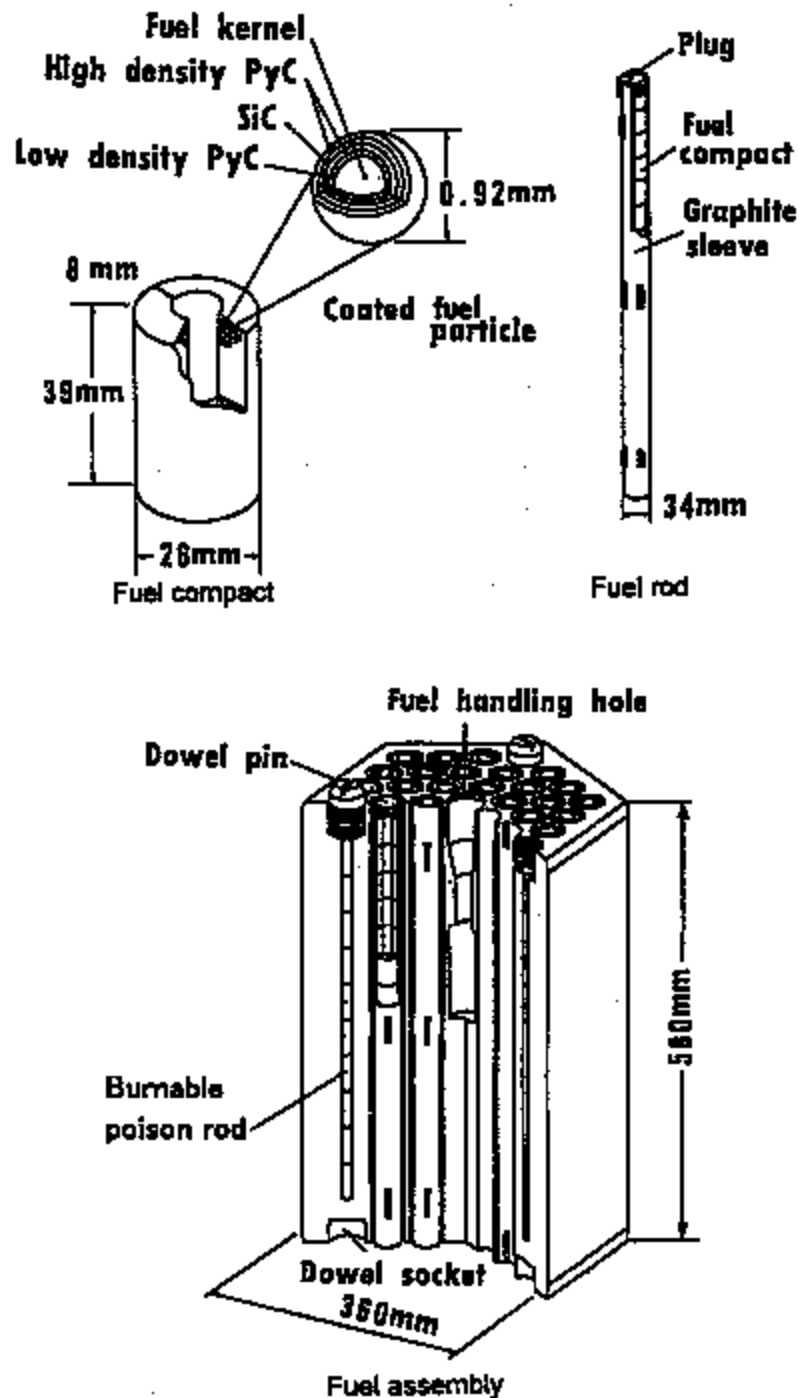
FIG. 2.8: Structure of fuel assembly.

The top of the control rod guide columns and irradiation columns are 100mm lower than that of the fuel columns because the 9th layer block of these columns are 480mm in height. Each horizontal gap width between two columns is 2mm in average.

Reactivity is controlled by 16 pairs of control rods. A pair of control rods is individually moved by a control rod drive mechanism located in stand-pipes connected to the hemispherical top head closure of the RPV. The control rods are inserted into two channels of the control rod guide columns in the active core and in the replaceable reflector regions.

Fuel loading scheme

Before fuel loading, the whole fuel region in the core is filled with graphite dummy blocks. There are two types of dummy blocks: graphite blocks with three large holes and those with three small holes. The graphite blocks with three large holes were actually used as control rod guide columns for out-pile seismic tests of the core structure. The others with three small holes were newly produced as dummy fuel blocks. The primary coolant system is filled with helium at normal atmospheric pressure and is not in operation during fuel loading. The core is at room temperature. Fuel loading is carried out by replacing the dummy blocks with the fuel assemblies, column by column. The fuel loading scheme is shown in Figure 2.6. The fuel blocks are loaded from the periphery to the center, and thin and thick annular cores are made at 18 and 24 fuel-column-loaded core, respectively.

The approach to criticality was observed by monitoring the inverse of the neutron multiplication fraction. The core is regarded as critical when the neutron density is maintained constant after removing the temporary neutron source. After the first criticality, the increment in reactivity was measured by the inverse kinetic method. The excess reactivity of the core was obtained by adding all increments of the reactivity from the first criticality to the fully-loaded core.

Configuration and composition of components

For the calculations, the detailed data of the active core, the adjacent replaceable reflector region and the permanent reflector region were necessary. Configuration of the components in the above mentioned regions is described as follows: The position of blocks in the core is noted by vertical position number and column number. The vertical number is 1, 2, . . . , 9 as from the top blocks in the 1st layer to the bottom blocks in the 9th layer, with the column number named according to Figure 2.9. For example, "4C05" means that the block is placed at the 4th block from the top, the 2nd ring from the core center, and the 5th block from the north in clockwise direction. In all, 30 fuel columns are grouped concentrically into 4 fuel zones as shown in Figure 2.9.

Fuel assembly

A fuel assembly consists of fuel rods, two burnable poison (BP) rods and a fuel graphite block. Each fuel rod consists of a graphite sleeve and 14 fuel compacts containing coated fuel particles (CFPs). The fuel rods are inserted into vertical holes of 41mm diameter in the fuel graphite block and form annular coolant channels between the vertical holes and the fuel rods. Figure 2.8 shows the structure of fuel assembly. There are two types of fuel graphite blocks having 31 or 33 fuel rods. The number of different uranium enrichments are 12 in the core. The uranium enrichment of all compacts in a fuel assembly is not changed. The fuel assembly is classified by the uranium enrichment, the number of fuel rods and the type of BPs. The fuel assembly arrangement in the core is shown in Figure 2.9.

A CFP consists of a spherical fuel kernel of low enriched UO_2 with TRISO coating. The TRISO coating consists of a low-density, porous pyrolytic carbon (PyC) buffer layer adjacent to the fuel kernel, followed by high density isotropic PyC layer, a SiC layer and a final outer PyC layer. The CFPs are embedded in graphite matrix of the fuel compact. The CFPs are classified into 12 sorts by their uranium enrichments. The form of the CFPs is given in Figure 2.10.

Layer number from top block	Layer number from top fuel block	Items	Fuel zone number			
			1	2	3	4
3	1	Uranium enrichment (wt%)	6.88	7.82	9.38	9.81
		Number of fuel rod of graphite block	33	33	31	31
		Type of burnable poisons	H-I	H-I	H-I	H-I
4	2	Uranium enrichment (wt%)	5.16	6.25	7.19	7.82
		Number of fuel rod of graphite block	33	33	31	31
		Type of burnable poisons	H-II	H-II	H-II	H-II
5	3	Uranium enrichment (wt%)	4.29	5.16	5.91	6.25
		Number of fuel rod of graphite block	33	33	31	31
		Type of burnable poisons	H-II	H-II	H-II	H-II
6	4	Uranium enrichment (wt%)	3.30	3.86	4.29	4.79
		Number of fuel rod of graphite block	33	33	31	31
		Type of burnable poisons	H-I	H-I	H-I	H-I
7	5	Uranium enrichment (wt%)	3.30	3.86	4.29	4.79
		Number of fuel rod of graphite block	33	33	31	31
		Type of burnable poisons	H-I	H-I	H-I	H-I

Note:
Fuel zone number is shown in the below figure.
Type of burnable poisons is shown in Table 2-3.
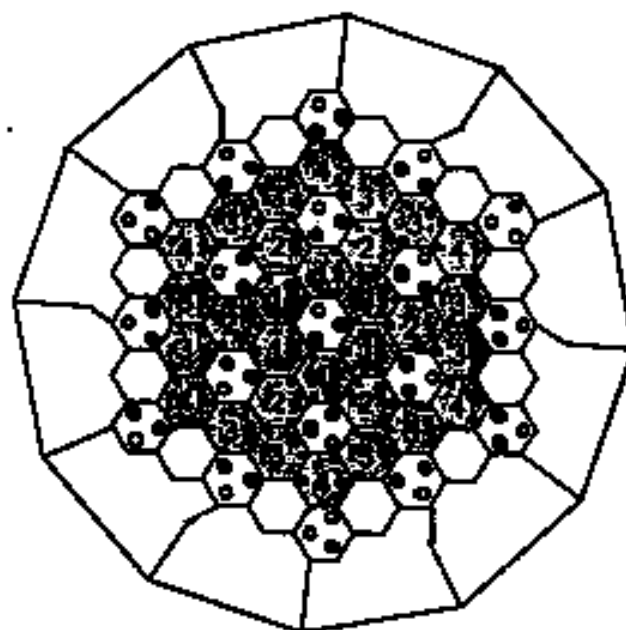
⟨N⟩ N : Fuel zone number
· : Burnable posion

FIG. 2.9. Fuel assembly arrangement in the HTTR core.
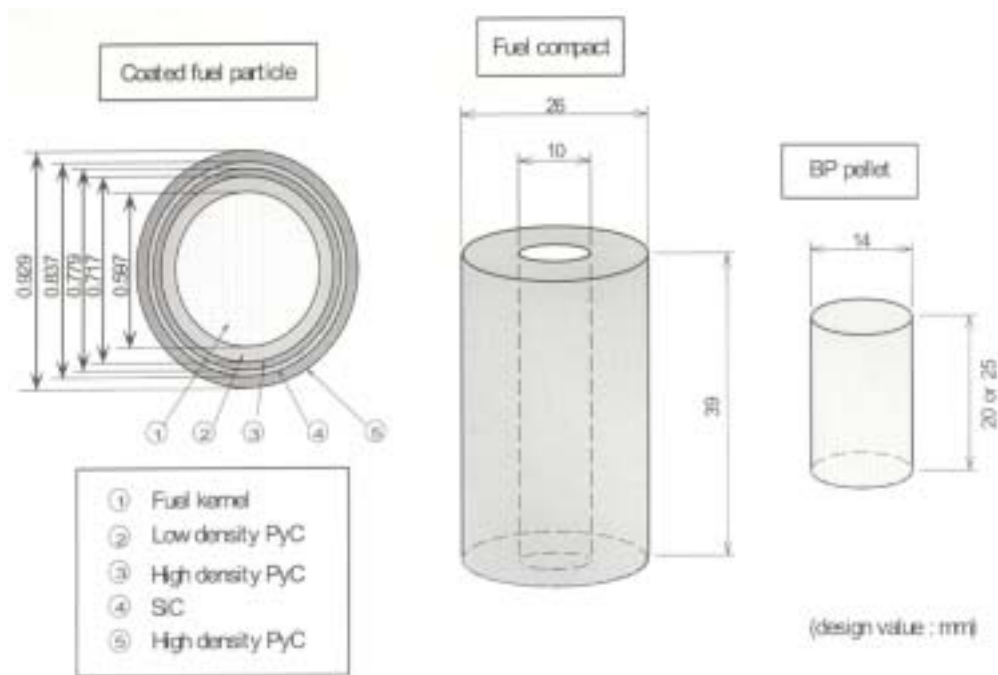
FIG. 2.10. Coated fuel particle, fuel compact and burnable poison pellet.

The fuel compact consists of CFPs and graphite matrix. The form is a hollow cylinder of 10mm in inner diameter, 26mm in outer diameter and 39mm in height.

The fuel rod consists of a graphite sleeve containing 14 fuel compacts. It is inserted into the coolant channel of the fuel graphite block. The form of the fuel rod is given in Figure 2.11. The fuel graphite block is a prismatic hexagonal block 580mm in height and 360mm in width across the flats. The block has 33 fuel holes in the fuel zones 1 and 2, and 31 fuel holes in the fuel zone 3 and 4. The fuel zone numbers are defined in Fig. 2.7. The form of the block is given in Figure 2.12 and Figure 2.13.
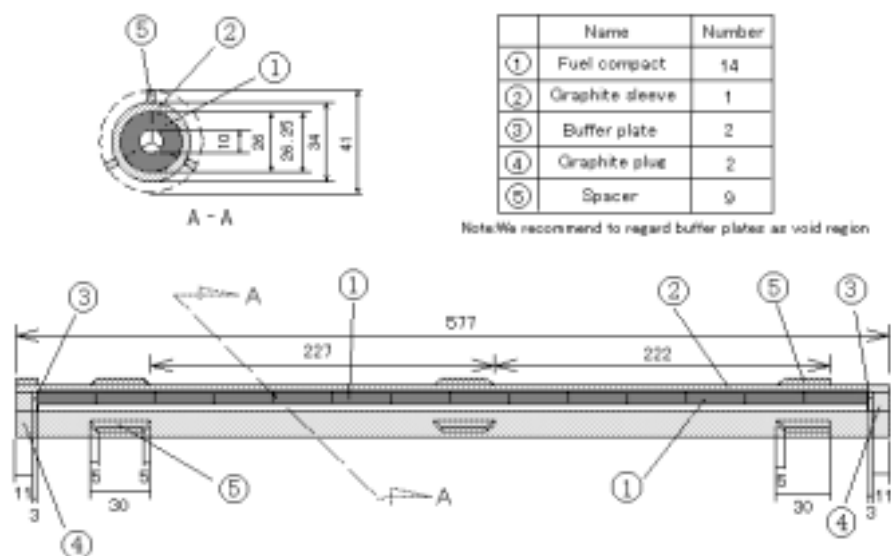
FIG. 2.11. Fuel rod.

TABLE   2   Burnable poisons and Graphite discks

Burnable poison pellet

Material B_4C-C composite

Boron arrangements   shown in Fig.5

Type	H-I	H-II
Density (g/cm^3)	1.79	1.82
Natural boron concentration (wt%)	2.22	2.74
Diameter (mm)	13.9	13.9
^{10}B abundance ratio (wt%)	18.7	18.7

Graphite disk

Material   Graphite

Diameter (mm)	14.0
Density (g/cm^3)	1.77
Impurity (ppm)*	0.37

* Natural boron equivalent

Burnable poison rod

Number of BP rods in a fuel assembly   2   (shown in Fig.2)

Height   500 mm

Configuration of BP pellets and graphite disks in a BP rod are shown in the following figures

500 mm

10 BP pellets
200 mm

20 graphite disks
100 mm

10 BP pellets
200 mm

φ14 mm

H-I type

8 BP pellets
200 mm

20 graphite disks
100 mm

8 BP pellets
200 mm

φ14 mm

H-II type
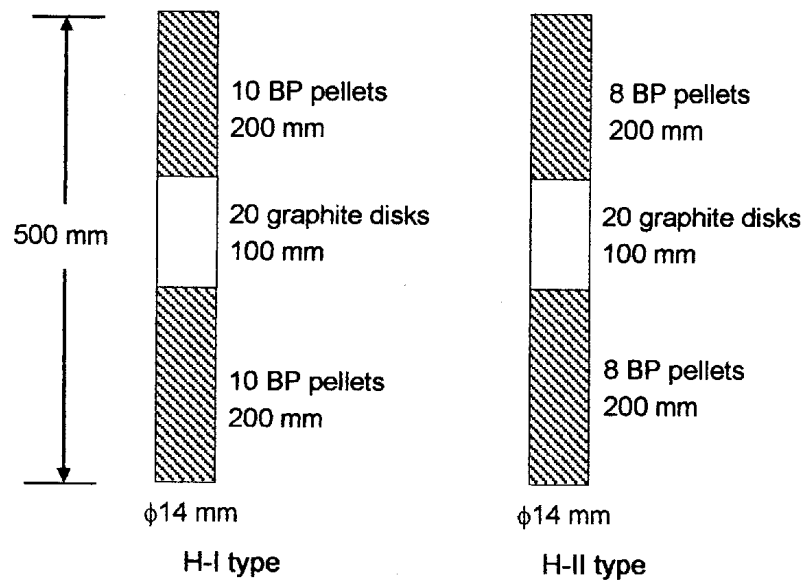
FIG. 2.12. Fuel block for 33 pin fuel assembly.
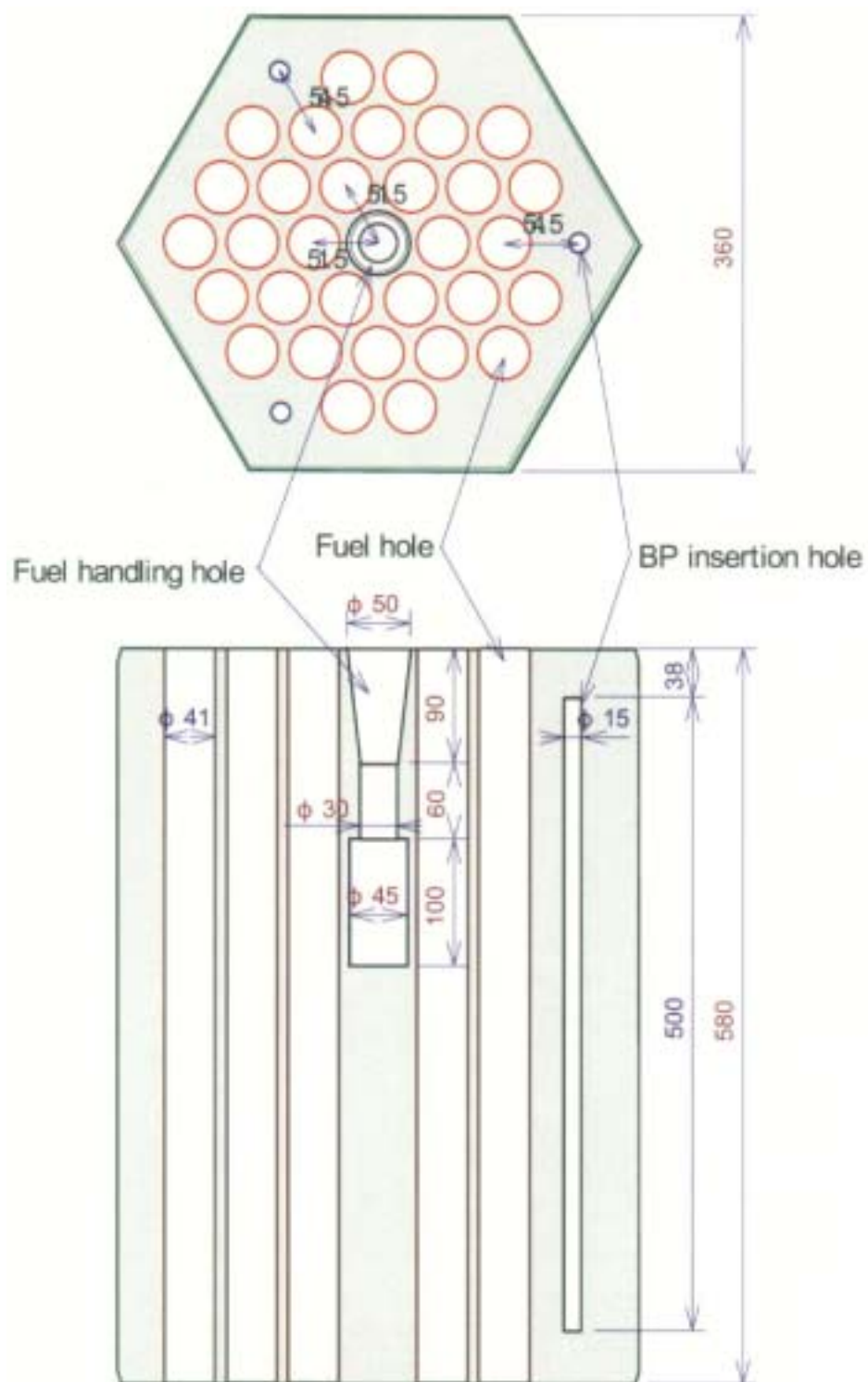
FIG. 2.13. Fuel graphite block for 31.pin fuel assembly.

Control rod insertion hole

108

360

Reserved shutdown pellet insertion hole

φ 50

90

φ 30

60

φ 45

100

φ 123

580

FIG. 2.14. Control rod guide block in layers 1 through 5.

Burnable poison (BP) rods are inserted into two of three BP insertion holes of a fuel graphite block as shown in Fig. 2.8. The BP insertion holes are under the 3 dowel pins of the fuel graphite block and are 15mm in inner diameter and 500mm in length. One hole without the BP rod is empty. Figure 2.6 shows positions of holes which are filled with BPs. The diameter of BP rod is 14mm. The BP r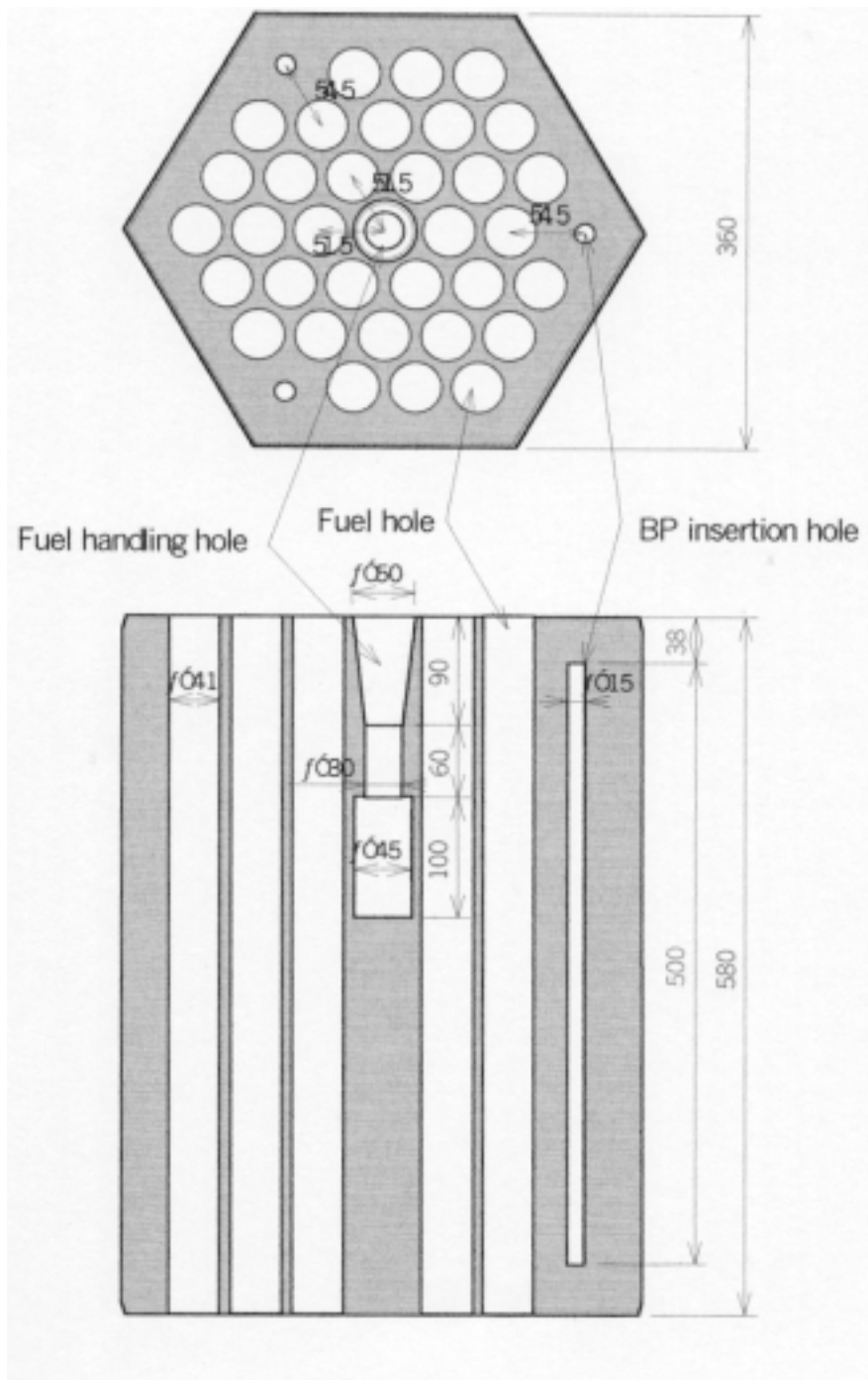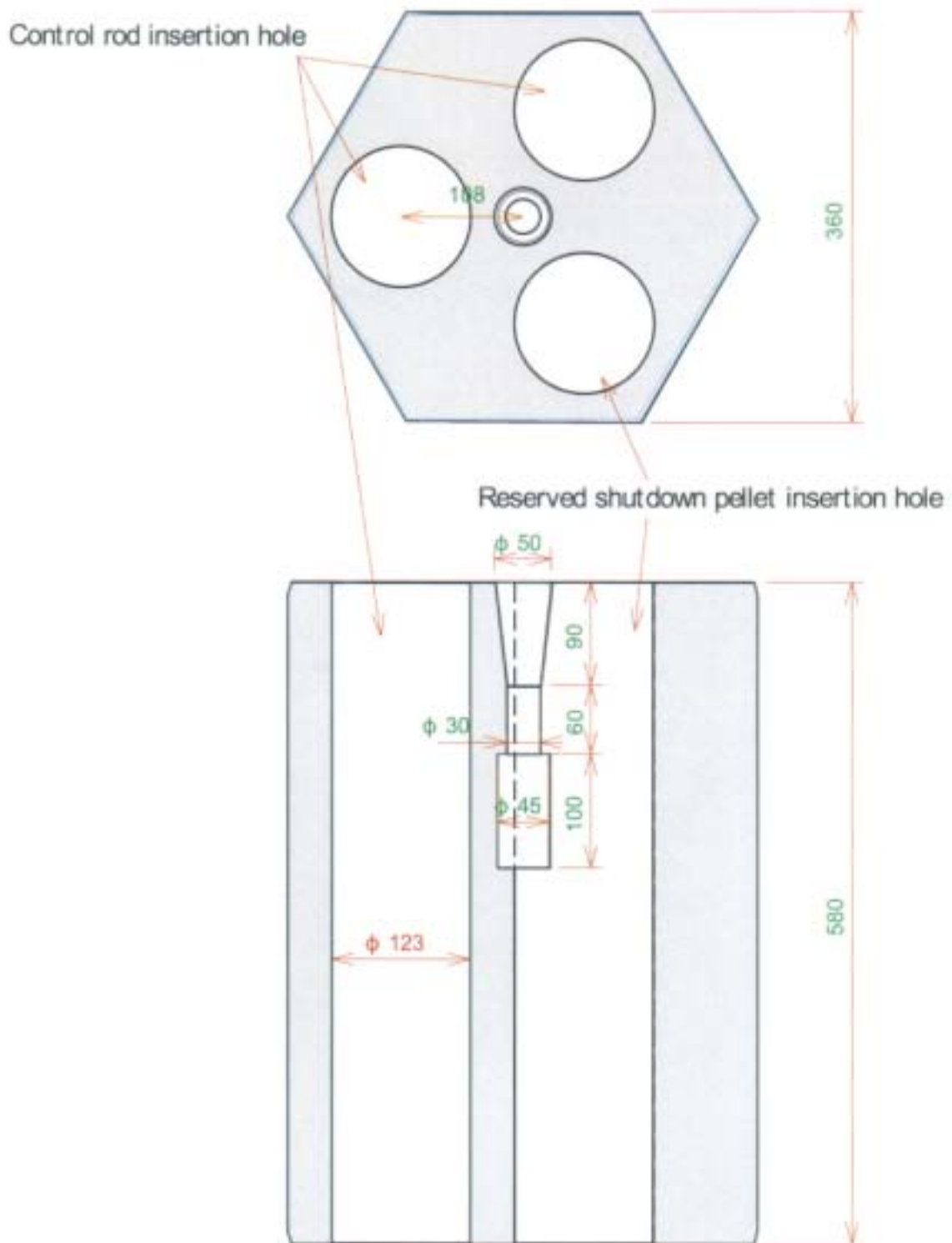od consists of BP pellets and graphite disks as shown in Table 2.2. The graphite disks are put between the BP pellets. The compositions of the BP pellets are B_4C and C. There are two types of BP pellets: H-I with 2.22wt% of natural boron concentration and H-II with 2.74wt%. The form of the BP pellets and graphite disks is given in Figure 2.10.

Control rod, reflector and dummy fuel blocks

There are 16 control rod guide columns each consisting of 9 control rod guide blocks. The control rod guide blocks have three holes. Two of them are control rod insertion holes. The third hole is a reserve shutdown system (RSS) hole which is used for emergency. Figure 2-6 shows the position of the control rod insertion holes and RSS holes in the core and the replaceable reflector region. Top and bottom replaceable reflector blocks are placed above and below the fuel assemblies. The arrangement of coolant channels (with 23mm in inner diameter) in the top replaceable reflector blocks corresponds to that of coolant channels (with 41mm in inner diameter) in the fuel assemblies within the same column. The upper bottom replaceable reflector block (the 8th layer) has the same arrangement of coolant channels as the top replaceable reflector block. The lower bottom replaceable reflector block (the 9th layer) has 6 large coolant channels.
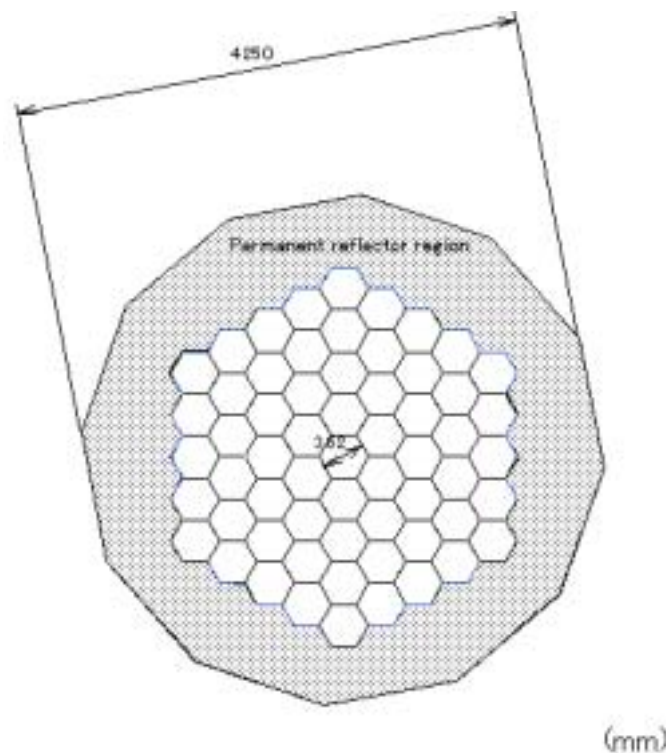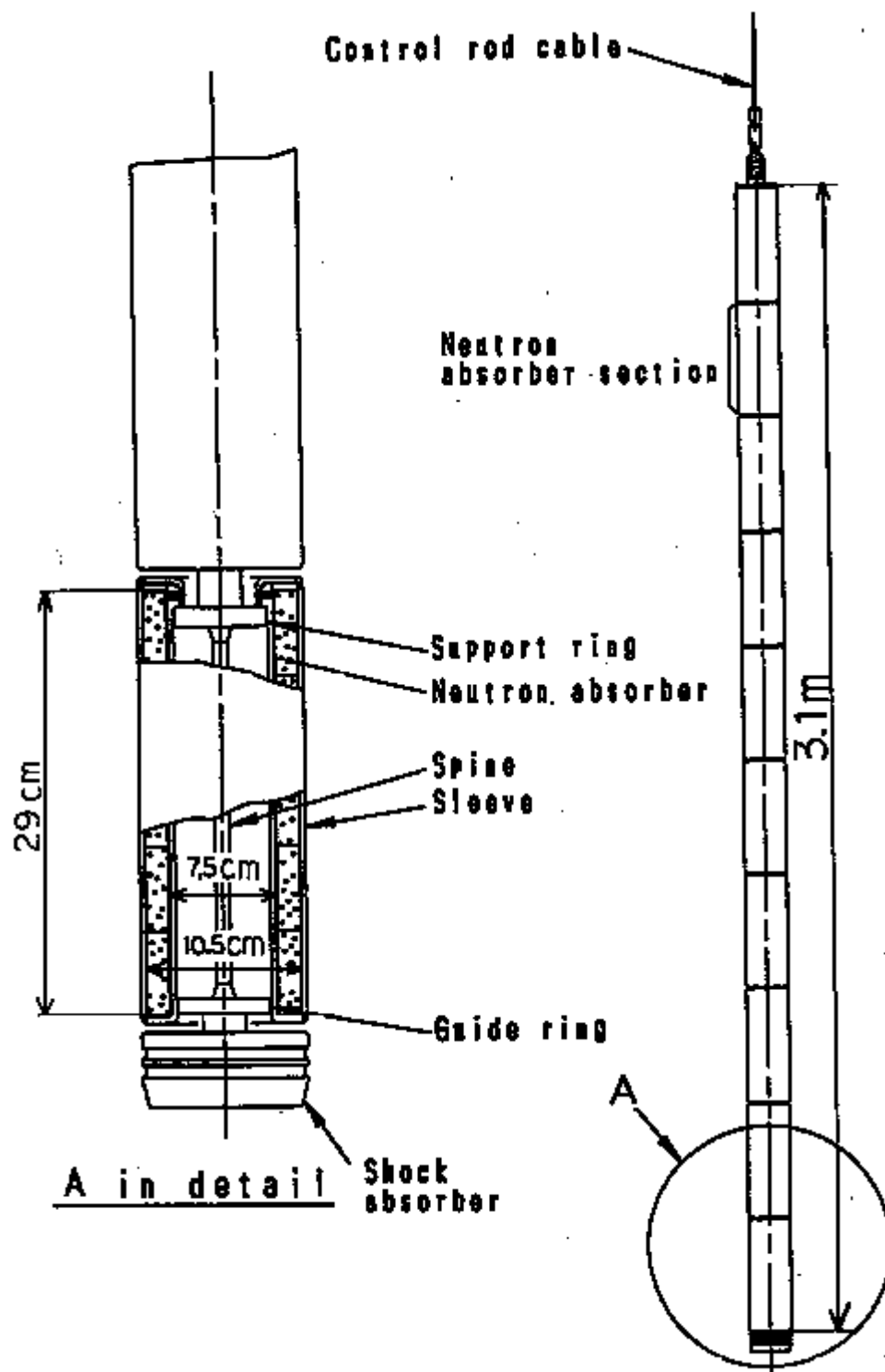

FIG. 2.15. Permanent reflector region.

FIG. 2.16. Schematic of control rod.
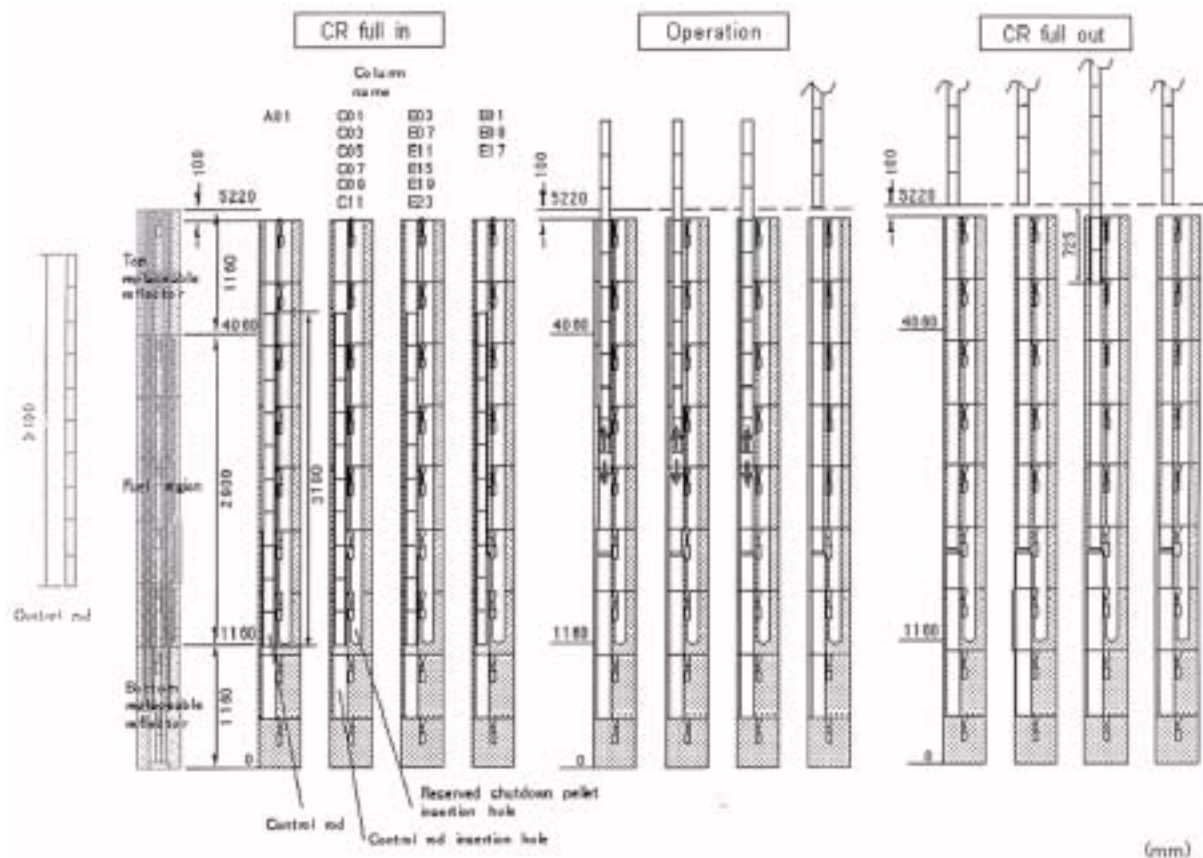
FIG. 2.17. Axial control rod position.

Dummy fuel blocks are placed in the active core before fuel loading as substitution for fuel assemblies. The external form of the dummy fuel block is the same as that of a fuel graphite block. The dummy fuel blocks contain higher impurity than the fuel graphite blocks. All dummy fuel blocks are replaced by fuel assemblies. All blocks except the bottom block of the control rod guide column and the irradiation column are 58 cm in height and 36 cm in width of across flats. The bottom blocks of the control rod guide and irradiation columns are 48 cm in height and 36 cm in width across the flats. A typical form of the control rod guide blocks for layers 1 through 5 is shown in Figure 2-14. Boron pins are installed into the lower parts of blocks in the 9th layer for neutron shielding. For benchmark problems, the neutron shielding pin region is considered as a black absorber or vacuum in calculation models.

Core components are horizontally surrounded by 12 permanent reflector blocks whose form is a large polygonal graphite block. The width across the flats of the core, including permanent reflector blocks, is 4250 mm as shown in Figure 2.15. The permanent reflector blocks have holes for irradiation tests and neutron detectors. The void fraction is 0.7 % due to the holes. Around the permanent reflector blocks, there are side shielding blocks consisting of B_4C/C. The structures outside of the permanent reflector region were neglected in the calculation models.

Control Rods

There are 16 pairs of control rods, 7 in the active core and 9 in the replaceable reflector region. A pair of control rods is inserted into holes of a control rod guide column.

Each control rod consists of 10 neutron absorber sections connected with metallic spines and support rings. Each section contains 5 sintered compacts of B_4C and C as neutron absorber in the annular space. The schematics of the control rod are shown in Figure 2. 16. The axial positions of the control rods are divided into three types as shown in Figure 2.17. When the control rods are fully inserted, the lower ends of all control rods are on the same plane with the bottom face of the 7th layer of a fuel column. In the first approach to criticality three pairs of control rods at columns E01, E09 and E17 in Figure 2.7 are fully withdrawn. These are not used to operate the reactor. The rest of 13 pairs of control rods are the withdrawn during the approach to criticality. At the critical condition, all control rod pairs except those of columns E01, E09, and E17 are adjusted so that their insertion depth will be the same. This insertion level is evaluated in the benchmark test HTTR-CR. When the control rods are fully withdrawn, their upper limit is the upper face of the 1st replaceable reflector block (over the fuel region) with the exception of those control rods (R2) at columns E03, E07, E11, E15, E19, and E23 in Figure 2.7. The control rods of these six columns have upper limits at 725mm below the top of the 1st block.

Further detailed data of the core, fuel assemblies and core internal components have been provided in [2-5].

Nuclear Instrumentation

Temporary neutron instrumentation consisting of three BF3 counters, three fission counters (FC), two gamma-ray-compensated ionization chambers (CIC) was used for the startup core physics tests. Positions of detectors were not arbitrarily chosen like liquid (water)-moderated reactors. Only the existing holes were available for the solid (graphite)-moderated reactor like the HTTR. However, the holes for control rods (CRs) and reserve shutdown systems could not be used due to safety-related restrictions. Thus the detectors are located in three irradiation columns as shown in Figure 2.18.
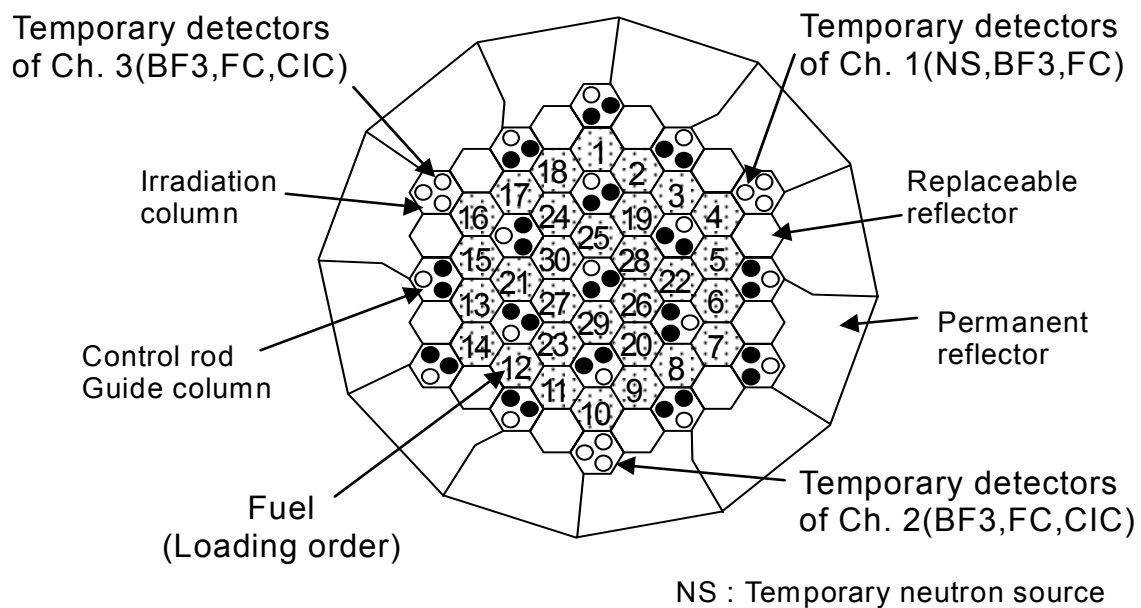
FIG. 2.18. Cross section of the HTTR and fuel loading order.

The BF3 is used for monitoring increase in the neutron density. The inverse of the multiplication factor was evaluated from the change in neutron density. The FC was used for measurement of the axial neutron flux distribution. The CIC was used for reactivity measurement by the Inverse Kinetic (IK) method. A temporary neutron source (Am-Be, 1.48×10^4 Bq) was inserted in irradiation test column. The vertical position of each detector is shown in Figure 2.19. The BF3 in Ch.1 is installed about 2 m apart from the neutron source to avoid the effect of direct-flying neutrons from the source. BF3 and FC in the same channel are located at the same vertical position in order to have redundancy for 1/M monitoring. FCs were movable in the vertical direction to measure the axial neutron flux distribution. The CICs were fixed in the

core. The temporary neutron source was withdrawn from the core to exclude the neutron source effect on the measurement.
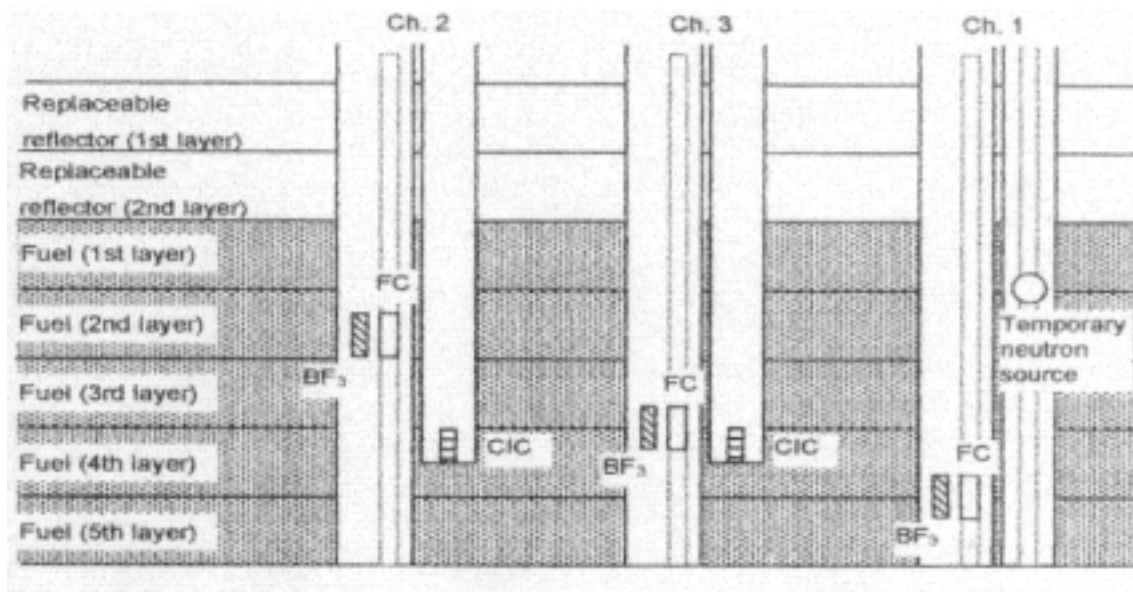
FIG. 2.19. Vertical location of temporary neutron detector system.

2.1.2. Benchmark Problem Descriptions

The benchmark problems addressed within this CRP include HTTR related start-up core physics tests and thermal hydraulics. General descriptions of these problems are included below. Details of the methodologies utilized and the results obtained for each problem by the individual CSIs are presented herein by each Member State.

2.1.2.1. Initial Criticality – [HTTR-FC] (Phase 1)

The number of fuel columns are evaluated for the first criticality, with the fuel columns charged from the outer region of the core. They are loaded clockwise, one by one. A small excess reactivity at the first criticality is also evaluated.

2.1.2.2. Initial Criticality – [HTTR-FC] (Phase 2)

The following effects are considered in the Phase 2 to improve the benchmark problem calculation accuracy:

1) Air in void of graphite
2) Revised impurity contents in dummy block
3) Aluminum in the temporary neutron detector holders.

2.1.2.3. Control Rod Position at Criticality – (HTTR-CR)

The control rod insertion depths are evaluated at the critical condition for the following three cases. All control rod insertion levels are adjusted on the same level except three pairs of control rods in the most outer region in the side reflectors. These three pairs of control rods should be fully withdrawn for the calculation.

1) 18 columns (thin annular core)
2) 24 columns (thick annular core)
3) 30 columns (fully-loaded core)

2.1.2.4. Excess Reactivity – (HTTR-EX)

The excess reactivity is evaluated for the three cases mentioned above. The room temperature of 300K is to be assumed as the moderator and fuel temperatures for the benchmark problem. One atmospheric pressure of helium is to be used as the primary coolant condition.

2.1.2.5. Scram Reactivity – (HTTR-SC)

The Scram reactivity is to be evaluated for the following two cases:

1) All reflector CRs are inserted at the critical condition
2) All CRs in reflector and core are inserted at the critical condition

The core condition for this benchmark problem is as follows:

-Fully-loaded core (30 column fuel core)
-Fresh fuel core

2.1.2.6. Isothermal Temperature Coefficient (HTTR-TC)

Isothermal temperature coefficients for the fully-loaded core are to be evaluated from the effective multiplication. The critical control rod positions are changed with temperature elevation in the real reactor operation. However, the control rod position is not to be changed in the calculation to obtain the reactivity difference. Critical control rod positions are to be evaluated at temperature of 480K.

2.2. REACTOR PHYSICS BENCHMARK ANALYSIS AND RESULTS

2.2.1. Japan

2.2.1.1 Analysis methodology and model description

Diffusion calculation [2-9, 2-10]

The calculations for the benchmark problems were carried out using a nuclear characteristics evaluation code system which was developed from an HTTR nuclear design code system [2-11]. The code system consists of the DELIGHT [2-12], TWOTRAN-II [2-13] and CITATION-1000VP [2-14] codes. An outline of the calculation codes and model is summarized in Table 2-3. The program structure of the system is shown in Figure 2.20.

Table 2-3. Codes, models and nuclear data library for diffusion calculation

Items	Name of country Japan
	Name of Institute JAERI
Nucl. Data file	ENDF/B-III, IV
Fuel cell code	DELIGHT
Theory	Collision probability
Model	Pin cell
Cut off energy	2.38eV
No. of groups	40
BP cell code	TWOTRAN-II
Theory	Transport
Model	2-D(r-Z)
No. of groups	6
Control rod cell code	TWOTRAN-II
Theory	Transport
Model	2-D (x-y)
No. of groups	6
Core cal. Code	CITATION
Model	3-D (Triangle)
No. of groups, (Fast +Thermal)	6, (3+3)

DELIGHT is an one-dimensional lattice burnup cell calculation code that has been developed in JAERI. TWOTRAN-II is a transport code that was used to provide average group constants of burnable absorber (BP) in fuel blocks and graphite blocks where control rods (CRs) are inserted. CITATION-1000VP is a reactor core analysis code. This code was developed from CITATION [2-15] so that nuclear characteristic analyses could be carried out with a three-dimensional whole core model of the HTTR in a short calculation time.
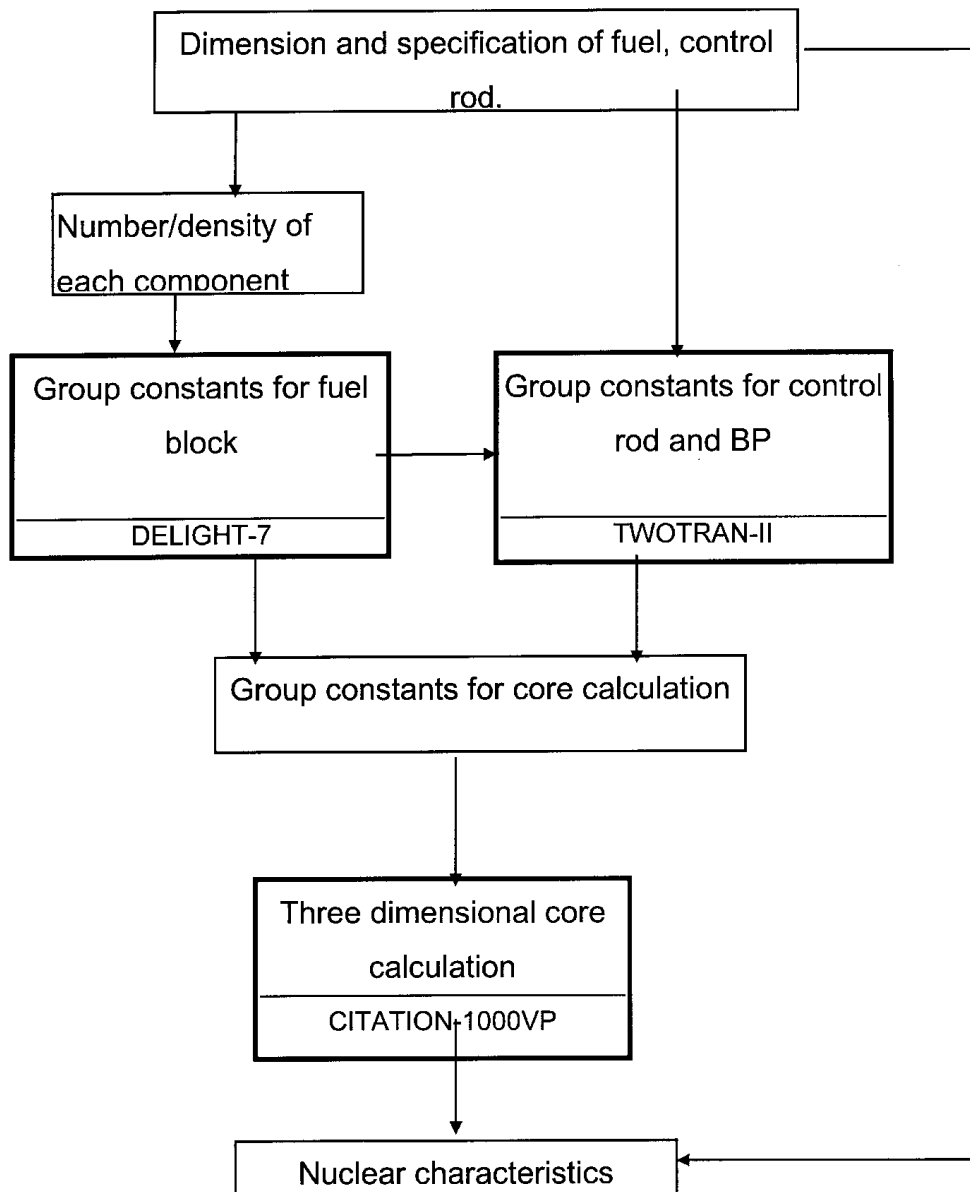
```
┌─────────────────────────────────────────┐
│  Dimension and specification of fuel, control │──────────┐
│                 rod.                     │          │
└─────────────────────────────────────────┘          │
        │                          │                  │
        ▼                          │                  │
┌──────────────────┐              │                  │
│ Number/density of │              │                  │
│ each component    │              │                  │
└──────────────────┘              │                  │
        │                          ▼                  │
        ▼                                             │
┌──────────────────────┐   ┌──────────────────────┐  │
│ Group constants for fuel │   │ Group constants for control │  │
│       block          │──▶│      rod and BP       │  │
│                      │   │                       │  │
│      DELIGHT-7       │   │      TWOTRAN-II       │  │
└──────────────────────┘   └──────────────────────┘  │
            │                      │                  │
            ▼                      ▼                  │
      ┌─────────────────────────────────┐            │
      │ Group constants for core calculation │        │
      └─────────────────────────────────┘            │
                    │                                 │
                    ▼                                 │
          ┌──────────────────────┐                   │
          │ Three dimensional core │                  │
          │     calculation        │                  │
          │                        │                  │
          │   CITATION-1000VP      │                  │
          └──────────────────────┘                   │
                    │                                 │
                    ▼                                 │
          ┌──────────────────────┐                   │
          │ Nuclear characteristics │◀────────────────┘
          └──────────────────────┘
```

FIG. 2.20. Program structure of the HTTR nuclear characteristics evaluation code system.

DELIGHT was used to provide group constants of fuel and graphite blocks for succeeding core calculations. Resonance, neutron spectrum, neutron flux distribution, criticality, and burn-up calculations were done sequentially. Nuclear data were based on ENDF/B-IV except burn-up chain data that were extracted from ENDF/B-III. In the resonance range, the code employs intermediate resonance approximation and can consider the effect of a double heterogeneity caused by coated fuel particles (CFPs) and assembled fuel rods. The average group constants of the whole fuel block were obtained by a fuel cell calculation as follows; The group constants of the fuel rods were calculated by using a one-dimensional cylindrical fuel cell model as shown in Figure 2.21. The fuel rods in a block are located in the inner position of the fuel block, and the outer region of a fuel block is graphite rich region. To simulate the harder neutron spectrum, the area of cross section of the fuel cell was determined by the pitch of fuel rods. The pitch of fuel rods is 5.15cm. Therefore, the outer radius of fuel cell is about 2.7cm.
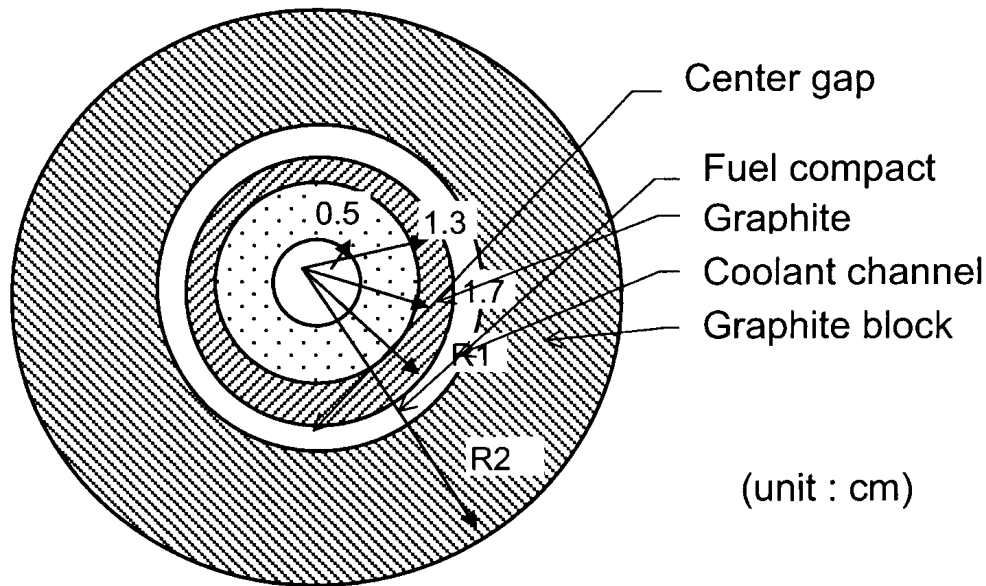
FIG. 2.21. Fuel cell model for DELIGHT code.

The group constants for BP and CR were calculated by TWOTRAN-II code.

BP cell model

The BP of the HTTR is a zebra type configuration. The average group constants of the zebra type BP was calculated by two-dimensional r-Z model of TWOTRAN-II code. The BP cell model is shown in Figure 2.22. The BP cell model corresponds to a quarter of a fuel block which contains half of the BP rod. BP rod consists of BP pellets and graphite pellets which are surrounded by graphite, the outer region contains homogenized fuel. Macroscopic cross section sets for the calculation were provided by the DELIGHT code.

In order to obtain the effective microscopic cross section, a homogenized region is determined to have the same cross section as the BP region in the core calculation model. Three kinds of σ_a for ^{10}B in the BP rod are evaluated for core calculations. The first one was for the fuel block with 7.9% enrichment of ^{235}U, 33 fuel pins and 2.0wt% of boron concentration in the BP rods. This σ_a-set was used for all BPs in the first layer of fuel blocks. The second one was for the fuel block with 6.3% enrichment of ^{235}U, 33 fuel pins and 2.5wt% of boron concentration in the BP rods which was used for all BPs with 2.5wt% of boron concentration. The third one was for the fuel block with 3.9% enrichment of ^{235}U, 33 fuel pins and 2.0wt% of boron concentration in the BP rods. This kind of σ_a was used for all BPs in the 4th and 5th layer of fuel blocks.

CR cell model

The average group constants of a pair of CRs and of the corresponding graphite block were obtained with the flux-weighting method. The neutron fluxes were calculated with a two-dimensional x-y model. The model is based on half of the graphite block where one CR is inserted.
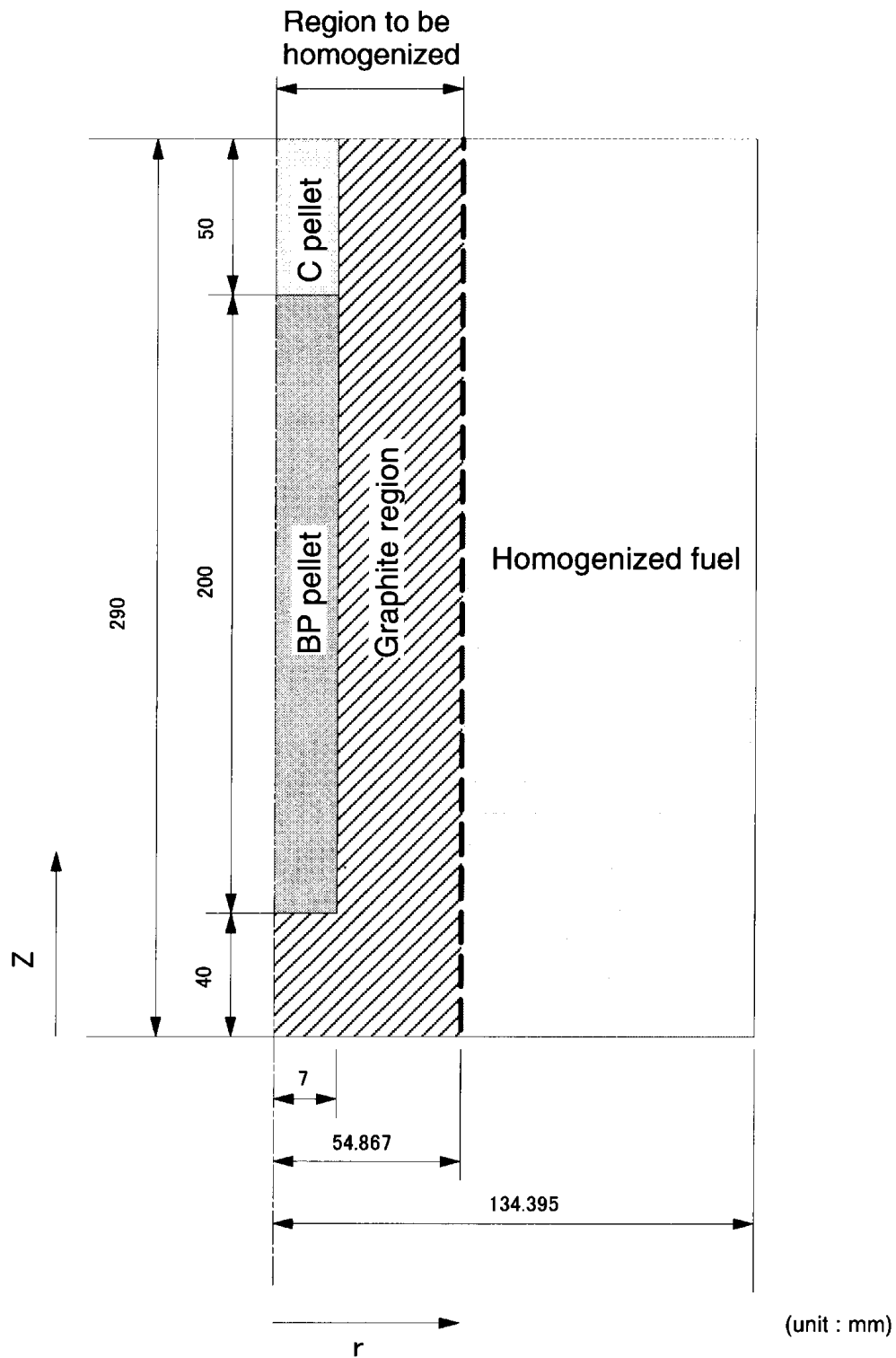
FIG. 2.22. BP cell model by TWOTRAN-II

The average group constant of CRs was obtained by smearing group constants in a region. For core calculations, two kinds of CR models were developed which are called as "CR-block model" and "CR-hex model". The smearing regions to obtain average group constants for CRs are different in the two models. The schematics for each model is shown in Figure 2.23. The CR-block model was used for all benchmark problems. The CR-hex model was used for HTTR-SC to check the effect of model.

i) CR-block model

The average group constants of CRs were homogenized in a CR guide block region. In the core calculation for the model, CR guide block was modeled as one region. This model is the same with the model used in the previous benchmark problem.

ii) CR-hex model

In the model, one CR rod is modeled as hexagonal shape which contains CR and surrounding graphite. The average group constant of CRs was obtained by smearing a narrow area in a CR guide block. In the core calculation for the model, the CR guide block is divided into three regions. One for CRs, one for a reserved shut down system pellet insertion hole, and one for graphite region. It is possible to consider the position of CRs in a control rod guide block at core calculations using the model.

In the benchmark problems, CR-block model was used as standard model. The effects of CR-block model and CR-hex model were evaluated in the benchmark of HTTR-SC.

The CITATION-1000VP is a reactor core analysis code based on the diffusion theory. This code was improved to enable a full core model calculation of the HTTR by extending the number of zones and meshes in the original CITATION code and enhancing the calculation speed by the vectorization of the code. This code was used for the analysis of the effective multiplication factor. The neutron energy group consists of 3 fast and 3 thermal groups.
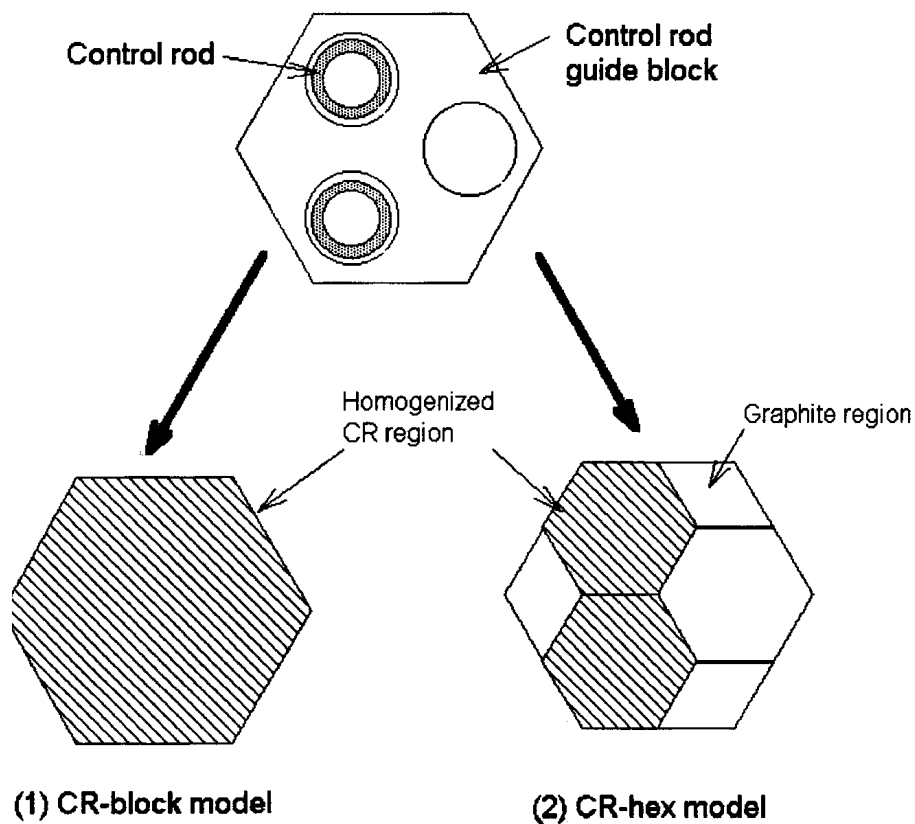

FIG. 2.23. Comparsion of CR model concrpt.

Fuel compact

BP rods

33 pin fuel block

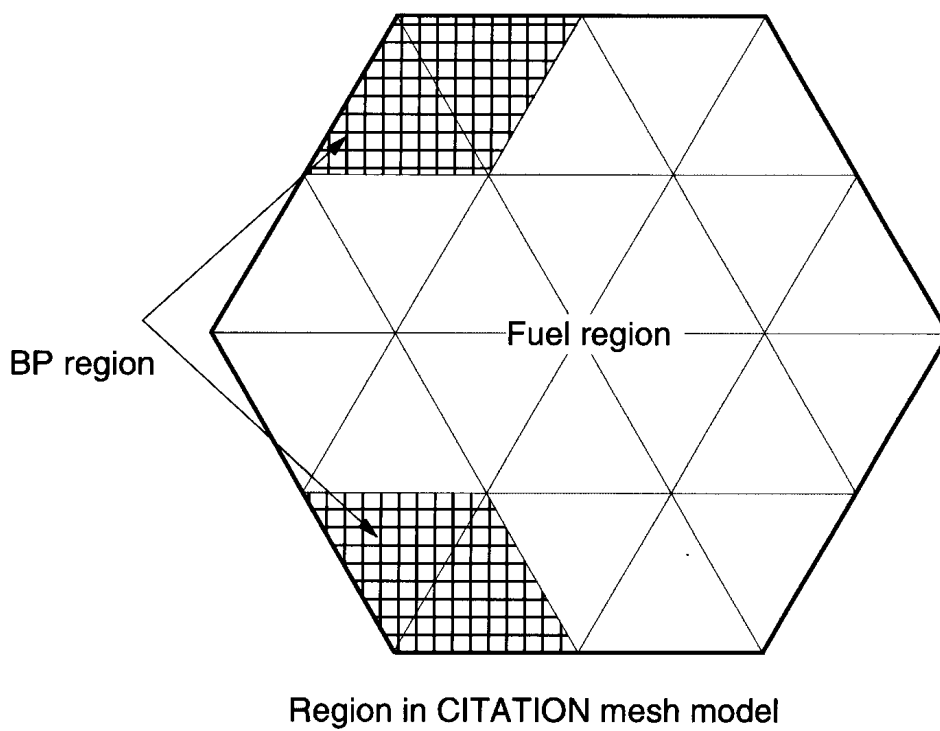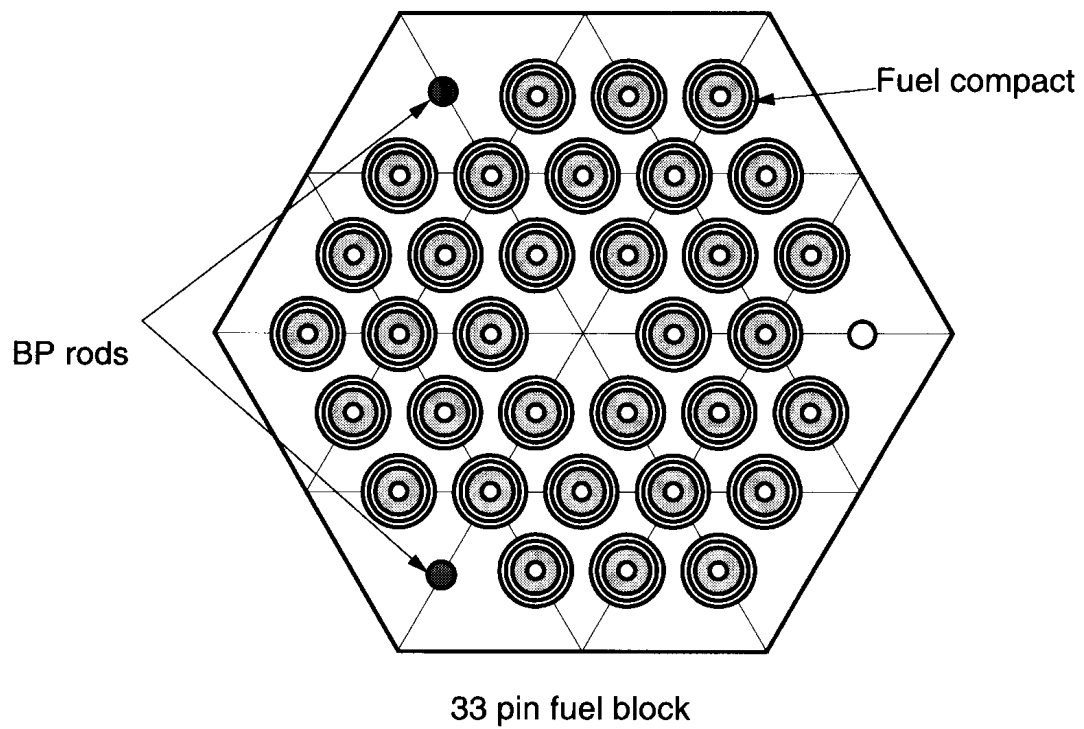BP region

Fuel region

Region in CITATION mesh model

FIG. 2.24. Configuration of regions in block for core calculation mode

A fuel block is divided into 24 triangular meshes horizontally and into 4 meshes vertically for the three-dimensional whole core calculation to simulate the position of the BP rods in a fuel block. In the horizontal plane, a fuel block was divided into BP region and fuel region as shown in Figure 2.24. ^{10}B and ^{11}B in a BP rod were distributed only in the BP region. Nuclides of the fuel, such as ^{235}U, ^{238}U, Si, were distributed only in the fuel region. Graphite is distributed homogeneously in the fuel and BP region. For the CR-block model, a CR guide block was modeled as one region.

Monte Carlo calculation

The whole core is presented with hexagonal lattices consisting of graphite reflector blocks and fuel blocks. The fuel block is also presented with hexagonal lattices consisting of fuel rods and BP rods. The fuel rod and BP rod are modeled with cylindrical body descriptions in hexagonal cells. Effective multiplication factors k_{eff} of different cores in fuel loading were calculated with MVP [2-16, 2-17] using the nuclear data of JENDL-3.2 [2-18]. The thermal neutron treatment for graphite in the JENDL-3.2 is based on $S(\alpha,\beta)$ of ENDF/III. The core temperature of 300K is assumed. The most probable value of k_{eff} was evaluated from track length, collision and analog estimators with the method of maximum likelihood. Number of histories per batch was 20,000 for all cases. Number of batches was 150. The first 5 batches were neglected for the statistical treatments. Although large number of scattering reactions must be calculated in one history for HTGR due to the low slowing down power of graphite, the CPU time is still reasonably small for the whole core analysis. The computation was carried out on the FACOM VPP-500.

In the geometry description, the hexagonal multiple lattice capability was used for periodical arrays of fuel rods in a fuel block and of hexagonal blocks in the core. The cross-sectional model of the 18 column, 24 column and whole core is given in Figures 2.15, 2.26, 2.28 and 2.27, respectively. The outer form of the permanent reflector blocks is modeled with a cylinder. The cross-sectional model of fuel block is shown in Figure 2-28. The cylindrical geometry of fuel rods and burnable poison rods were precisely modeled with body descriptions in hexagonal cells. The voids in control rod guide blocks and dummy fuel blocks increase neutron leakage because of the neutron streaming through them. They are also modeled with body descriptions in hexagonal cells. The CFPs in the compact are treated with the following three models:

(1) Homogeneous Model: All substances in CFPs are smeared with the graphite matrix in the compact.
(2) Corrected-homogeneous Model: Heterogeneity effect of CFPs, evaluated with collision probability theory [2-19], is added to the result of (1)
(3) Heterogeneous Model: Heterogeneity effect of CFPs is directory evaluated with Monte Carlo calculation using statistical geometry model based on MURATA's idea [2-20].
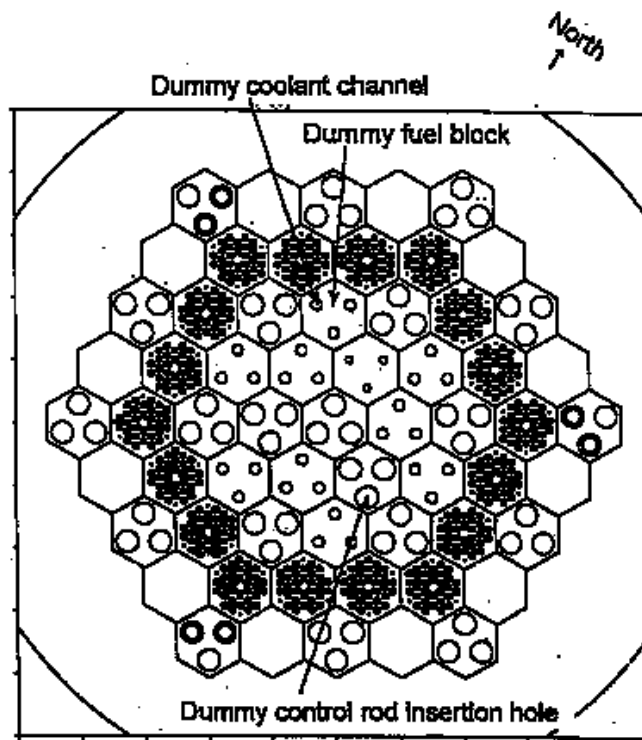
FIG. 2.25. Horizontal cross-section of 18 column core model.
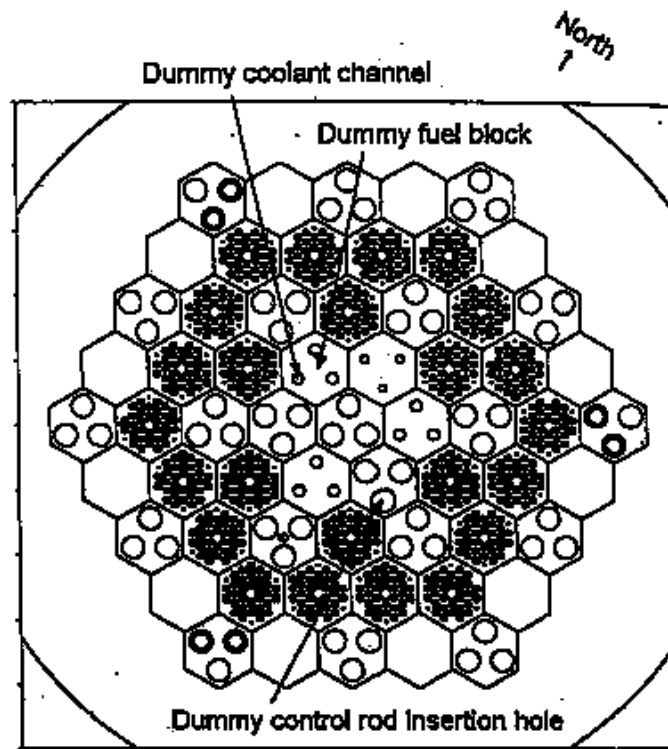
FIG. 2.26. Horizontal cross-section of 24 column core model.
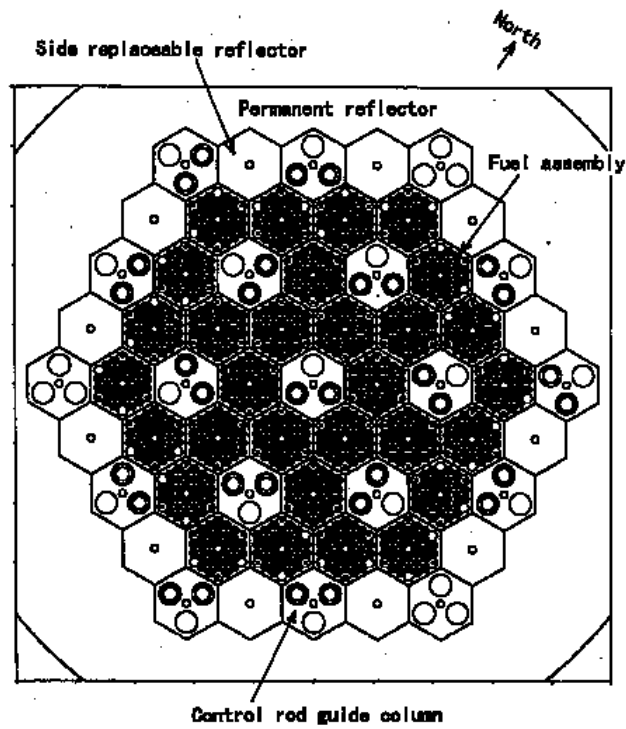
FIG.2.27. Horizontal cross-section of 30 column core model (fully-loaded core).
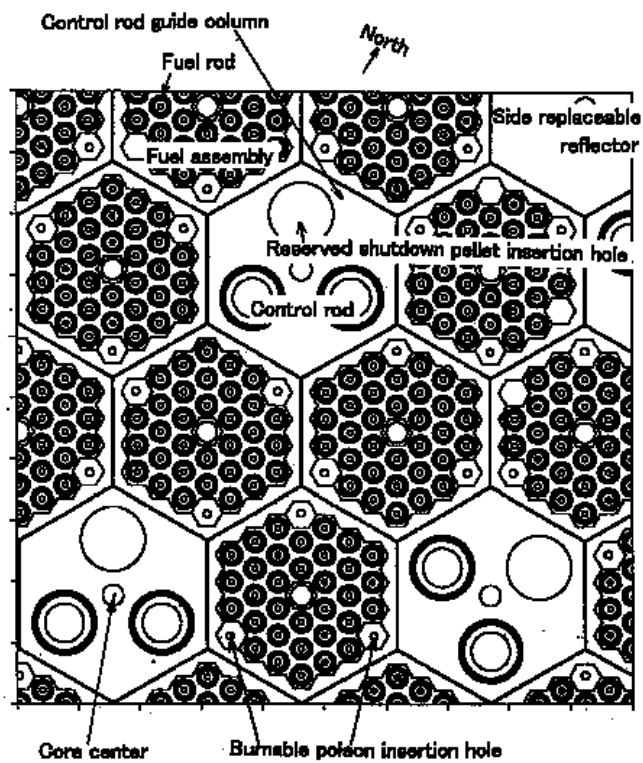
FIG: 2.28. Magnification of analytical model.
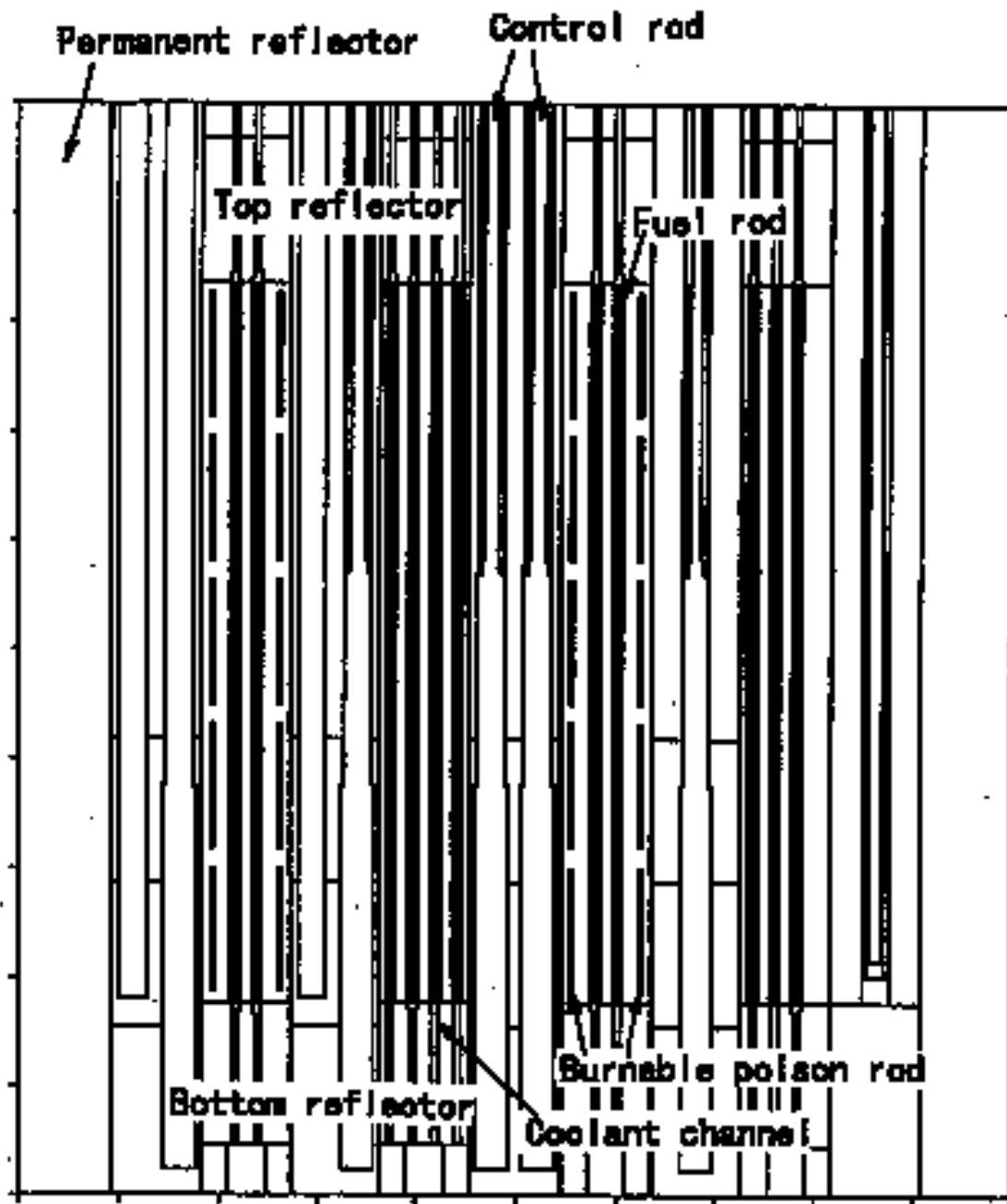
FIG. 2.29. Vertical cross-section of 30 column core model (fully loaded core).

Total amounts of material such as uranium, oxygen and carbon are conserved in the compact for each model. About 13,000 CFPs are distributed randomly in a fuel compact. The k_{eff} - calculations for fuel loading steps were carried out in the condition where CRs were fully withdrawn from the core and reflectors. The vertical cross-sectional model of core is shown in Figure 2.29.

The vertical length of each component is precisely modeled. The BP is separated in upper and lower parts in a fuel block. Graphite disks are inserted between upper and lower parts of BPs. The lengths of BP part and Graphite disk part are 40 and 10 cm, respectively.

2.2.1.2. Results of HTTR-FC calculation

The number of fuel columns are evaluated for the first criticality, when the fuels columns are charged from the outer region of the core. They are loaded clockwise, one by one. A small excess reactivity at the first criticality is also evaluated. For phase 2, the HTTR-FC is re-calculated considering the following effects:
1) Air in void of graphite
2) Revised impurity contents in dummy block
3) Aluminum in the temporary neutron detector holders.

The change in the effective multiplication factor at fuel loading was calculated. The R2 CRs remain in the top region of the core. The CR model was CR-block model. Fourteen kinds of microscopic cross section set of fuel were used for the calculations considering the kinds of ^{235}U enrichment and boron concentration in the burnable absorber rod.

HTTR-FC by diffusion calculation

The change in effective multiplication factor at fuel loading is shown in Table 2-4 and Figure 2.30. The number of fuel column at the first criticality is 17 columns and the excess reactivity at the first criticality is about 0.05%Δk/k.

Table 2-4. Calculation results of HTTR-FC

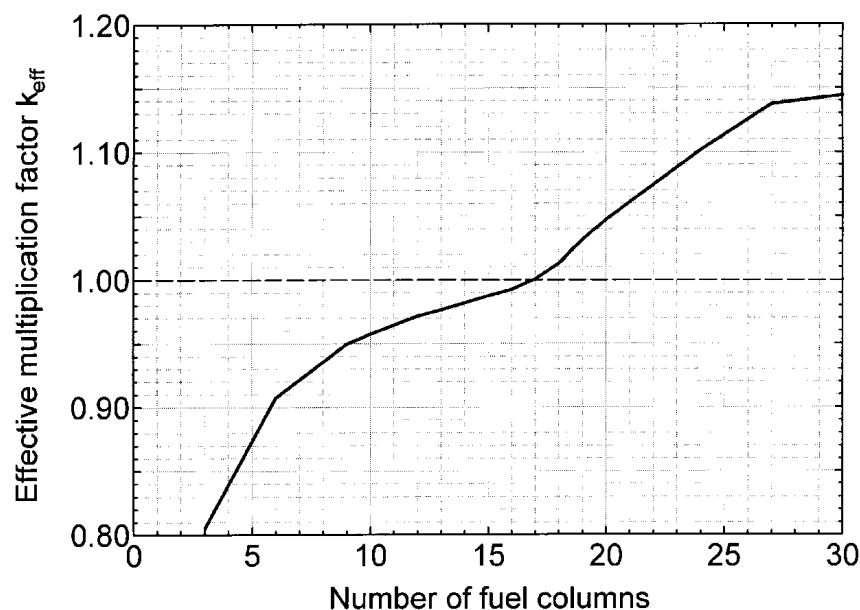| No. of fuel column	k_{eff} [-]	Excess reactivity [%Δk/k]
16	0.9921520	-0.79
17	1.0005451	0.05

FIG. 2.30. Change in k_{eff} at fuel loading.

HTTR-FC by Monte Carlo

The change in effective multiplication factors and excess reactivitys are given in Figure 2.31 and Table 2-5. The CFP's heterogeneity effect evaluated with the collision probability theory was 0.012 Δk for the HTTR fuel. This effect was added to the calculated k_{eff} - values for the corrected-homo. Model. The heterogeneity effect of CFP was evaluated also from difference in keff of the Homo- and Hetero- models. The results are given in Table 2-6. Six pairs of control rods in side reflector can not be withdrawn form the top reflector perfectly, because a sufficient negative reactivity addition rate must be supplied for reactor scrams. The CR insertion was simulated in the calculation. The fuel number for the first criticality is estimated for 18 fuel columns (Hetero. model).

Table 2-5. Calculated k_{eff} and excess reactivity to loaded fuel columns

Fuel columns	Heterogeneous model		Homogeneous model	
	k_{eff}*	ρ_{ex}**	k_{eff}	ρ_{ex}
12	0.959596 ± 0.00051	-4.21	–	–
14	0.97429 ± 0.00056	-2.64	–	–
16	0.98461 ± 0.00055	-1.56	0.98052 ± 0.00054	-1.99
17	0.99506 ± 0.00052	-0.50	–	–
18	1.00609 ± 0.00047	0.61	1.00266 ± 0.00050	0.27
19	1.01626 ± 0.00046	1.60	–	–
21	1.04827 ± 0.00047	4.60	–	–
24	1.09968 ± 0.00047	9.06	1.09350 ± 0.00039	8.55
27	1.13399 ± 0.00044	11.82	–	–
30	1.14278 ± 0.00039	12.49	1.13258 ± 0.00045	11.71

*: k_{eff} is Effective multiplication factor. The variation shows the statistical error.

**: ρ_{ex} is Excess reactivity in %$\Delta k/k$.

Table 2-6. Heterogeneity effects of CFP

Fuel columns	ρ_{ex}(heterogeneous)-ρ_{ex}(homogeneous) (%$\Delta k/k$)
16	0.43
18	0.34
24	0.51
30	0.78
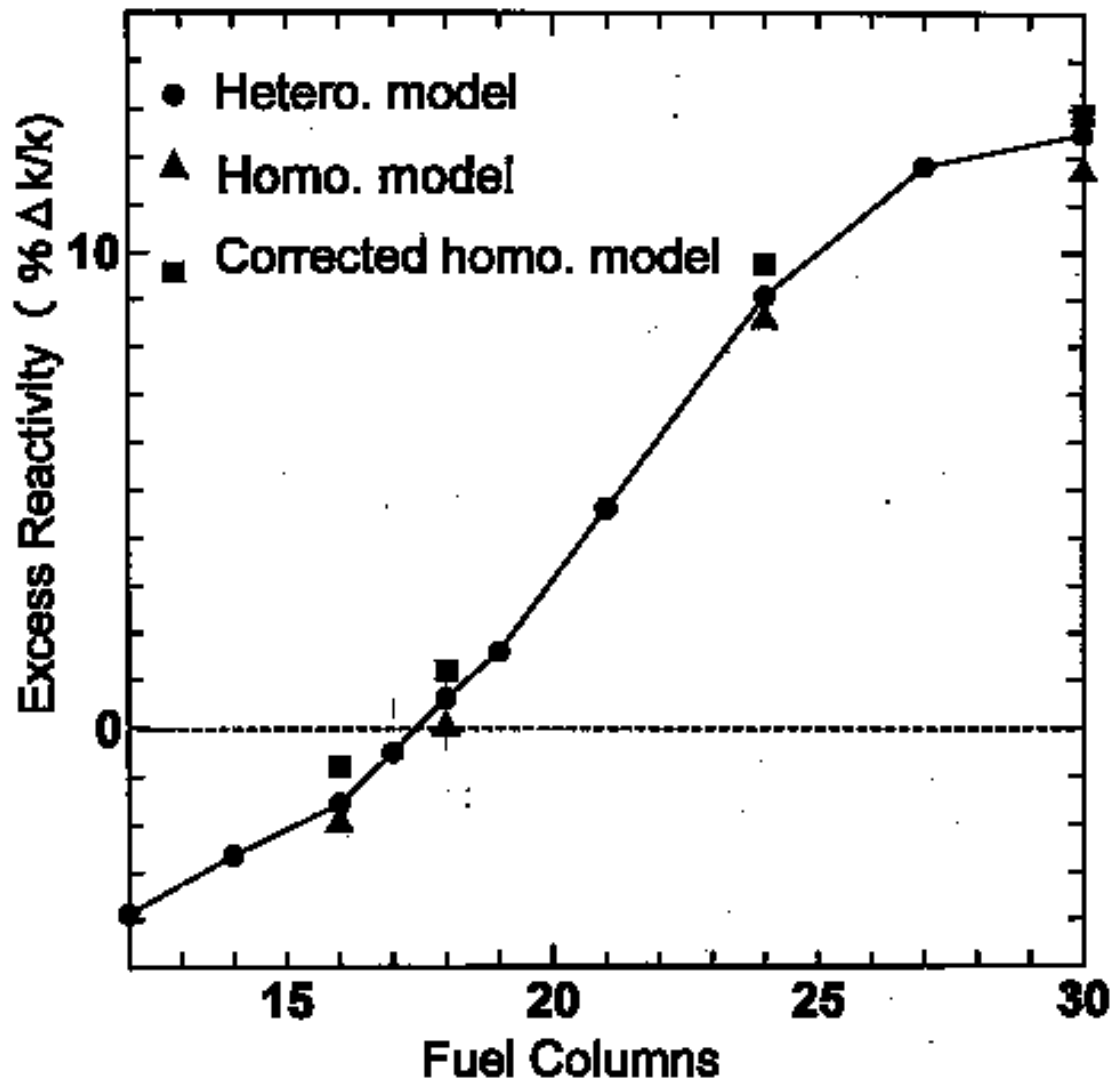
FIG.2.31. Change in excess reactivity with fuel loading.

The experimental results for HTTR-FC were as follows: The fuel loading was started from the core periphery to core center so that the annular core will be constructed on the way to the full core, to obtain the nuclear characteristics. Fuel blocks are loaded clockwise in the core periphery as shown in Figure 2.25. The fuel loading was carried out by replacing dummy blocks with fuel blocks. The annular core was made when the core was loaded with fuel columns from 18 to 24. Inverse multiplication factors (1/M) were evaluated at 0, 6, 9, 12, 15, 16, 17 and 18 fuel column-loaded cores to predict the first criticality. The first criticality was achieved at the 19 fuel-column-loaded core.

2.2.1.3. HTTR-CR

The control rod insertion depths are evaluated at the critical condition for the following three cases:

1)   18 columns (thin annular core)
2)   24 columns (thick annular core)
3)   30 columns (fully loaded core)

All control rod insertion levels are adjusted on the same level except three pairs of control rods in the most outer region in the side reflectors. These three pairs of control rods are fully withdrawn for the calculation. (The fully withdrawn position of CRs (C, R1, R3) are over the top of the replaceable reflector. The "fully withdrawn" position of the six control rods of R2 is 725 mm below the top of the 1st replaceable reflector block.)

HTTR-CR by diffusion calculation

The control rod position at criticality for 18-columns loaded core, 24 columns-loaded core and fully loaded core are shown in Table 2-7.

Table 2-7. Calculation results of HTTR-CR

No. of fuel column	Control rod position at criticality [mm]
18	3035
24	2055
30	1665

HTTR-CR by Monte Carlo calculation

The analytical method for HTTR-CR is as same as that for HTTR-FC. The results are as follows:

Model and column number	CR position (mm)
18 (Corrected homo. model)	2810
24 (Corrected homo model)	2080
30 (Hetero model)	1800

The experimental results for HTTR-CR were as follows: The reactor was made critical in every fuel loading step after the first criticality to the full core. The steps were 21, 24, 27 and 30 columns. The CR position at every critical condition was measured to evaluate calculation accuracy. The CRs are inserted from top to bottom. The tops of C-, R1- and R2-CRs were kept the same level at critical conditions. The R3-CRs were fully withdrawn. The CR position is defined as distance from the boundary between the fuel region and the bottom reflector. The change in the critical CR position is given in the following Table 2-8:

Table 2-8. Measured critical control rod positions

Fuel column	21	24	27	30
Rod position(mm)*	2646±5	2215±5	1899±5	1775±5

*Distance from the boundary between fuel region and the bottom reflector. Sinking of CR driving mechanism (14mm) was considered.

The excess reactivity is evaluated for the three cases mentioned in HTTR-CR. The room temperature of 300K is assumed as the moderator and fuel temperatures for the benchmark problem. One atmospheric pressure of helium is used as the primary coolant condition.

HTTR-EX by diffusion calculation

The excess reactivity at 18-columns loaded core, 24 columns-loaded core and fully loaded core are shown in Table 2-9.

Table 2-9. Calculation results of HTTR-EX

No. of fuel column	k_{eff} [-]	Excess reactivity [%Δk/k]
18	1.0126343	1.2
24	1.1014290	9.2
30	1.1442246	12.6

HTTR-EX by Monte Carlo calculation

The analytical method for HTTR-EX is as same as that for HTTR-FC. The results are as follows:

Model and column number	Excess reactivity (%Δk/k)
18 (Hetero. model)	0.61
24 (Hetero. model)	9.06
30 (Hetero model)	12.5

The experimental results are as follows: Fuel addition method was applied for the excess reactivity measurement. The increment in excess reactivity was measured by IK method at 21, 24, 27, and 30 column-loaded core. The measurement was affected by the negative shadowing effect. The measured increments in excess reactivity were revised with following relation to correct the shadowing effect. The excess reactivity for each core are given in Table 2-10.

$$\rho_{ex} = \sum \Delta\rho_{ex}$$

$$\Delta\rho_{ex} = \Delta\rho_{ikm} \cdot R$$

$$R = \frac{\Delta\rho_{excal}}{\Delta\rho_{ikcal}}$$

ρ_{ex} :Excess reactivity (%Δk/k)

$\Delta\rho_{ex}$:Increment in excess reactivity (%Δk/k)

$\Delta\rho_{ikm}$:Increment in excess reactivity measured with IK method (%Δk/k)

$\Delta\rho_{excal}$: Increment in excess reactivity calculated after definition.

All control rods are fully withdrawn from the critical rod position (%Δk/k)

$\Delta\rho_{ikcal}$: Increment in excess reactivity calculated after IK measurement procedure (%Δk/k)

R: Revising factor

Table 2-10. Excess reactivity

Fuel columns	ρ_{ikm} (%Δk/k)	$\Delta\rho_{ikm}$ (%Δk/k)	R	$\Delta\rho_{ex}$ (%Δk/k)	ρ_{ex} (%Δk/k)
21	2.3 ±0 .23	2.3 ± 0.23	1.69 ± 0.12	4.0 ± 1.1	4.0 ± 1.1
24	5.0 ± 0.50	2.7 ± 0.27	1.40 ± 0.11	3.7 ± 1.0	7.7 ± 2.1
27	7.4 ± 0.74	2.4 ± 0.24	1.26 ± 0.15	3.0 ± 0.9	10.7 ± 3.0
30	8.5 ± 0.85	1.1 ± 0.11	1.19 ± 0.04	1.3 ± 0.3	12.0 ± 3.3

(β_{eff}=0.0065)

2.2.1.5. HTTR-SC

The core condition is as follows:

-Fully-loaded core (30 column fuel core)
-Fresh fuel core

The following two cases are investigated the HTTR-SC:

1) Scram reactivity of reflector CRs (R2 and R3)

The Scram reactivity of the reflector CRs is evaluated for the fully-loaded core as follows.

$$\rho_R = \frac{k_{Crit.} - k_{RCR-in}}{k_{Crit.} \cdot k_{RCR-in}} \cdot$$

Where:

ρ_R: Scram reactivity of reflector CRs (Δk/k)

$k_{Crit.}$: Effective multiplication factor at critical CR position

k_{RCR-in}: Effective multiplication factor at CR position after scram

The effective multiplication factors is calculated at the critical CR positions and the CR positions after scram. The CR positions are given in Table 2-11. The reflector CRs are fully inserted after scram. The positions of the in-core CRs are not changed. The temperature for core and reflector is 300K.

Table 2-11. Control rod position before and after scram of reflector CRs*

CR Group	Critical position (mm)	Position after scram (mm)	Remark
C	1775	1775	Not changed
R1	1775	1775	Not changed
R2	1775	-55**	
R3	Full out	-55	

*:Case (T4-3005), No neutron source
**:Control rods are inserted slightly into the top of the bottom reflector

2) Scram reactivity of all control rods (C, R1,R2 and R3):

The scram reactivity of all CRs is evaluated from the effective multiplication factors as follows:

$$\rho_A = \frac{k_{Crit.} - k_{ACR-in}}{k_{Crit.} \cdot k_{ACR-in}} \cdot$$

Where:

$\rho_{A:}$ Scram reactivity of all CRs ($\Delta k/k$)

$k_{Crit.}$: Effective multiplication factor at critical CR position

k_{ACR-in}: Effective multiplication factor at CR position after scram

The effective multiplication factors is calculated at the critical CR positions and the CR positions after scram. The CR positions are given in Table 2-12. The all CRs are fully inserted after scram. The temperature for core and reflector is 300K.

Table 2-12. Control rod positions before and after scram of reflector and in-core CRs*

CR Group	Critical positions (mm)	Positions after scram (mm)	Remark
C	1775	-55**	
R1	1775	-55	
R2	1775	-55	
R3	Full out	-55	

*:Case (T4-3005), No neutron source

**:Control rods are inserted slightly into the top of the bottom reflector

.

The measured scram reactivity was 0.46$\Delta k/k$

HTTR-SC by diffusion calculation

The scram reactivity should be calculated from the criticality condition with CR position at 1789mm. In the calculation model, it is difficult to set the CR position at 1789mm because the vertical mesh division is 145mm. The scram reactivity was evaluated by interpolating the results of 1740mm and 2030mm.

The calculated results of HTTR-SC by the CR-block model and the CR-hex model are shown in Table 2-13. The results of CR-block model was smaller than that of the CR-hex model. In the CR-hex model, reflector CRs are nearer to the core than in the CR-block model. Therefore, scram reactivity becomes larger.

The comparison of measured and calculated value of the scram reactivity are shown in Table 2-14. For the results of all CRs, the error of CR-block model and CR-hex model are about –7% and –4%, respectively. The difference of both models is small. Both model show good agreement with measured results.

For the results of reflector CRs, the error of CR-block model and CR-hex model are about –31% and –26%, respectively. The CR-hex model shows less error than CR-block mode, but still shows more than 20% of error. The calculation model should be further revision.

Table 2-13. Calculated results of HTTR-SC

(1)Scram reactivity of reflector CRs(R2 and R3)

CR model		CR-block model		CR-hex model	
CR position before scram [mm]		1740	2030	1740	2030
k_{eff}	Before scram	1.0093164	1.0418115	1.0084132	1.0409116
	R2, R3 full in (0mm)	0.9311435	0.9599020	0.9247989	0.9534538
Scram reactivity [%Δk/k]		8.32	8.19	8.97	8.81
Scram reactivity from 1789 mm [%Δk/k]		8.30		8.94	

(2) Scram reactivity of all CRs

CR model		CR-block model		CR-hex model	
CR position before scram [mm]		1740	2030	1740	2030
k_{eff}	Before scram	1.0093164	1.0418115	1.0084132	1.0409116
	All CRs full in (0mm)	0.7069916		0.6980522	
Scram reactivity [%Δk/k]		42.37	45.46	44.09	47.19
Scram reactivity from 1789 mm [%Δk/k]		42.9		44.6	

Table 2-14. Comparison to the measured value

(1) CR-block model

	Scram reactivity [%Δk/k]		Error [%]
	Measured (E)	Calculated (C)	C/E-1
Reflector CRs	12.1	8.30	-31.4
All CRs	46.3	42.9	-7.3

(2) CR-hex model

	Scram reactivity [%Δk/k]		Error [%]
	Measured (E)	Calculated (C)	C/E-1
Reflector CRs	12.1	8.94	-26.1.
All CRs	46.3	44.6	-3.7

HTTR-SC by Monte Carlo Calculation

The analytical method for HTTR-SC is the same as that for HTTR-FC. The results are given in Table 2-15:

A two-step scram will be performed in the HTTR to prohibit the high temperature exposure of the in-core CRs in full power operation. The in-core CRs are inserted when the core temperature becomes less than 750°C or 2400 seconds passes after insertion of reflector CRs. The simulation of the two-steps scram was conducted in startup core physics. The in-core CRs were inserted in the time delay of 20 seconds after insertion of the reflector CRs. The time delay was determined so that the neutron density signal from the CIC did not become too small for reactivity measurement. The reactivity was measured continuously by the IK method. Digital computer was used to evaluate the reactivity from change in neutron density signal.

Table 2-15. Scram reactivity of control rods

Items	Scram Reactivity
1) Scram reactivity of reflector CRs k_{crit} k_{RCR-in} $\rho_R(\Delta k/k)$	0.99908 ± 0.00045 0.91222 ± 0.00058 0.0953 ± 0.0007
2) Scram reactivity of all CRs k_{crit} k_{ACR-in} $\rho_A(\Delta k/k)$	0.99908 ±0.00045 0.68873 ± 0.00064 0.4510 ± 0.0008

Table 2-16. CR position at two step scram*

R	CR position [mm]		
	Before scram	First step scram	Second step scram
1	1775±5	1775±5	-55±5**
1	1775±5	1775±5	-55±5**
2	1775±5	-55±5**	-55±5**
3	Full out	-55±5**	-55±5**

*:Sinking of CR driving mechanism was considered
**: Control rods are inserted slightly below 0 mm at scram.

Table 2-17. Scram reactivity at two-step scram

Scram	Measured scram reactivity [$\Delta k/k$]	Error C/E-1 (%)
Reflector CRs	0.12±0.012	-17
All CRs	0.46±0.046	10

(β_{eff}=0.007)

2.2.1.6. HTTR-TC

Isothermal temperature coefficients for fully-loaded core are evaluated from the effective multiplication factors by the following relation:

$$\rho_n = \frac{k_{n+1} - k_n}{k_{n+1} \cdot k_n} \cdot \frac{1}{(T_{n+1} - T_n)}$$

Where: ρ_n: Temperature coefficient between T_n and T_{n+1} ($\Delta k/k/K$)
T_n: Core temperature at nth measurement (K)
T_{n+1}: Core temperature at n+1th measurement (K)
k_n: Effective multiplication factor at T_n
k_{n+1}: Effective multiplication factor at T_{n+1}

The critical control rod positions are changed with temperature elevation in the real reactor operation. However, the control rod position should not be changed in calculation to obtain the reactivity difference. The critical positions given in Table 2-18 as CR position are to be used for calculation of effective multiplication factors. The effective multiplication factors are calculated for the following temperatures:

280, 300, 340, 380, 420, 460, 480 (K)

Temperature coefficient for following temperatures are evaluated from the effective temperature coefficients with the above relation.

290   320 360 400 440   470   (K)

Additionally, the critical control rod positions are evaluated at temperature of 480K. The insertion depths of C, R1 and R2 are at the same level. All of R3 is fully withdrawn.

Table 2-18. Control rod position for temperature coefficient evaluation

CR Group	Critical positions* (mm)
C	1777
R1	1777
R2	1777
R3	Full out

*These values are obtained from the critical positions (T4-3005) by correcting with lifting effect of CR driving mechanism (about -14mm) and temperature effect from 25 to 27 (about 2mm).

HTTR-TC by diffusion calculation

The isothermal temperature coefficients were evaluated using the CR-block model. It was impossible to calculate isothermal temperature coefficients directly due to mesh division of the core calculation model. Therefore, the isothermal temperature coefficients at 1776mm were evaluated by interpolating the results at 1740mm and 2030mm. In the calculation, four kinds of microscopic cross section set were used. Each layer of fuel block use same microscopic cross section set. Air in void of graphite and Al of temporary neutron detector holders were not considered.

The calculation results are shown in Table 2-19 and Figure 2.32. Due to our convenience, calculated temperature points are not same to the problem description. Therefore, isothermal temperature coefficients at the temperature point described in the problem definition are evaluated by the calculated results. The results are provided in Table 2-19. The average temperature coefficient within the temperature range is about $-1.3 \times 10^{-4} \Delta k/k/K$.

The criticality CR position at 480K was evaluated by the results already shown in Table 2-19. The results are shown in Table 2-20.

Table 2-19: Calculated results of HTTR-TC (by CR-block model)

(1) Effective multiplication factors

CR position [mm]		1740	2030
Temperature [K]	300	1.0169601	1.0497657
	320	1.0145556	1.0474498
	340	1.0119939	1.0449780
	380	1.0065323	1.0396969
	420	1.0011004	1.0344445
	460	0.9957035	1.0292383
	480	0.9901534	1.0238264

(2) Isothermal temperature coefficients

CR position [mm]		Temperature coefficients [$\Delta k/k/K$]		
		1740	2030	1776*
Temperature [K]	310	-1.16596×10^{-4}	-1.05309×10^{-4}	-1.15×10^{-4}
	330	-1.24751×10^{-4}	-1.12913×10^{-4}	-1.23×10^{-4}
	360	-1.34046×10^{-4}	-1.21521×10^{-4}	-1.32×10^{-4}
	400	-1.34768×10^{-4}	-1.22091×10^{-4}	-1.33×10^{-4}
	440	-1.35356×10^{-4}	-1.22247×10^{-4}	-1.34×10^{-4}
	480	-1.40737×10^{-4}	-1.28395×10^{-4}	-1.39×10^{-4}

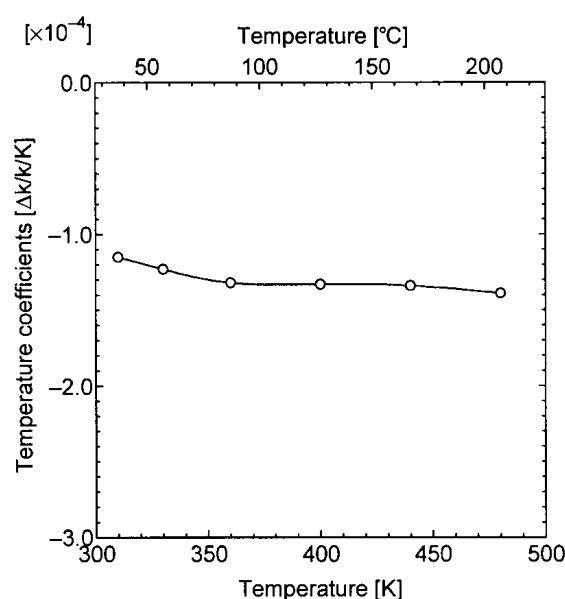* : Interpolated by the results of 1740mm and 2030mm.

FIG. 2.32. Calculated results of temperature coefficients (CR position: 1776mm).

Table 2-20. Criticality CR position at 480K

	CR position [mm]
C, R1, R2	1825
R3	4060

HTTR-TC by Monte Carlo Calculation

The analytical method for HTTR-TC is as same as that for HTTR-FC. The results are given in Table 2-21:

Table 2-21. Temperature coefficients of HTTR core

Items	Temperature coefficients
Effective multiplication factor for different temperatures	
k_{300}	0.99762 ± 0.00054
k_{340}	0.99273 ± 0.00051
k_{380}	0.98621 ± 0.00050
k_{420}	0.97990 ± 0.00050
k_{460}	0.97393 ± 0.00057
k_{480}	0.97221 ± 0.00051
Temperature coefficients ($\Delta k/k/K$)	
ρ_{320}	-1.23×10^{-4}
ρ_{360}	-1.66×10^{-4}
ρ_{400}	-1.63×10^{-4}
ρ_{440}	-1.56×10^{-4}
ρ_{470}	-0.91×10^{-4}
Critical control rod position at 480K	
C, R1, and R2 (mm)	1789
R3	Full out

The control rod positions at critical condition were measured for three different core temperatures (T). The core temperature was obtained by averaging core-inlet and -outlet coolant temperatures. The control rod positions and core temperatures are summarized in Table 2-22:

Table 2-22.　Control rod positions and core temperature

CR group	CR position (mm)		
	T=22.7	T=122.0	T=144.9
C	1751*±5	1873±5	1903±5
R1	1751*±5	1873±5	1903±5
R2	1751*±5	1873±5	1903±5
R3	Full out	Full out	Full out

*:Sinking of CR driving mechanism (14mm) was considered.
**After taking out temporary detectors from core

The temperature effect was evaluated from CR positions, using calculated control rod worth curve. The isothermal temperature coefficients are given in the following Table:

Table 2-23. Isothermal temperature coefficient

Temperature range (　)	Iso.temp.coeff. ($\Delta k/k/T$)
22.7~122.0	-1.34E-4*
122.0~144.9	-1.42E-4*

2.2.2. France

2.2.2.1 General analysis method and model description

Codes and calculation scheme

The French reactor physics code system SAPHYR has been used in the following HTTR calculations. SAPHYR gathers several codes developed at CEA like APOLLO2 [2-23] (transport) based on a database produced with THEMIS/NJOY, CRONOS2 [2-24] (diffusion-transport), FLICA4 (3D- thermal hydraulics), ..., which are interconnected. This code system, initially dedicated to PWR calculations and research & development purposes, seems to be well adapted for the assessment of the HTGR performances and characteristics. Finally, the Monte-Carlo code TRIPOLI4 [2-25] has also been used throughout the study.

All the HTTR problems proposed in reference [2-21] have been treated considering two calculation methods: one based on a Transport – Diffusion calculation scheme and a second one based on a Transport – Monte-Carlo calculation scheme. Figure 2.33 illustrates the general procedure. The standard 172-groups or point-wise cross sections library issued mainly from JEF-2.2 are used for the calculations.
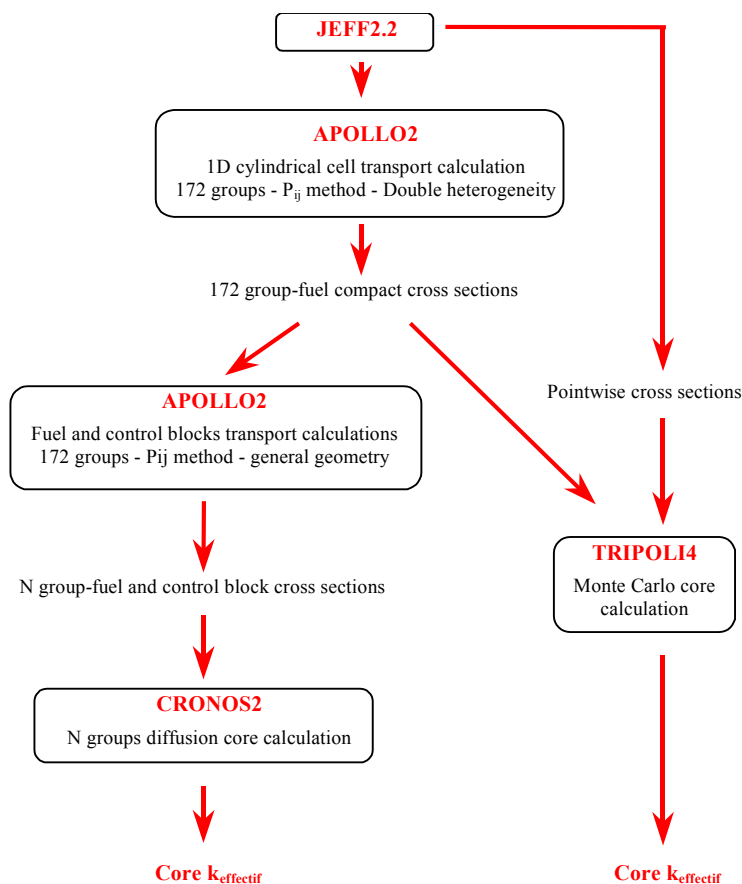

FIG. 2.33. Description of both calculation schemes.

It is noteworthy that as far as the Transport-Diffusion calculations are concerned, two different approaches have been used in terms of core modelling. The first one, a rough model with strong hypotheses (homogenised fuel block, no streaming effect, …) led to preliminary predictions of the HTTR-FC, EX and CR problems (**first results**). Then, enhancements to

improve the modelisation have been identified, assessed and finally implemented in course of revised calculations using new benchmark data proposed in [2-27]. This has been done for all the HTTR benchmarks (FC, EX, CR, SC and TC) and constitutes the second prediction (**final results**).

Cylindrical calculation of the fuel compact

Knowing that the stochastic geometries calculations (coated fuel particles - CFP - randomly distributed in the fuel compact) is not available in the Monte-Carlo code TRIPOLI4, a 1D-cell calculation has been performed as a first step. It takes into account a precise spherical description of the particles with all their coatings which themselves fill the annular part of the cylindrical geometry of the fuel compact (Figure 3.34) with a packing density around 30 %. The self-shielding of the uranium is calculated during this calculation stage. A collision probability method is used to solve the transport equation with 172 energy groups. The critical buckling search allows taking into account the neutron leakage by the addition of a homogeneous leakage term in the form of $DB^2\Phi$. The extra region of the cylindrical cell is representative of the other fuel cells disposed around with the triangular pitch of the fuel rods in the assembly.
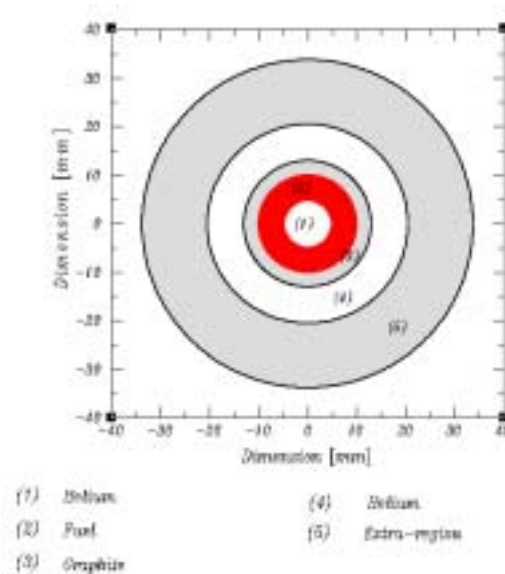

FIG. 2.34. Cylindrical Fuel Cell Model.

This first stage provides **fuel compact-homogenized 172-group cross sections** for Monte-Carlo core calculations (TRIPOLI4). Therefore, in the core calculations performed by TRIPOLI4, point-wise cross sections are used everywhere in the core
except in the fuel rod region where the multigroup cross sections have been generated with APOLLO2.

Although that the CFP might be directly considered in the 2D fuel element calculations, as for TRIPOLI4 the same **fuel compact averaged 172-group cross sections** have been used in the 2D transport model described hereafter. This avoids calculating the self-shielding in the 2D configuration and results in a large saving of CPU time without making severe assumption.

Fuel block 2D-calculations

This stage must lead to an averaged flux weighted library of the different fuel blocks existing in the core. This library of n-group-constants is directly read during the core diffusion calculations. The energy structures (n = 2 to 20) are given in annexe. A 172 group-collision probability method is used in the 2D-fuel block geometry (Figure 2.35). The fuel handling hole zone is modelled by a lower graphite density. As far as the burnable poisons (BP) are concerned, the B_4C and graphite pellets are **axially homogenised** with the graphite matrix in order to reduce the number of calculations from 32 to 16 and to simplify the core calculations. The impact of this axial homogenisation is important and has been evaluated hereafter.
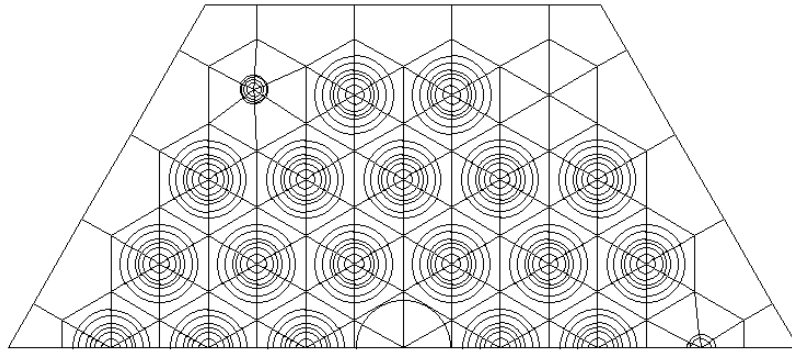
FIG. 2.35. 2D-fuel block geometry.

These 2D calculations were performed in infinite medium with a critical buckling search. A B1 homogeneous neutron leakage model has been retained as a first step. This led to **isotropic diffusion coefficients** and did not allow taking into account the streaming effect. The P_{ij} model gives a flux evaluation in each region depicted in Figure 2.35. An example of the power distribution in a fuel block is given in Figure 2.36 (the map is normalised to 100).

FIG. 2.36. Power Distribution in the f343320 fuel block.

The 2D-results of the fuel blocks in fundamental mode are gathered in the Table 2-24 below and an example of the average neutron flux obtained for the lower and the higher enriched fuel blocks are given in Figure 2.37.
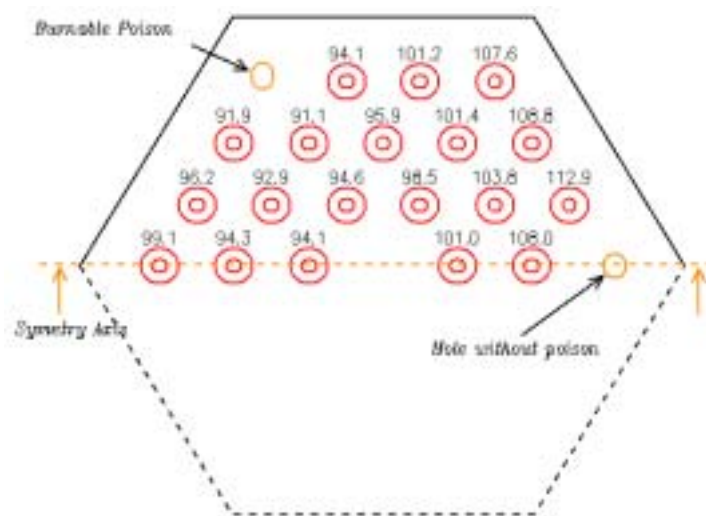
Table 2-24. 2D-Transport Calculations on the Fuel Blocks

Fuel Block	Enrichment [% masse]	Multiplication factor	Migration Area [cm^2]
f343320	3,4	1,10650	491,05
f393320	3,9	1,14991	487,14
f433120	4,3	1,18391	486,43
f483120	4,8	1,21366	481,82
f433325	4,3	1,15656	476,90
f523325	5,2	1,20380	470,53
f593125	5,9	1,24481	469,50
f633125	6,3	1,25798	468,43
f633325	6,3	1,24962	465,50
f723125	7,2	1,28937	463,70
f793125	7,9	1,30862	457,99
f673320	4,6	1,28423	467,60
f793320	7,9	1,31733	459,52
f943120	9,4	1,36335	458,81
f993120	9,9	1,37213	455,45
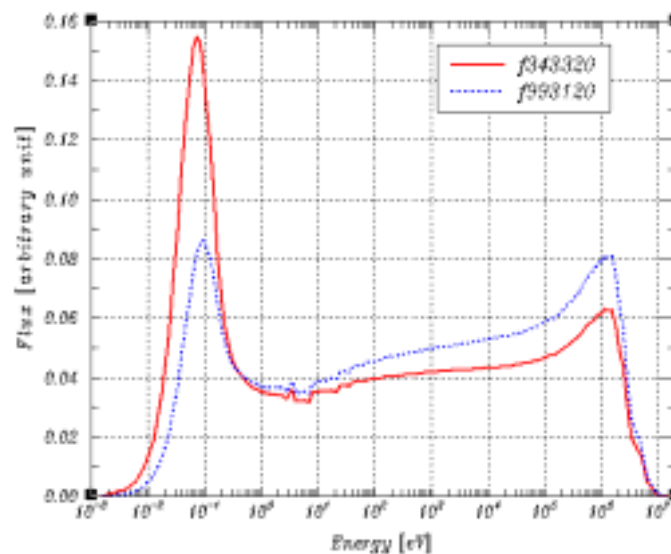
FIG. 2.37. Neutron Spectrum in the fuel block

Control blocks 2D-calculations

From the previous calculations, the average fluxes of the fuel blocks were used as a 172 group-neutron source placed at the periphery of the control blocks to generate the averaged weighted library needed for core diffusion calculation. A similar collision probability method has been used in the 2D-geometry shown in Figure 2.38 for the control blocks with and without the control rods inserted.

As for the fuel blocks, the n-group-constants have been created by spatial homogenisation on the overall control block geometry. Indeed, among the finite element meshes available in the CRONOS2 diffusion code, it was first impossible to take into account the position and the orientation of the fuel and control blocks by an heterogeneous geometric description of these elements. Moreover, no transport-diffusion equivalence factors have been considered for the control blocks when the control rods are inserted. The averaged neutron fluxes obtained in the control blocks are given in Figure 2.39.
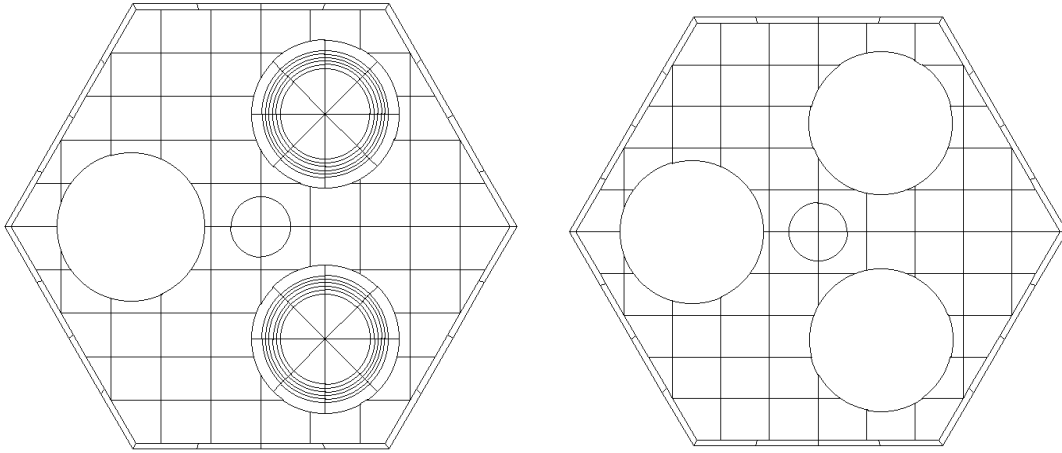

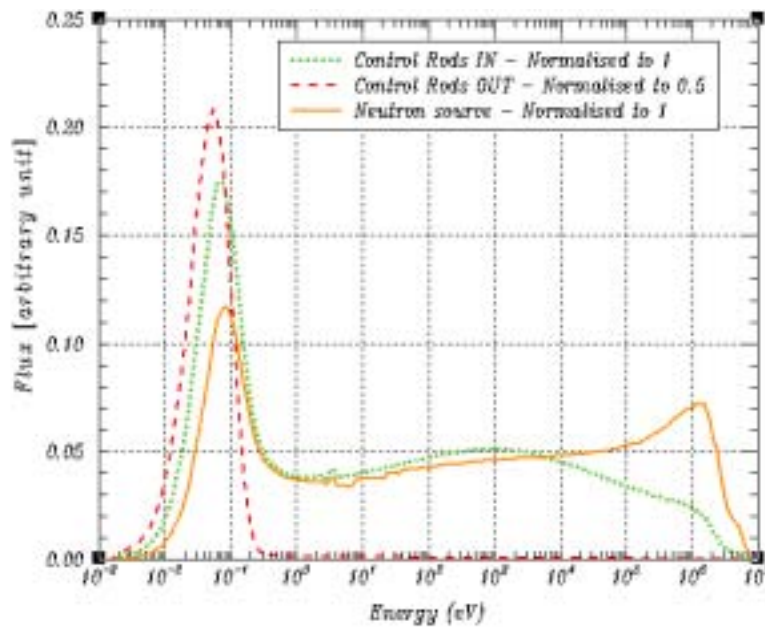*FIG. 2.38. 2D-Control Rod Blocks Geometry.*

FIG. 2.39. Neutron Spectrum in the Control Rod Blocks.

Reflector cross section generation

In the diffusion calculations, the n-group-cross sections of the replaceable reflector have been evaluated with similar methods to those described in the previous section where a neutron source is placed at the periphery of the blocks. As far as the permanent reflector region is concerned, the cross sections come from a 1D-cylindrical core transport calculation (in its fully loaded configuration) performed with the S_n method.

Core diffusion calculations

An hexagonal 3D-geometry has been used for the core description. Each fuel and control block is represented by a **hexagon with a homogeneous composition**. On this hexagonal mesh, the *finite element method* provides several polynomial approximations. In this case, a second order exact integration (standard parabolic Lagrange) has been adopted horizontally and leads to 19 flux values per mesh (equivalent to a 24 homogeneous meshes in finite difference method).
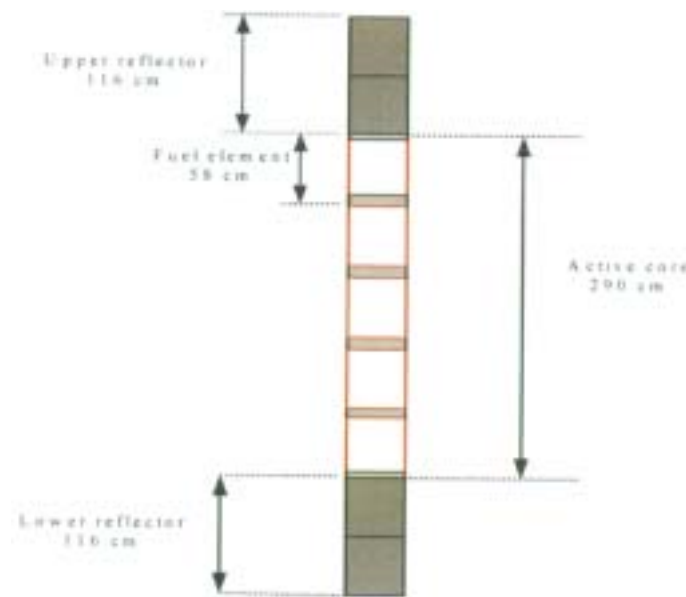
FIG. 2.40. Core Axial Description for CRONOS2 code.

Axially, a linear Lagrange method using Gauss Formula has been applied. Each fuel section (14 fuel compact stack) was divided into 6 meshes and the inter-space between fuel sections (3.4 cm of graphite) has been described explicitly per Fig. 2.40.

Transport-Monte Carlo core calculations

In spite of the homogenised fuel compacts, the core model developed here is a very detailed 3D-model of the HTTR with all components modelled explicitly. For these components, point-wise cross sections based on the JEF2.2 evaluation were used. The fuel compact was represented by a set of 172-group-constants coming from the previous transport calculation. It is noteworthy that in this case the burnable poison had the exact axial description in opposition to the homogeneous axial description used in the core diffusion calculations.
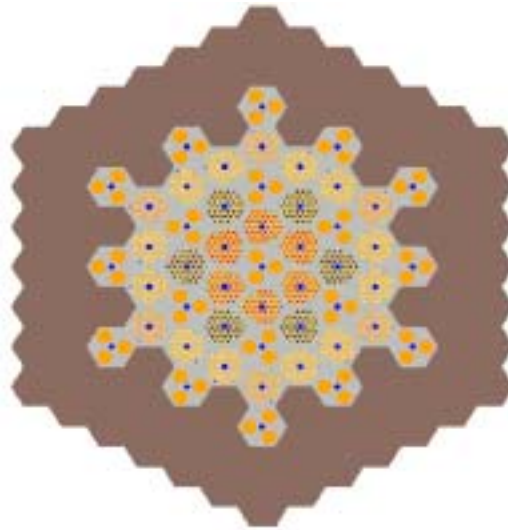
FIG. 2.41. Cross Section of Fully Loaded Core for TRIPOLI4 code.

Only the core configurations with 18 and 30 columns have been considered here. Figures 2.41 and 2.42 show a cross section view of the fully loaded core and detailed axial and radial cross section views of the control rod and fuel blocks.
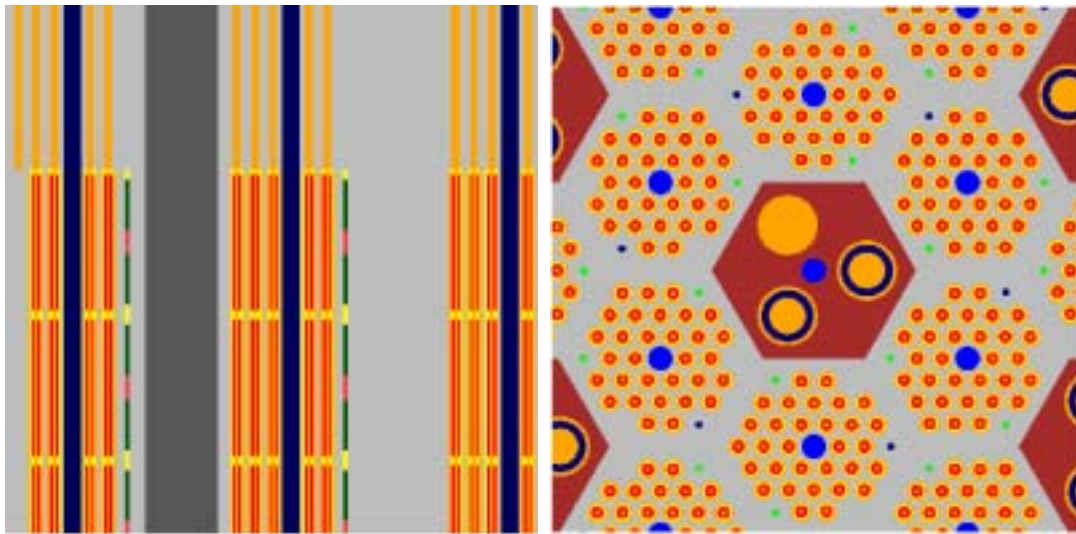
FIG. 2.42. Details of the Geometry used in the TRIPOLI4 code.

Synthesis of the assumption of the initial diffusion calculation scheme

The key factors in modelling the HTTR with the *transport-diffusion* calculation scheme are the following:
- the BP are axially homogenized
- the streaming effect is not taken into account everywhere in the core
- homogenised hexagons are considered without equivalent factor in order to respect the absorption rates of the BP and the control rod (CR) between both transport and diffusion calculation stages
- flux-weighted cross sections are used for the reflector
- CR insertion on the top reflector not taken into account

The following section provides the results taking into account these assumptions. Then, their impacts on the results have been assessed. They have been reconsidered in course of the revised calculations according to the results of these assessments.

2.2.2.2 First Results

HTTR-FC and EX

The calculations performed with the two different methods are gathered in Table 2-25. It is important to note that all the k_{eff}-values of the Table 2-25 are corrected with a Δk of - 0.004 in order to take into account the presence of the control not fully withdrawn to the top of the reflector and not considered in the core models.

All the preliminary calculations underestimated the number of fuel columns needed to achieve the first criticality (Diffusion calculations: **10 columns**; Monte-Carlo calculations: **17 fuel columns**). As it can be seen in Table 2-25, the discrepancy between the calculations and the experiment at least ranges from $\Delta k = 0.017$ to 0.058 at 18 fuel columns loading and from $\Delta k = 0.01$ to 0.033 at full core.

It is noteworthy that the observed discrepancies decrease with increasing number of fuel columns in the core. Due to the large experimental uncertainty at 30 fuel columns loading, the differences between the calculations and the experiment are within the error bar, whereas at the thin annular core assembly the discrepancies are significant. Two reasons for the latter circumstance can be proposed. The first would be that the two steps transport-diffusion calculation based on the fundamental mode assumption would be less and less appropriate as one goes toward the annular core configuration. The second would concern the level of the actual boron impurity in the dummy fuel blocks and of the residual air (instead of helium) in the graphite pores. As far as the latter is concerned, the impurities of some dummy fuel blocks have been re-measured by JAERI and revised data [2-27] have been recommended for the recalculation of the first criticality (HTTR-FC2).

Table 2-25. Experimental, Monte-Carlo and First Diffusion Results

	CRONOS2 3D - (first model) • *diffusion 8 gr* • *homog. Fuel block* • *no streaming* • *axially homog. BP*	Δk [%$\Delta k/k$]	TRIPOLI4 3D *Monte-Carlo* *172 gr & pointwise*	Δk [%$\Delta k/k$]	EXPERIMENT
30 col	**1.1698**	**14.5 %**	**1.14630 ± 0.0009**	**12.8 %**	**1.13630 ± (> 3.6%)**
28	1.1691	14.5 %			
26	1.1596	13.8 %			
24	**1.1399**	**12.3 %**			
22	1.1158	10.4 %			
20	1.0886	8.14 %			
19	1.0745	6.93 %			
18 col	**1.0580**	**5.48 %**	**1.01710 ± 0.0009**	**1.68 %**	**subcritical**
16	1.0383	3.69 %			
14	1.0284	2.76 %			
12	1.0184	1.81 %			
10	1.0044	0.44 %			
9	.9970	- 0.3 %			

In the course of the studies, the following reasons for the above mentioned discrepancies (especially for the simplified Transport – Diffusion calculation scheme) have been identified and quantified:

- A non-adequate treatment of the axial self-shielding in the BP rods,
- An underestimation of the neutron streaming (due to large channels of the CR blocks),
- The neglect of the detailed structure of the HTTR fuel block in the core calculations.

These main physical effects and their impacts on the core reactivity are briefly depicted in Figure 2.43 for the case of the annular core configuration. Similar tendencies can be observed for the full core configuration. Nevertheless, different absolute values (into bracket Figure 2.43) are obtained for the quantified physical effects due to the harder neutron spectrum in the fully loaded core. Indeed, the observed weight of the boron absorption in the BP is different in this case.
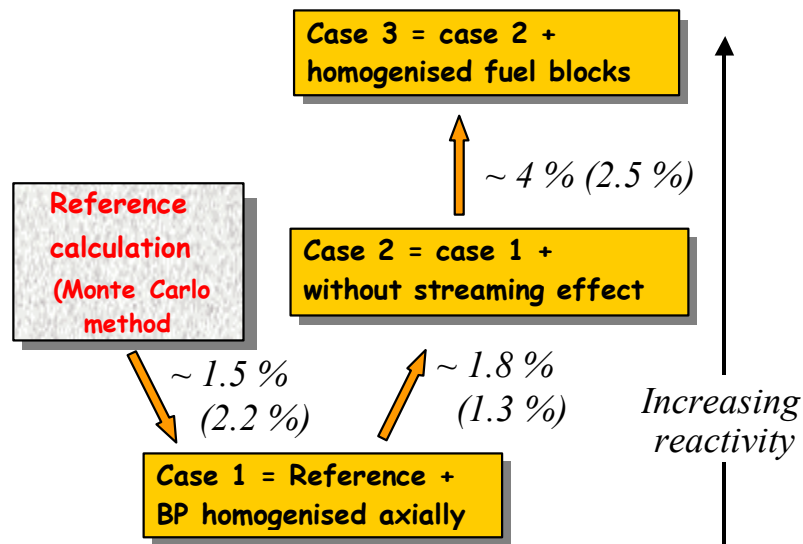
FIG. 2.43. Key factors in modelling and their impact on the reactivity for the 18 fuel columns core configuration (and full core).

For the thin annular core, starting from a best estimate calculation and neglecting the fact that the burnable poison was axially a succession of boron and graphite pellets leads to a predicted reactivity 1.5 % lower than considering the actual heterogeneous composition of these burnable poisons (3D Monte Carlo estimation). On the opposite, a core calculation that does not take into account the streaming effect will result in an increase of the reactivity of about 1.8 %. At this stage, it is interesting to note that by making two strong physical hypotheses a result not far from the best estimate calculation can be obtained. Finally, a discrepancy on the order of 4 % can be achieved if an insufficient description of the fuel block is used to model the high level of radial heterogeneity (2D Monte Carlo estimation).

Therefore, the HTTR-FC2 benchmark has been a good opportunity to implement the new enhanced methods coming from this analysis and to evaluate the progress considering the new data.

HTTR-CR

Transport-diffusion calculations

The control rod insertion depths have also been evaluated to achieve criticality in the three configurations recommended by the benchmark problem HTTR-CR (thin and thick annular core and fully loaded core). The results corresponding to the *transport-diffusion* method are given in the following Table 2-26 with the calculational approach illustrated in Figure 2.44.

Table 2-26. Critical Insertion Depths of the Control Rod

Configuration: Number of fuel columns	Control rod critical positions from the bottom of the active core
(thin annular core) 18	**251 cm**
(thick annular core) 24	**181 cm**
(fully loaded core) 30	**151 cm**
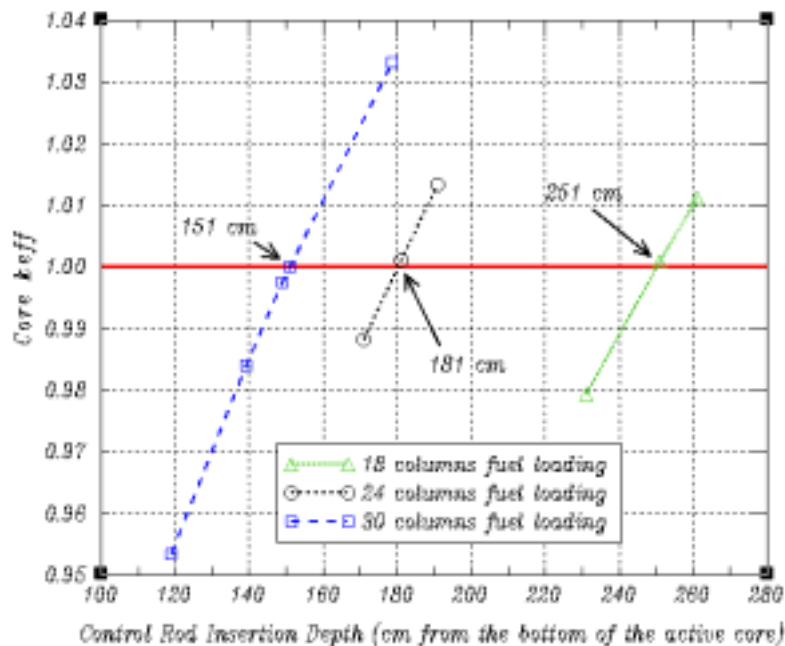
FIG. 2.44. *Effective multiplication factor as a function of the control rod position.*

It should be noted that the core model used here does not allow taking into account the orientation of the control rods in the homogeneous block description, as it is also the case for the position of the burnable poison in the fuel element.

Transport-Monte Carlo Core Calculations

As far as the second method is concerned (*transport-Monte Carlo*) it is noteworthy that, as recommended by the benchmark problem, the structural materials of the control rod have not been taken into account. Conversely, a detailed axial description of the control rods has been done as depicted in Figure 2.45.
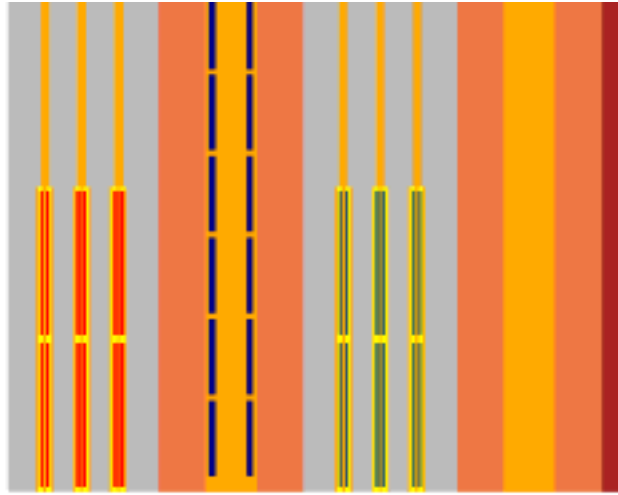
FIG. 2.45. Axial Cross Section View of the Inserted Control Rods.

The calculations aimed to tentatively evaluate the critical insertion depth of the control rod in the fully loaded core configuration have been performed. Two control rod insertion depths have been considered. The first one *-178.7 cm-* is the experimental value and the second one *-170 cm-* comes from an estimation of the control rod efficiency obtained in the diffusion calculations. The results are given in the Table 2-27 below:

Table 2-27. Reactivity for Two Control Rod Positions (Full Core)

Configuration: Number of fuel columns	*Control rod position from the bottom of the active core*	k_{eff}
(fully loaded core) 30	**178.7 cm**	**1.00850±0.0009**
(fully loaded core) 30	**170.0 cm**	**0.99840±0.0009**

From the results above, the critical rod position can be evaluated to **171 cm**. As a conclusion, one can note that, compared with the Monte Carlo, the control rod worth is overestimated with the diffusion method (without utilizing equivalence factor).

2.2.2.3 Modification to Model and Assessment of Improvements

 New finite elements in the core diffusion model

New finite elements recently implemented in CRONOS-2 have been used. They allow taking into account the exact position of the burnable poison in the fuel blocks and the fuel element orientation in the core.

Indeed, from the 2D transport calculations illustrated on the Figure 2.34, the fuel element was initially homogenised in one hexagonal finite element. Then, with the help of the new available finite elements, two different meshes were considered to describe the fuel elements with 24 radial meshes: 24 equilateral triangles (type I) or the cutting out depicted in Figure 2.46 (type II). Only the last one has been kept in the final model because of the fact that it is the only one that allows homogenising the poison with its associated graphite without homogenising partially the fuel compacts. Therefore, the fuel element structure is described by using three different mediums and the flux is calculated for each point described in Figure 2.46 (61 points for the hexagonal element).

Fuel element geometry

Fuel element description
in transport calculations (APOLLO2)

Fuel element description
in diffusion calculations (CRONOS2)
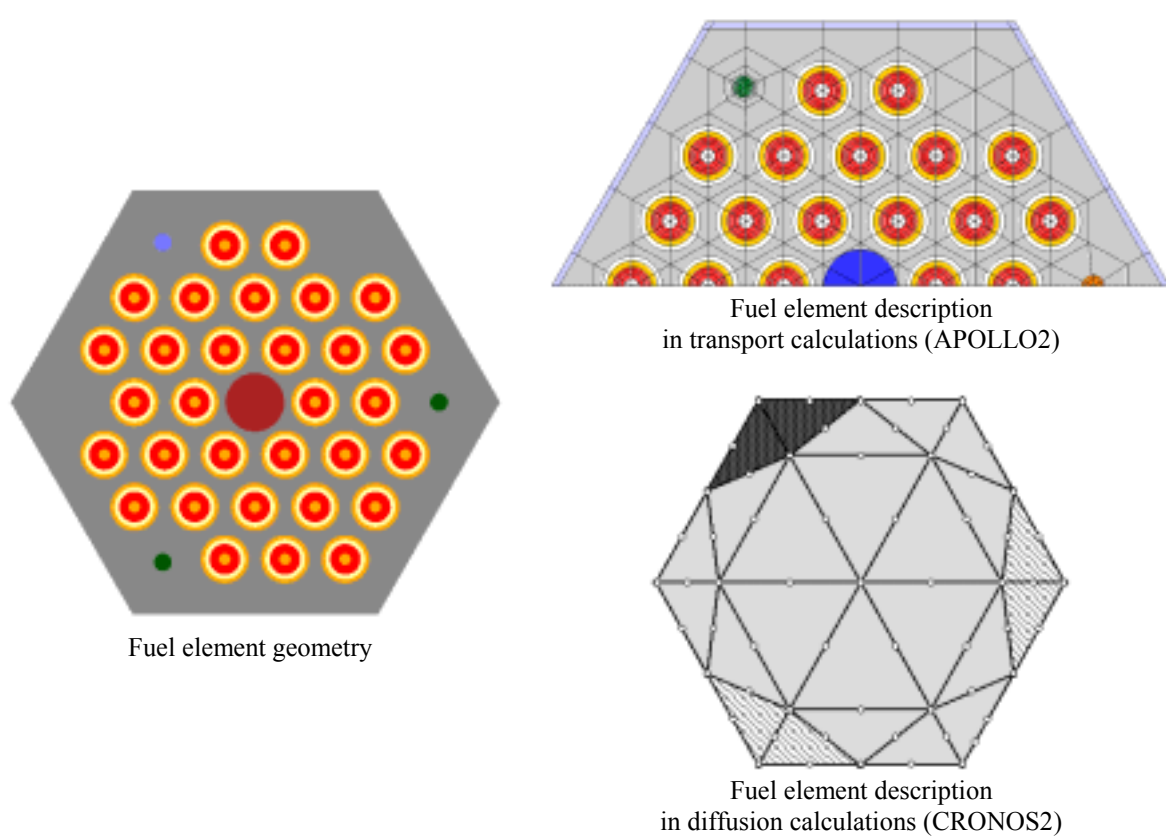
FIG. 2.46. Fuel element modelling in the improved Transport – Diffusion calculation scheme.

When such a heterogeneous fuel block geometry is used in the diffusion calculations, the impact have been evaluated for the three core configurations with 18, 24 and 30 columns, on the basis of a 2D simplified core with no axial leakage and with an average uranium enrichment. The diffusion calculations are compared to the Monte Carlo one. The results obtained for the first configuration are presented in Figure 2.47.
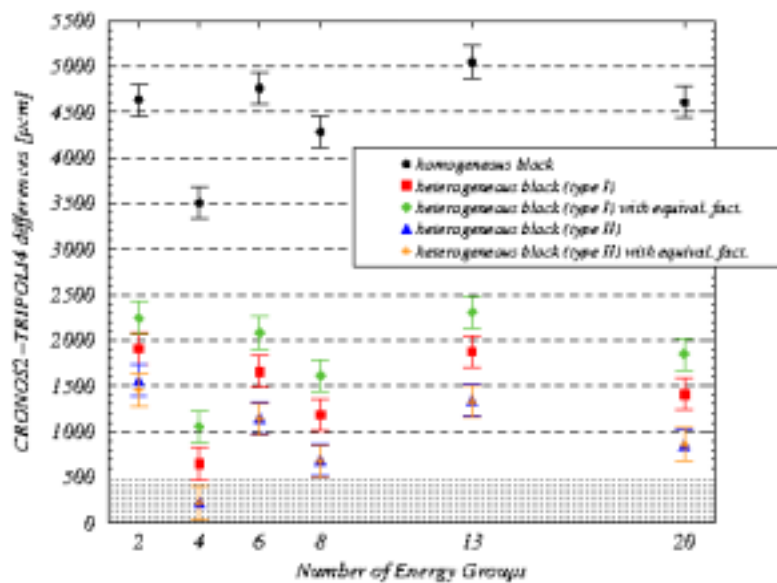
FIG. 2.47. 2D calculation comparison for different energy group structure in the diffusion calculation - 18 columns core -

As previously mentioned, the most important impact is obtained for the 18 columns core loading. As far as the **full core** is concerned, the diffusion-Monte Carlo 2D-discrepancies become **quite acceptable** with the use of the new finite elements. Moreover, the use of equivalence factors has been implemented in order to respect the global absorption rate between the APOLLO-2 transport calculations (172 groups) and the CRONOS-2 diffusion calculations with few groups. This option has not been considered afterwards because of it small impact (Figure 2.47) on the finite element of type II.

As a conclusion, a detailed description of the fuel block improves largely the results by giving a higher weight to the BP absorption in the fuel blocks. It allows getting quite acceptable values comparing to the reference TRIPOLI4 2D-calculation for the full core but a remaining discrepancy of about 1% can be observed for the annular core. This could be attributed to the cross section generation stage where the environment of the BP would not be representative of the one existing in the annular core configuration. Indeed, in this configuration the BP is surrounded by much more graphite (reflector) that thus increases the absorption flux-weighted cross-section. Besides, it would appear that there is actually no specific trend concerning the energy structure to be retained in the CRONOS-2 calculations.

Streaming modelling in the transport calculations

For improving the Transport – Diffusion calculation scheme, the streaming effect has been taken into account by using **anisotropic diffusion coefficients** in the core calculations. These diffusion coefficients have been evaluated in the fuel element transport calculation performed by APOLLO2. The Benoist method [2-29] available in APOLLO2 (called *TIBERE* model) is based on the B1 heterogeneous neutron leakage model. However, it might not be applicable in the large HTTR channels of the control rod graphite blocks (three large channels per block). Therefore, another analytical model (Benoist [2-30]) has also been tested on one control rod block alone and compared to the *TIBERE* model. With this formulation, the corrected diffusion coefficient is given by:

$$\frac{D_k}{\frac{1}{3}\lambda_m} = 1 + \frac{V_c}{V_t}\left(1 + \frac{c}{\lambda_m}Q_k\right) \tag{1}$$

where:

- $Q_r = 1 - 1/\Delta$ $\qquad Q_Z = 2 - \frac{3\pi}{4}B_Z c$ $\qquad k = r, z$ *(radial or axial)*

- c is the channel radius, λ_m is the mean free path of the moderator (graphite)

- $V_c = \pi c^2$ is the channel volume, V_t is the cell volume, B_Z is the axial buckling

and: $\Delta = \dfrac{\gamma}{\gamma + 1 - \dfrac{2b'}{1 - b'\dfrac{V_c}{V_t}}}$, $b' = \dfrac{\gamma + \dfrac{1}{2}}{\gamma + 1}$, $\gamma = \dfrac{c}{\lambda_m}$

In order to validate these models (*TIBERE* and analytical model), Monte-Carlo and diffusion calculations have been performed on the simplified geometry: the control rod block is surrounded by fuel elements and the axial structure of the geometry is the same as HTTR's core. The results are gathered in Table 2-28.

TABLE 2-28. Streaming Effect Calculated on the Simplified Core

	TRIPOLI4 $k_{effectif} \pm 3\sigma$	CRONOS2 2 gr.	8 gr.
Homogeneous control block	1,27958 ± 0,00090	1,26320	1.27397
Heterogeneous control block			
TIBERE	1,27247 ± 0,00100	1,26040	1,27057
Analytical formulation		1,25657	1,26672
Streaming effect [pcm]			
TIBERE		222	267
Analytical formulation	560 ± 135	526	570

The streaming effect calculated by CRONOS2 is underestimated when the anisotropic diffusion coefficients are evaluated by the *TIBERE* model. The underestimation of the streaming effect is the consequence of a non-adequate calculation of the axial diffusion coefficient (underestimation of − 20 to − 25 % on D_z calculation). On the other hand, the use of an analytical model for the axial diffusion coefficient allows obtaining results in good agreement with the reference (Monte-Carlo method).

2.2.2.4 New Results

New available data

The new data benchmark (HTTR-FC2) has been defined by JAERI [2-27]. It has been a good opportunity to implement the new enhanced methods coming from the previous analyses. Besides, the impact of these new data on the reactivity has been evaluated on the basis of the Monte Carlo calculations and of the improved core diffusion calculations. These effects are listed in Table 2-29.

Table 2-29. Analysis of the Benchmark Data Impact on the Results

	Number of fuel columns 18	30
Residual air in the graphite porosity and re-evaluated impurities in the dummy fuel blocks	− 0.82 % [1]	− 0.3 % [1]
Worth of the CR insertion to the top of the reflector (R2 group)	− 0.22 % [1] − 0.32 % [2]	− 0.25 % [2]
Temporary neutron detector	non evaluated	non evaluated

[1] *Evaluated with the Transport – Monte-Carlo calculation scheme*
[2] *Evaluated with the Transport - Diffusion calculation scheme*

The overall effect can exceed 1 % according to the core configuration. One can note that the impact of the residual air in porosities and the impurities in graphite are much more higher in the thin annular core configuration. This could explain the decrease of the discrepancies between the experiment and the first calculation results, correlated to the number of dummy fuel blocks (graphite) discharged during the criticality approach.

Diffusion calculation results

As far as the diffusion calculations are concerned, new developments carried out in APOLLO2 and CRONOS2 take into account:

- the exact position of the BP in the fuel block, by using new finite elements mesh in the core model
- the streaming effect, by generating anisotropic diffusion coefficients from both 2D-Pij calculations and analytical formulation.

The use of the HTTR-FC2 data associated with a complete description of the axial heterogeneity of the BP poison led to new core diffusion calculation results. This was done for several energy structures in CRONOS2 without observing a main trend which would allow to select a reference as energy mesh.

The final results are partially gathered in Figures 2.48 and 2.49. Figure 2.48 illustrates, with 8 energy groups, the impact of the different model assumptions on the reactivity as a function of the number of fuel columns loaded into the core. Figure 2.49 shows a streaming effect ranging from 2.25 % in the 18 columns core configuration to 1.8 % in the full core configuration. These results highlight also the importance of the used leakage model for evaluating the neutron streaming in the control rods graphite blocks. Indeed, the first model (*TIBERE* model) gave some values varying from 1.8 to 1.5 %.
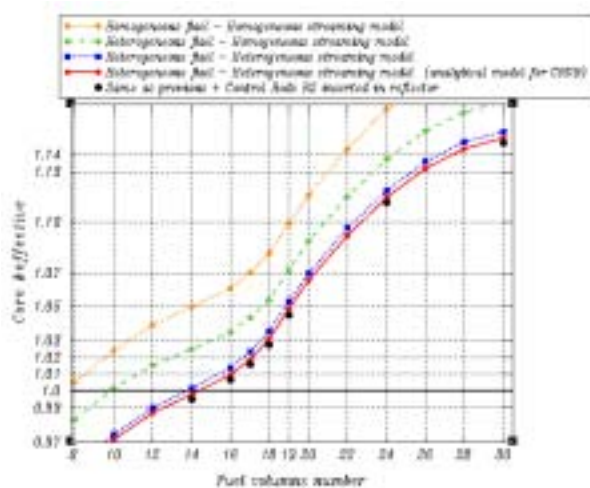
FIG. 2.48. k_{eff} values obtained with different core models.   *FIG. 2.49. Neutron streaming and fuel block homogenisation effect.*
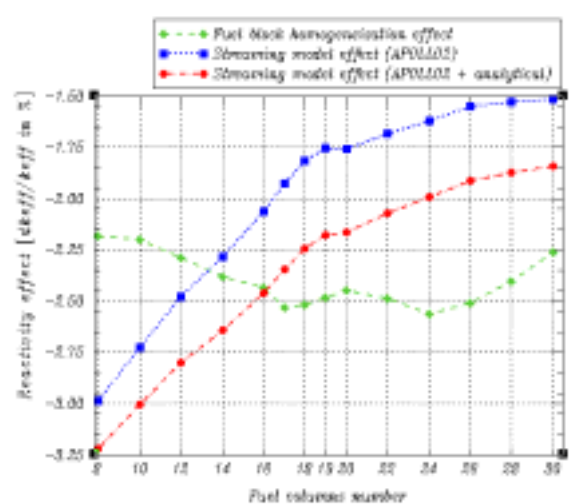
It is noticeable that the number of fuel columns needed to achieve criticality increases by about 7 in comparison with the first results (Table 2-25) when considering the presence of the detectors and the CR inserted in the upper reflector. However, at first criticality, a discrepancy remains between the diffusion and the Monte-Carlo calculations (0.9 % < Δk/k < 1.7 %). This underscores the limits of a method based on a cross section homogenisation from a fundamental mode calculation (infinite medium) that is barely pertinent for the 18 columns core configuration. The actual environment (reflector blocks) should be considered and should take place instead of the white boundary condition in the 2D APOLLO2 transport calculations, before homogenising and collapsing locally the cross sections inside the fuel element.

Final results of the HTTR-FC2 problem

All the final results are gathered in Table 2-30. In the case of the Monte Carlo code TRIPOLI4, the discrepancy between the measurement and the calculation for the 18 fuel columns configuration is reduced to $\Delta k/k \sim 0.8\ \%$, when considering the revised data of the HTTR benchmark.

As far as diffusion calculations are concerned, the discrepancy is now reduced to $\Delta k/k \sim 2.7$ or $1.7\ \%$ (depending on the number of energy groups), when taking into account the improved models and the revised data. After all, it must be stressed that all the calculation results obtained for the fully loaded core configuration fit the experiment, especially if one consider the experimental uncertainties.

Table 2-30. Experimental, Monte-Carlo and Final Diffusion Results

	TRIPOLI4 [1] *3D Monte Carlo* *172 gr & pointwise*	CRONOS2 [1] **(Final model)** • 3D *Diffusion* • *4 groups - 8 groups*	EXPERIMENT
30 col.	1.13833 ± 0.00090	1.1362 - 1.1451	$1.1363 \pm (> 3.6\ \%)$
24 col.	*	1.1000 - 1.1096	$1.0834 \pm (> 2\ \%)$
19 col.	1.02692 ± 0.00043	1.0351 - 1.0432	$1.0152 \pm\ ?$
18 col.	1.00855 ± 0.00090	1.0178 - 1.0275	subcritical

[1] *detector impact included ($\Delta k = 0.002$) but not modelised*

Excess reactivity HTTR-EX

All the excess reactivity are gathered below according to the previous values and the definition of the excess reactivity given in [2-22].

Table 2-31. Excess Reactivity for Different Core Configurations

Excess Reactivity [1]	**Number of loaded fuel columns**			
$(k_{eff} - 1)/k_{eff}$ **[%]**	**18**	**19**	**24**	**30**
Diffusion	$1.7 < \Delta k/k < 2.7$	$3.4 < \Delta k/k < 4.1$	$9.1 < \Delta k/k < 9,9$	$12,0 < \Delta k/k < 12,7$
Monte-Carlo	$+ 0.85$	$+ 2.6$	Non evaluated	$+ 12,15$

[1] *detector impact included ($\Delta k = 0.002$) but not modelised*

Control rod position for criticality: HTTR-CR

The results presented in Table 2-32 correspond to the fully loaded core configuration. The control rod positions for obtaining criticality with all the inserted CR are: **178.7 cm** with the diffusion calculations and **177.9 cm** with Monte-Carlo code.

Table 2-32: k_{EFF} for Different CR Insertion Depths. Full Core

Control Rod Insertion Depth [cm]	APOLLO2 – TRIPOLI4	APOLLO2 – CRONOS2	Exp.
178,9	$1,00117 \pm 0,00024$	1,00020	critical
177,6	$0,99972 \pm 0,00038$	0,99840	*

It is noteworthy that the CR insertion depth is well evaluated with the diffusion core calculation despite of the discrepancies with the Monte Carlo results observed in this configuration without the inserted CR. This remark underscores the fact that the CR worth is overestimated with the diffusion method especially in this case where no equivalence factors have been used in order to respect either the flux or the absorption rates between the multigroup transport calculations and the broad group diffusion core calculations.

Scram reactivity: HTTR-SC

In this section, the CR worth has been evaluated (Table 2-33) in the fully loaded core configuration and according to:

$$\rho = \frac{k_{crit.} - k_{Control\ Rods\ IN}}{k_{crit.} \times k_{Control\ Rods\ IN}}$$

As far as the CR insertion in the reflector is concerned, an unexplained result has been observed with the Monte Carlo calculation, whilst a good agreement can be observed for the overall CR worth inserted in the core. Once again, these results highlight the overestimation of the absorbant in the diffusion calculation when one compares the CRONOS2 results to those of TRIPOLI4.

Table 2-33. Control Rod Worth

	TRIPOLI4 (Monte Carlo)	CRONOS2 (diffusion)	Exp.
CR inserted in the reflector			
$k_{critique}$	$1,00117 \pm 0,00024$	1,00020	*
k_{RCR}	$0,92215 \pm 0,00040$	0,90245	*
ρ_{RCR} [%]	**8,56**	**10,83**	**12,0 $\pm$ 1,2**
All the CR inserted in the core			
$k_{critique}$	$1,00117 \pm 0,00024$	1,00020	
k_{RCR}	$0,68396 \pm 0,00030$	0,63982	
ρ_{RCR} [%]	**46,32**	**56,31**	**46,0 $\pm$ 4,6**

Isothermal temperature coefficient in the core : HTTR-TC

The temperature coefficients have been evaluated from the following expression:

$$\rho_{12} \quad = \quad \frac{k_{T_1} - k_{T_2}}{k_{T_1} \times k_{T_2}} \cdot \frac{1}{(T_1 - T_2)}$$

They have been estimated only from k_{eff} of the core diffusion calculations performed at different temperature (Table 2-34).

Table 2-34. K_{EFF} as Function of the Temperature

Temperature [K]	APOLLO2 – CRONOS2
300	1,00395
340	0,99724
380	0,99088
420	0,98455
460	0,97823
480	0,97525

According to the results gathered in Table 2-35, the temperature coefficients range from - 15 to - 16 pcm/°K between 300 to 420 K.

Table 2-35. Isothermal Temperature Coefficients

Temperature coefficients [pcm/°K]	APOLLO2 – CRONOS2
ρ_{320}	− 16,75
ρ_{360}	− 16,09
ρ_{400}	− 16,22
ρ_{440}	− 16,40
ρ_{470}	− 15,62

2.2.2.5 Concluding Remarks

The HTTR's core physics benchmarks have been treated with two different calculation scheme: a transport-diffusion method and a transport-Monte Carlo one. These benchmarks constitute the first opportunity in reactor physics to model and benchmark the codes and methods in thin **annular core geometry**. This important point led to the limitations of the classical two-steps core modeling based on a transport-diffusion chained calculations in order to take accurately into account the **core/reflector interface**. Moreover, one of the other characteristics of the HTTR core in its annular configuration was the presence of a large number of uncommon **big channels** offering the possibility for the neutrons to leak from the active zone (*streaming effect*). In addition to that, the **important axial and radial heterogeneities** in the core (burnable poison, many different enrichments) make the HTTR a real challenge in reactor physics.

Quite acceptable results are obtained in the **fully loaded core configuration**. Besides, some **discrepancies** between the calculations and the experiment appear for intermediate core configuration (**thin annular core**) close to criticality. Parts of these

discrepancies were reduced to **Δk/k ~ 0.85 %** with the Monte-Carlo calculations taking into account the new benchmark data (air in porosity and impurities in graphite). As far as the deterministic approach is concerned, the discrepancies were analysed and tackled by different treatments. However, a difference of at least **1 %** remains between the diffusion and the Monte Carlo calculations in the **annular core** configuration when considering revised data.

2.2.2.6 Addendum

Several energy structure have been tested in course of this study for the core diffusion calculations (see Table 2-36): the 2, 4, 8 and 20 group meshes, currently applied in the PWR studies and the 6 and 13 groups which have already been used in the GT-MHR related analyses.

Table 2-36. Group Structures for Core Diffusion Calculations

13 gr	6 gr	Limite inférieure en énergie [Mev]
1	1	$1,8315,10^{-1}$
2	2	$1,0104,10^{-3}$
3		$1,6745,10^{-5}$
4	3	$4,1293,10^{-6}$
5		$2,13,10^{-6}$
6	4	$1,305,10^{-6}$
7		$7,90,10^{-7}$
8		$6,2501,10^{-7}$
9	5	$3,91,10^{-7}$
10		$3,145,10^{-7}$
11		$1,15,10^{-7}$
12	6	$5,9,10^{-10}$
13		$1,1,10^{-10}$

The 6 and 13 group structures

8 gr	4 gr	2 gr	Limite inférieure en énergie [Mev]
1	1	1	$9,0718,10^{-1}$
2	2		$2,7324,10^{-3}$
3			$5,0045,10^{-3}$
4	3		$2,7679,10^{-6}$
5			$1,67,10^{-6}$
6			$6,2501,10^{-7}$
7	4	2	$1,6,10^{-7}$
8			$1,1,10^{-10}$

The 2, 4 and 8 group structures

20 gr	Limite inférieure en énergie [Mev]	20 gr	Limite inférieure en énergie [Mev]
1	4,493	11	$5,560.10^{-5}$
2	2,231	12	$4,000.10^{-6}$
3	1,353	13	$6,250.10^{-7}$
4	$4,979.10^{-1}$	14	$3,500.10^{-7}$
5	$1,832.10^{-1}$	15	$2,200.10^{-7}$
6	$6,738.10^{-2}$	16	$1,340.10^{-7}$
7	$2,479.10^{-2}$	17	$7,700.10^{-8}$
8	$9,119.10^{-3}$	18	$3,000.10^{-8}$
9	$2,035.10^{-3}$	19	$1,000.10^{-8}$
10	$4,540.10^{-4}$	20	$1,1.10^{-10}$

The 20 group structure

2.2.3. Germany [2-44]

2.2.3.1. Introduction

The calculations described in this report were performed within the framework of the IAEA Co-ordinated Research Programme (CRP) on "Evaluation of the High Temperature Gas Cooled Reactor Performance". The benchmark problems of the HTTR's start-up core physics experiments have been defined by the Oarai Research Establishment, JAERI. The ISR of Research Centre Jülich joined this CRP with the aim of testing its reactor code system. The intention is to use the HTTR's start-up core experiments in order to find validation criteria for the calculational methods hitherto used and the scope within which they can be applied. Pre-test and post-test results have been obtained for the benchmark problems HTTR-FC and HTTR-EX described in detail in [2-34]: the number of fuel columns has been evaluated for the approach to first criticality when the fuel columns are charged from the core periphery, and the excess reactivities for 18, 24, and 30 fuel columns have been determined.

2.2.3.2. Computational Methods and Nuclear Data

An overview of the code system used in the criticality calculations is given in Figure 2.50. All calculations performed are based on a 123-group cross section library which was generated from the JEF-2.2 nuclear data files [2-35]. The NITAWL module of the AMPX-77 system [2-36] was used to calculate shielded cross sections in the resonance region where the Nordheim integral treatment is employed. The double heterogeneity of the fuel due to the coated particles (cp) and the fuel rod assembly was taken into account by Dancoff factors which were calculated by the ZUT code [2-37] and supplied as input data for NITAWL. The 1-d cell calculations were performed by the TOTMOS code [2-38], a one-dimensional transport-corrected integral spectrum code for eigenvalue calculations and the generation of homogenized broad group constants. In order to evaluate the effect of the inhomogeneous distribution of the burnable poison (BP) in the axial direction, additional cell calculations in two-dimensional r-z geometry were performed by the discrete ordinates transport code DORT [2-39]. The eigenvalues and flux distributions of the whole reactor were calculated by the diffusion code CITATION [2-40] in 3-d triangular-z geometry. The OCTAGN module was used to transform the cell-weighted broad group cross section data into a format such that they can be used in the CITATION code. To take into account the effect of increased neutron streaming in the coolant channels and in the large holes of the core and the reflector, anisotropic diffusion coefficients were used. These were calculated by the MARCOPOLO code on the basis of the multigroup integral transport theory [2-41]. In order to estimate the influence of this effect the calculations for the whole reactor were performed with and without streaming corrections.

The geometric dimensions of the fuel and core components and the atom number densities of the materials given in Ref. [2-34] were used in the pre-test calculations. In the post-test calculations residual air in the pores of the graphite, aluminium in the temporary neutron detector holders and a revised boron impurity in some dummy fuel blocks were taken into account [2-42].

Dancoff Factors

The NITAWL code considers the double heterogeneity of a system by Dancoff factors. The Dancoff factor is defined as the probability that a neutron emitted from the surface of the fuel region of the fuel element under consideration will have its next collision

in the fuel region of any other fuel element. Applying this definition to a fuel rod lattice filled with fuel in the form of coated particles the ZUT code calculates the Dancoff factor as a sum of the single rod Dancoff factor and the probability that a neutron leaving the first rod will reach another fuel rod and be absorbed there. The Dancoff factors were calculated for all the different types of compacts and are listed in Table 1 together with the corresponding U^{238} resonance integrals. The Dancoff factors remain nearly constant because they are only dependent on the slightly varying geometric dimensions of the fuel compacts and rods, and on the density of the graphite matrix. In pre-test and post-test prediction the Dancoff factors are the same.
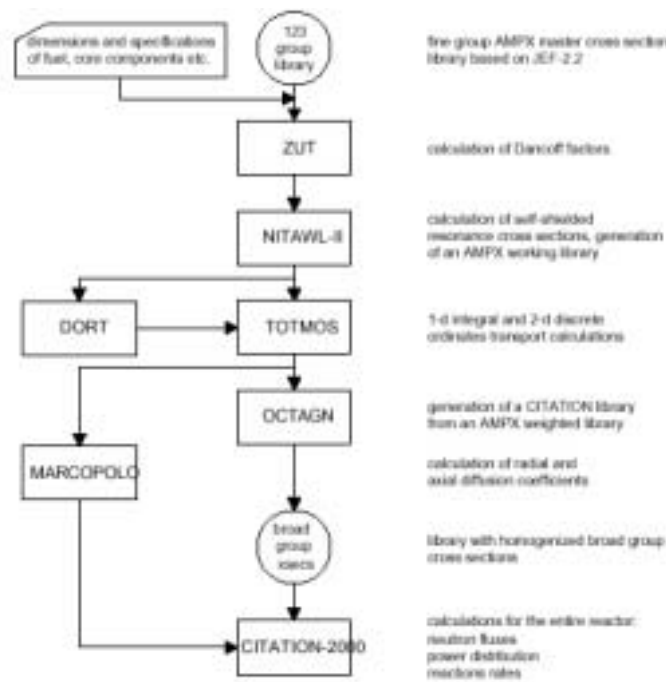
FIG. 2.50. Programme Structure of HTTR Calculations.

Table 2-37. Dancoff Factors and U^{238} Resonance Integrals for the Different Uranium Enrichments

Enrichment (wt.%)	Packing Frac.	Vol. of Fuel Comp. (cm3)	Boron Imp. (ppm)	Dancoff Factor	U^{238} Res.Int.
3.301	29.6	17.63	0.95	0.7225	43.82
3.864	30.4	17.69	0.91	0.7283	44.12
4.290	30.5	17.70	0.90	0.7284	44.17
4.794	30.3	17.72	0.88	0.7296	44.20
5.162	30.5	17.65	0.90	0.7300	44.36
5.914	30.3	17.70	0.51	0.7280	44.67
6.254	29.9	17.69	0.54	0.7270	44.85
6.681	30.3	17.65	0.50	0.7280	44.91
7.189	30.8	17.69	0.85	0.7258	45.09
7.820	28.8	17.67	0.87	0.7214	44.97
9.358	29.8	17.72	0.89	0.7223	45.91
9.810	29.3	17.71	0.90	0.7245	45.89

2.2.3.3. Pre-Test Calculations

1-d Cell Calculations

For the 15 types of BP-fuel combinations given in Appendix B of [2-34], one-dimensional cell calculations were performed by the TOTMOS code using the following scheme:

1. 123 cell-weighted group constants of the cp-cell-model were calculated in spherical geometry using a 123 group cross section library. The cell model consists of 3 zones: the kernel, the coatings, and the corresponding matrix zone. A white boundary condition was used at the outer surface of the cell.

2. Subsequently, 123 cell-weighted group constants of the fuel rod cell were calculated in cylindrical geometry and with the same group structure as used for the cp cell. The zones of the cylindrical fuel rod cell were: the central hole, the fuel compact, the graphite sleeve, the coolant channel, and the corresponding graphite block. The fuel rod cell is shown in Figure 2.51. The group constants of the materials in the fuel zone were the cell-weighted cross sections resulting from the cp cell calculation. The cross section of the fuel cell was equivalent to the cross section of the fuel block divided by the number of fuel rods. A white boundary condition was used at the outer surface of the cell.

3. In a subsequent third cell calculation, the cylindrical cell model shown in Figure 2.52 consists of a BP rod surrounded by a second zone representing the remaining fuel block. The group constants of the materials in this second zone were the cell-averaged 123 group constants resulting from the fuel rod cell calculation. The cross section of the BP cell was the same as the cross section of the fuel block divided by the number of BP rods. Again a white boundary condition was used at the outer cell surface. In this last step of the cell calculations, cell-weighted condensation was performed to four broad energy groups used in the calculations of the whole reactor. The energy group structure of the four groups is given in Table 2-38.

The k_∞-values of the cp-, fuel- and BP-cell calculations are given in Table 2-39 for all 15 types of BP-fuel combinations.
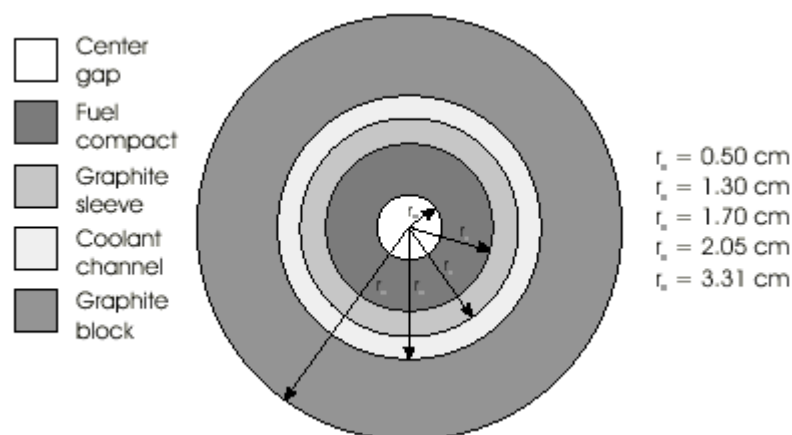
FIG. 2.51. Pre-Test 1-d Cylindrical Model of the Fuel Rod Cell for TOTMOS.
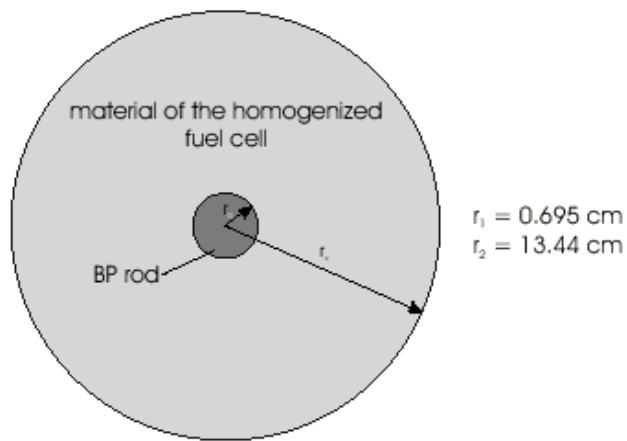
FIG. 2.52. Pre-Test 1-d Cylindrical Model of the BP Cell for TOTMOS

Table 2-38. Group Structure in the Diffusion Calculation

4 Group Set (Pre-Test)		26 Group Set (Post-Test)	
Group	Upper Energy Boundaries (eV)	Group	Upper Energy Boundaries (eV)
1	$1.492*10^7$	1 2 3 4	$1.492*10^7$ $7.408*10^6$ $3.679*10^6$ $6.721*10^5$
2	$1.111*10^5$	5 6 7 8 9 10 11 12	$1.111*10^5$ $1.931*10^4$ $3.355*10^3$ $1.585*10^3$ $7.485*10^2$ $2.754*10^2$ $1.301*10^2$ $6.144*10^1$
3	29.0	13 14 15 16	29.0 13.7 8.32 5.04
4	1.86	17 18 19 20 21 22 23 24 25 26	2.38 1.29 0.65 0.35 0.20 0.12 0.08 0.05 0.02 0.01

Table 2-39. Pre-Test Results of the TOTMOS Cell Calculations; No BP Adjustment

ID. No.	Enr. (wt.%)	k_∞-Values of the		
		Cp Cell	Fuel Cell	BP Cell
343320	3.4	0.6282	1.4285	1.1309
393320	3.9	0.6562	1.4604	1.1819
673320	6.7	0.7782	1.5457	1.3355
793320	7.9	0.8208	1.5610	1.3716
433120	4.3	0.6771	1.4957	1.2167
483120	4.8	0.6995	1.5142	1.2514
943120	9.4	0.8713	1.5996	1.4161
993120	9.9	0.8854	1.6021	1.4254
433325	4.3	0.6771	1.4790	1.1887
523325	5.2	0.7163	1.5095	1.2437
633325	6.3	0.7619	1.5376	1.2955
593125	5.9	0.7484	1.5476	1.2855
633125	6.3	0.7619	1.5559	1.3002
723125	7.2	0.7969	1.5726	1.3351
793125	7.9	0.8208	1.5802	1.3565

2-d cell calculations and BP adjustment

In the 1-d TOTMOS cell calculations, the axial heterogeneity of the BP is not explicitly taken into account. Thus, the efficiency of the BP is overestimated since the axial self-shielding of the BP cannot be considered. In order to find out the influence of the axial heterogeneity of the BP, 2-d cell calculations were performed by the discrete ordinates transport code DORT. For this purpose two series of 2-d cell calculations were performed:

1. In a first series of DORT calculations, the BP region is homogenized as in the 1-d cell. The results are given in Table 2-40 and compared with the corresponding results obtained by the TOTMOS code. It is seen that there is quite good agreement between the two computational methods.

2. In a second series of calculations the axial heterogeneity of the BP is explicitly considered in the 2-d DORT calculations. The geometric model is shown in Figure 2.53 and the results are presented in Table 2-40. It can be seen that the heterogeneity has quite a large influence on the infinite multiplication constant of the BP cell and considerably reduces the efficiency of the BP in comparison to the 1-d cell calculations.

In order to transfer this information into the 1-d cell calculation the B^{10} concentration was reduced in such a way that the resulting Δk was the same as that obtained in the two series of DORT calculations. In all BP-fuel combinations, the B^{10} concentration had to be reduced by 22% to 30 %.

Table 2-40. Pre-Test Infinite Multiplication Factors of the BP Cell Obtained by Different Methods

Case	k_∞-Values of the BP Cell				
	TOTMOS Homog.	DORT Homog.	Δk (TOTM.-DORT)	DORT Heterog.	Δk (DORT$_{Het.}$-DORT$_{Hom.}$)
343320	1.1309	1.1347	0.0038	1.1741	0.0394
393320	1.1819	1.1855	0.0036	1.2225	0.0370
673320	1.3355	1.3376	0.0023	1.3654	0.0275
793320	1.3716	1.3737	0.0021	1.3981	0.0244
433120	1.2167	1.2204	0.0037	1.2575	0.0371
483120	1.2514	1.2548	0.0034	1.2896	0.0348
943120	1.4161	1.4181	0.0020	1.4417	0.0236
993120	1.4254	1.4274	0.0019	1.4499	0.0225
433325	1.1887	1.1929	0.0041	1.2343	0.0414
523325	1.2437	1.2475	0.0037	1.2852	0.0378
633325	1.2955	1.2988	0.0033	1.3329	0.0342
593125	1.2855	1.2892	0.0037	1.3264	0.0373
633125	1.3002	1.3037	0.0036	1.3401	0.0363
723125	1.3351	1.3383	0.0032	1.3719	0.0335
793125	1.3565	1.3594	0.0029	1.3908	0.0313

horizontal view   (not drawn to scale)

material of the homogenized
fuel cell

BP rod

r. = 0.695 cm
r. = 13.44 cm

vertical view   (not drawn to scale)
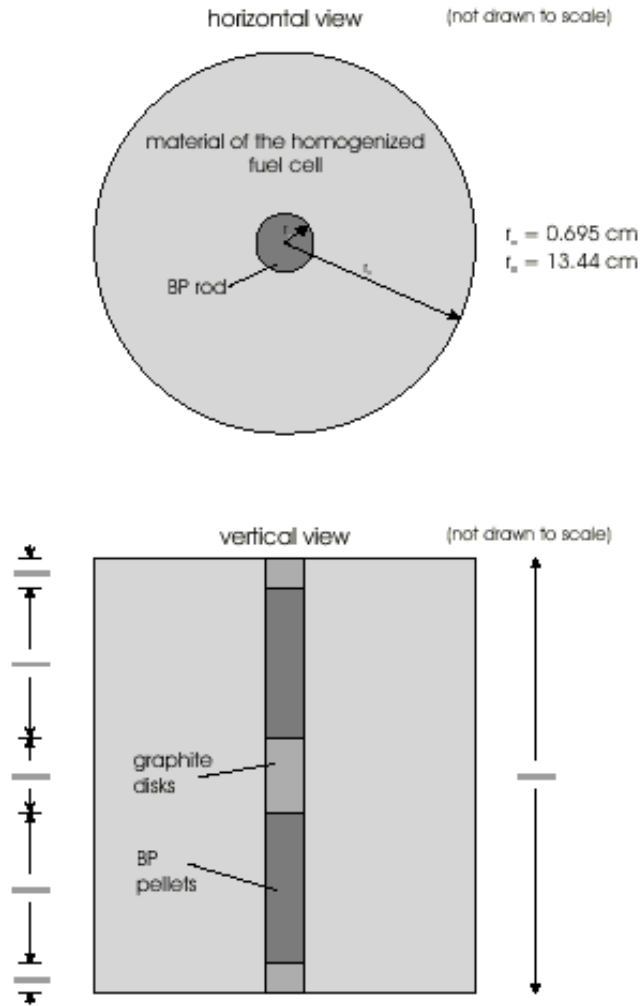
graphite
disks

BP
pellets

FIG. 2.53. Pre-Test 2-d Cylindrical Model of the BP Cell for DORT.

Streaming correction

The presence of the insertion holes in the control rod guide blocks and of the coolant channels in the fuel and reflector blocks leads to an increased neutron streaming in the axial direction. A possibility of treating this effect within the diffusion theory is the use of anisotropic diffusion coefficients. These are determined by the MARCOPOLO code which calculates anisotropic multigroup diffusion coefficients from the leakages of a heterogeneous lattice cell. For all types of blocks with insertion holes or coolant channels, 1-d cylindrical cells are defined which, in most situations, consist of a central hole representative of the block and surrounded by an associated material zone. As typical examples, the cell models of the dummy fuel block MB-2 and of the control rod guide block CB-1 are shown in Figures 2.54 and 2.55. The MARCOPOLO code allows the calculation of the buckling-independent diffusion constants D^g_k (k=r,z) in these cells taking into account linear anisotropic scattering. The group constants used in the MARCOPOLO calculations were provided by the TOTMOS code. For the control rod guide blocks CB-1 and CB-2 and the reflector block RB-1, the ratio of the anisotropic diffusion coefficients to the homogeneous diffusion coefficients are given in Table 2-41. The resulting values for all block types of interest are input into the CITATION code in the form of these streaming correction factors.
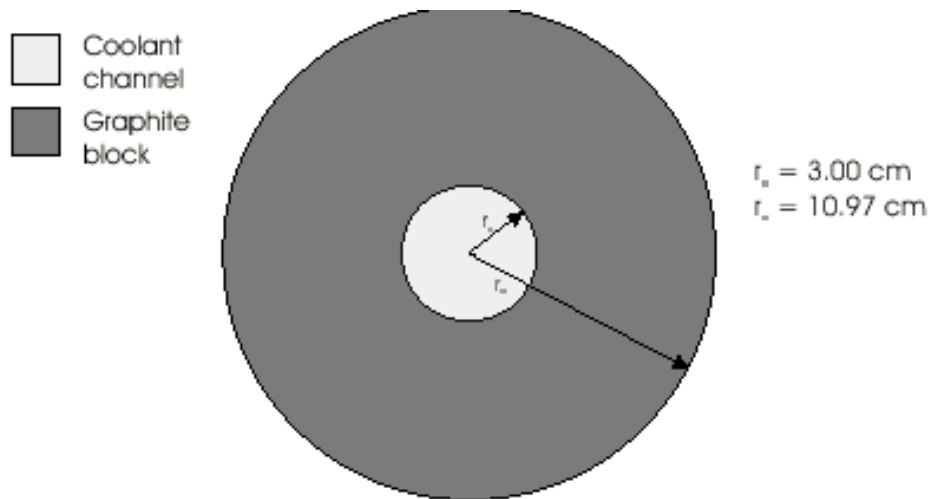
FIG. 2.54. 1-d Cylindrical Model of the Simplified Dummy Fuel Block B (MB-2).
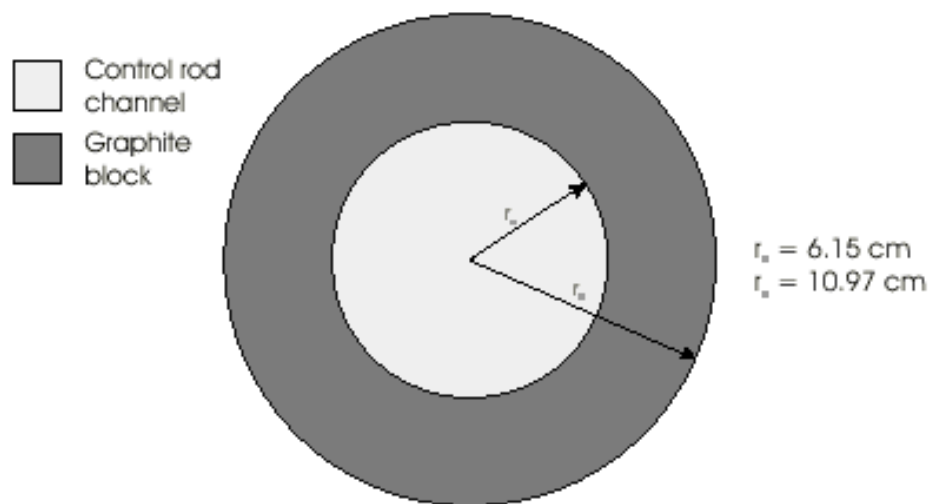
FIG. 2.55. 1-d Cylindrical Model of the Control Rod Guide Block CB-1.

Table 2-41. Pre-Test Streaming Correction Factors Obtained by the MARCOPOLO Code

| Group | Streaming Correction Factors | | | | | |
| | CR Guide Block CB-1 | | CR Guide Block CB-3 | | Repl.Refl.Block RB-1 | |
	D_r/D_{hom}	D_z/D_{hom}	D_r/D_{hom}	D_z/D_{hom}	D_r/D_{hom}	D_z/D_{hom}
1	1.1403	1.5740	1.1562	1.6317	1.0199	1.0513
2	1.1761	1.9333	1.1963	2.0358	1.0246	1.0786
3	1.1812	1.9497	1.2016	2.0537	1.0286	1.0836
4	1.1877	2.0243	1.2090	2.1369	1.0307	1.0908

Whole reactor calculations

Using the 4-group cross sections from the NITAWL-TOTMOS cell calculations the whole HTTR reactor was modelled with the CITATION diffusion code. A 3-dimensional triangular-z model was chosen. Each block was divided horizontally into 6 meshes and vertically into 4 meshes. The assembly was modelled by dividing the volume into spectral zones related to the material compositions. There are 45 different material zones.

Six pairs of control rods in the side reflector of the HTTR cannot be fully withdrawn to the top of the reflector. The effect of this CR insertion on reactivity is given as $\Delta k = 0.004$ in Ref. [2-34] and is subtracted from the calculated k_{eff}-values. Fuel columns are loaded clockwise from the periphery to the centre according to the loading order given in Ref. [2-34]. A thin annular core is formed at 18 fuel column loading, and a thick annular core is achieved when 24 fuel columns are loaded. A full core contains 30 fuel columns. According to this loading scheme four series of diffusion calculations were performed for 9 up to 30 fuel columns in the core:

- without streaming correction of the diffusion constant and without BP adjustment,
- with streaming correction, but without BP adjustment,
- with BP adjustment, but without streaming correction,
- with both corrections.

The k_{eff}-values of these four series are shown in Figures 2.56 and 2.57, respectively. As can be seen, the influence of the streaming correction is nearly independent of the BP adjustment. With and without BP adjustment the streaming correction causes a difference in k_{eff} from $\Delta k = 0.02$ at a loading with 9 fuel columns down to $\Delta k = 0.015$ for the case of a fully loaded core. This decrease in Δk can be explained by the fact that dummy fuel blocks with large holes and a great neutron streaming effect are subsequently replaced by fuel blocks which exhibit nearly no streaming effect. Moreover, it is found that the neutron streaming in the coolant channels of the top and bottom replaceable reflector can be neglected, because the decrease in k_{eff} caused by this effect was only $\Delta k = 0.08$ %.

On the other hand, the effective multiplication constants are increased by the BP adjustment: the "boron adjusted" k_{eff}-values are greater than the uncorrected ones, and the difference in k_{eff} increases with the increasing number of fuel rods. But it is evident that the increase of the effective multiplication constant due to the BP adjustment is not compensated by the effect of neutron streaming.

When taking into account the neutron streaming in the channels and holes of core and reflector, the neutron shielding in the BP rods, and when the reactivity of the CR insertion is subtracted, the first criticality will be achieved at 16 fuel columns loading. The excess reactivity amounts to $\Delta k/k = 0.42$ %. The excess reactivity of the thin, thick, and the fully loaded core is 2.48 %, 10.27 %, and 13.85 %, respectively. All results are shown in Tables 2-42 and 2-43.

These results agree very well with the average results of the deterministic calculations of all CRP-5 participants presented at the 1st Research Coordination Meeting [2-22].

Table 2-42. Pre-Test Effective Multiplication Factor and Excess Reactivity at the First Criticality

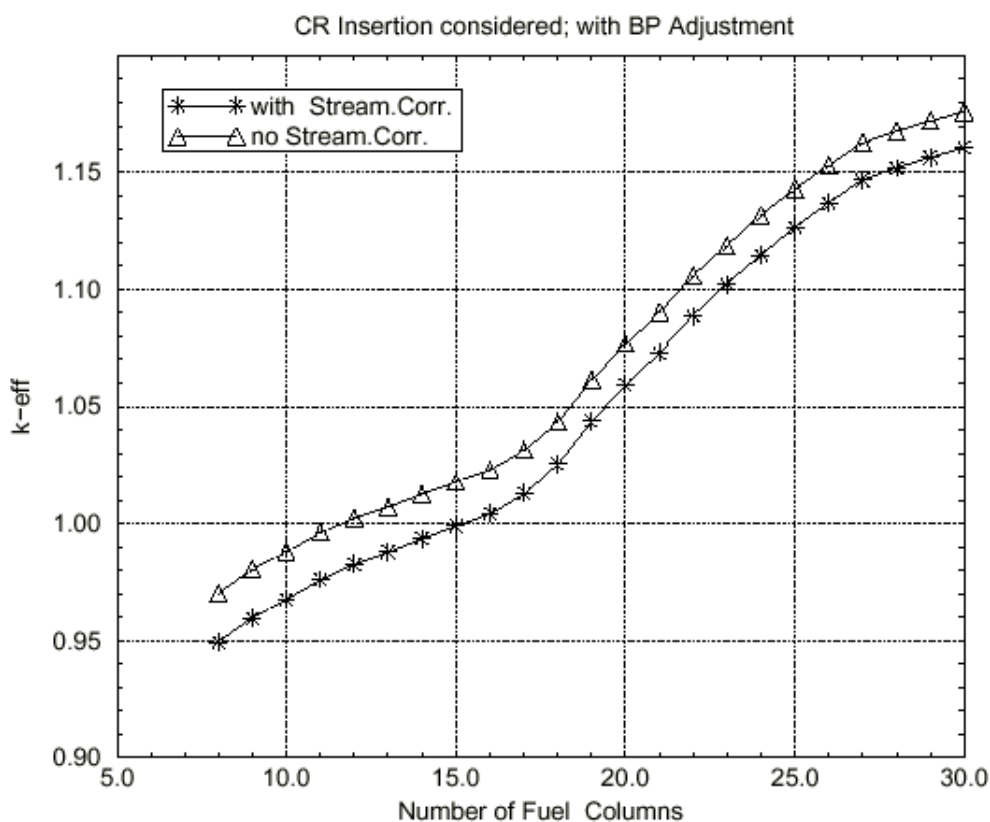| No. of Fuel Columns	k_{eff}	ρ [%Δk/k]
15 16	0.9991 1.0042	-0.90 +0.42

FIG. 2.56. Pre-Test Effective Multiplication Factor as a Function of the Number of Fuel Columns.

Table 2-43. Pre-Test Effective Multiplication Factor and Excess Reactivity at 18, 24, and 30 Fuel Columns Loading

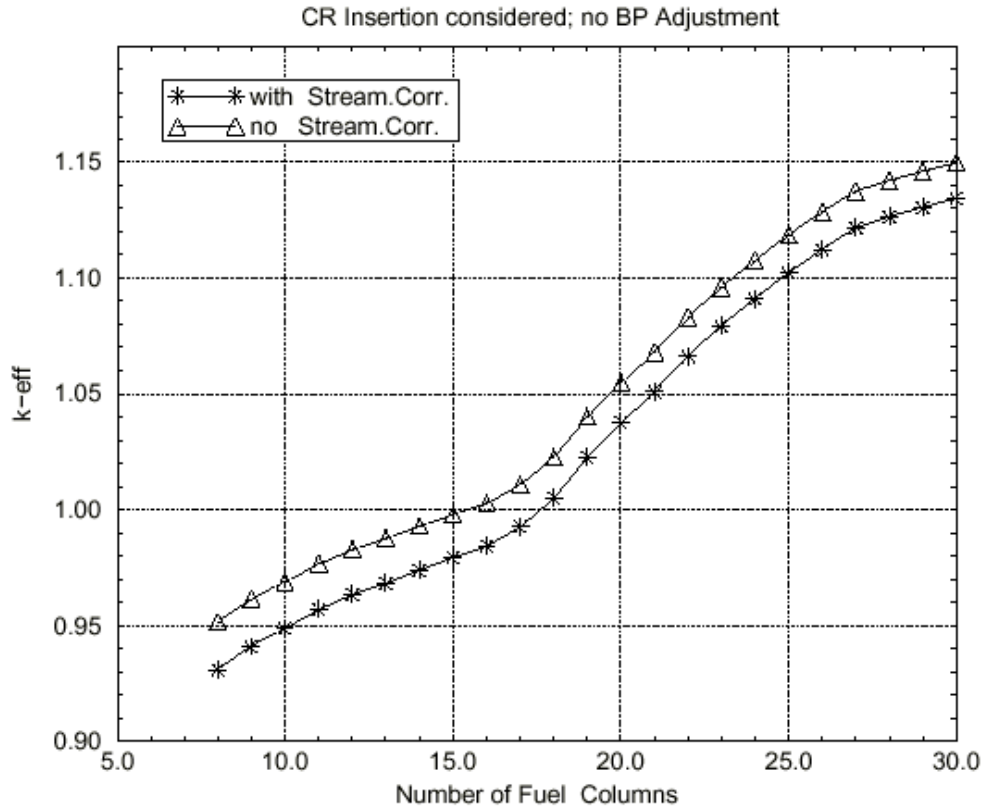| No. of Fuel Columns	k_{eff}	ρ [%Δk/k]
18 24 30	1.0254 1.1145 1.1607	2.48 10.27 13.85

FIG. 2.57. Pre-Test Effective Multiplication Factor as a Function of the Number of Fuel Columns.

Discussion of the pre-test results

In the pre-test diffusion calculation the first criticality of the HTTR was achieved with 16 fuel columns in the case of fuel columns loading from the core periphery. This corresponds to a critical mass of 29.6 kg U^{235}. It turned out that the burnable poison in the fuel blocks and the neutron streaming in the holes of the CR guide columns had a great influence on the neutronic characteristics of the HTTR and that an accurate treatment of these effects is required.

The experiment showed that the HTTR got critical with 19 fuel columns with an excess reactivity of about $\Delta k/k=1.5\%$. The discrepancy between measurement and the FZJ pre-test calculation amounted to $\Delta k=0.0287$ at the first criticality for a 4 group diffusion calculation with no leakage iteration; at 30 fuel columns in the core this difference was with $\Delta k=0.0261$ of the same order as can be seen on Table 2-44. Only at 27 and 30 fuel columns loading the calculated excess reactivities were in the experimental error intervals, showing some error compensating effects in the calculations. Six possible reasons for these discrepancies are given in the following:

- a non-adequate modelling of the fuel and BP unit cells,
- the neglect of the detailed structure of the HTTR fuel block in the whole core calculations,
- the use of few group homogenized cross sections in the whole core diffusion calculation without leakage iteration,

- the consideration of another than the actual boron impurity in some dummy fuel blocks and of helium instead of air in the graphite pores,
- a not yet adequate treatment of the self-shielding in the BP rods,
- and an underestimation of the neutron streaming.

Table 2-44. Results of the Pre-Test Diffusion Calculations together with the Experimental Results

No. of Fuel Columns	k_{eff} Calc.	k_{eff} Exper.	Δk Calc.-Exp.	ρ [% $\Delta k/k$] Calc.	ρ [% $\Delta k/k$] Exper.
9	0.9596	0.9282	0.0314	-4.21	-7.7[a]
12	0.9827	0.9481	0.0346	-1.76	-5.5[a]
15	0.9991	0.9652	0.0339	-0.09	-3.6[a]
16	1.0042	0.9701	0.0341	0.42	-3.1[a]
17	1.0129	0.9785	0.0344	1.27	-2.2[a]
18	1.0254	0.9913	0.0341	2.48	-1.0[a]
19	1.0439	1.0152	0.0287	4.21	1.5
21	1.0731	1.0417	0.0314	6.81	4.0±1.1[b]
24	1.1145	1.0834	0.0311	10.27	7.7±2.1[b]
27	1.1469	1.1198	0.0271	12.81	10.7±3.0[b]
30	1.1607	1.1346	0.0261	13.85	12.0±3.3[b]

 (CR Insertion considered Δk=0.004)
[a] from 1/M Measurement [2-43]
[b] from IK Method

2.2.3.4. Post-Test Calculations

Assessment of differences

The first four possible reasons of the differencies between pre-test prediction and experiment were analysed in more detail using simplified (1-d and 2-d) models of a thin annular core with 18 fuel columns:

- improved modelling of the fuel and burnable poison (BP) unit cells,
- consideration of the exact position of the BP rods in the fuel blocks,
- use of many group homogenized cross sections or accurate leakage iteration in the whole core diffusion calculation,
- and consideration of the revised boron impurity in some dummy fuel blocks and of residual air in the pores of the graphite, as proposed by JAERI [2-42].

In the course of these studies it turned out that the change in the unit cell models, the increase of the boron impurity in some dummy fuel blocks and the replacement of the helium in the pores of the graphite blocks by air reduced the multiplication constant of the simplified core models. However, this reduction was more than compensated by the increase of k_{eff} in a 26 groups diffusion calculation or a 4 groups diffusion calculation with leakage feedback used to describe the core/reflector coupling accurately.

In all pre-test calculations, the HTTR fuel blocks were homogenized with only six triangular meshes per fuel block and the **exact position** of the BP rods in the fuel blocks as mentioned in the 2nd item was not considered. When taking into account the detailed BP positions in the whole core diffusion calculations with 24 horizontal meshes per fuel block the multiplication constant decreased significantly, as can be seen on Table 2-45. Furthermore, it can be seen that the increase of the group number from 26 up to 52 in the whole core diffusion calculation has only a small influence on the k_{eff}-values. Thus, a group structure of 26 energy groups seems to be sufficient to get reliable results. The 26 energy group structures is given in Table 2-38.

Table 2-45. Effective Multiplication Constants and Δk Values for a Simplified 2-d, Triangular HTTR Core Model (18 Fuel Columns) Using Different Unit Cell Models and Group Structures (No Streaming Correction and BP Adjustment; Helium in Graphite Pores and Old Boron Impurity)

	k_{eff}		Δk
	Old Unit Cells 24 Mesh Hom. Model	New Unit Cells 24 Mesh Het. Model	New-Old Model
4 Groups	1.0484	0.9857	-0.0637
26 Groups	1.0840	1.0419	-0.0421
Δk 26-4 Groups	+0.0355	+0.0563	_
52 Groups	1.0842	1.0430	-0.0412
Δk 52-26 Groups	+0.0004	+0.0011	_

Concerning item 5 of the possible reasons for the discrepancies, the axial self-shielding in the BP rod was considered by a B^{10} adjustment in the 1-d cell calculations of the pre-test prediction. Now, an improved treatment of the axially heterogeneous distribution of the BP was performed by 2-d calculations.

As to item 6 of the possible reasons, the comparison with the Japanese Monte Carlo calculations shows, that the neutron streaming has been underestimated in the previous calculations. Therefore, modified diffusion constants for treating this effect were determined on the basis of the Japanese results.

Heterogeneity of the HTTR fuel block

In order to consider the exact position of the BP rods in the whole core diffusion calculation 24 horizontal meshes per fuel block have to be chosen and each fuel block has to be divided into three different regions:

- one fuel region, corresponding to 18/24 of the whole block,
- two BP regions, each corresponding to 2/24 of the whole block,
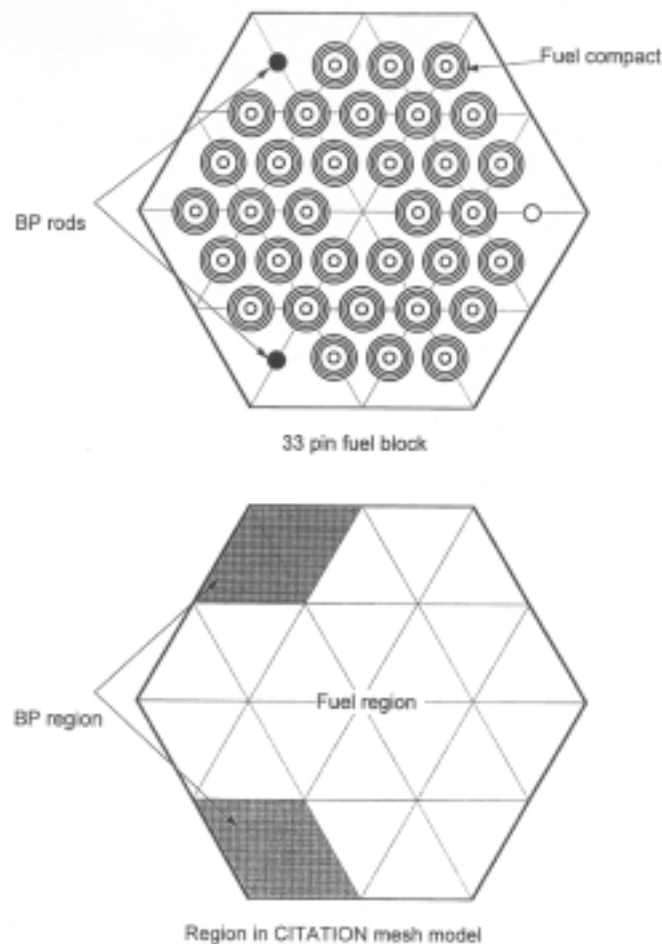- one "empty BP" region, according to 2/24 of the whole block.

FIG. 2.58. HTTR Fuel Block and Post-Test Model Used in the Diffusion Calculation with 24 Horizontal Meshes per Block.

The fuel block with 33 fuel pins is shown in Figure 2.58 together with the modelling of the different regions in the whole core diffusion calculation with 24 horizontal meshes per block. Basing on this subdivision of the fuel block it is necessary to create new unit cell models adapted to this situation.

New 1-d fuel cell model

The new fuel cell presented in Fig 2.59 together with the basic geometry has an outer radius of 2.70 cm corresponding to the pitch of the fuel rod lattice in the fuel block. Explicitely modelled are: the inner helium channel, the compact, the sleeve, and the outer helium gap. The cell-weighted 26 group cross sections generated on the basis of this new fuel cell model are used in the fuel region of each fuel block in the whole core diffusion calculation.
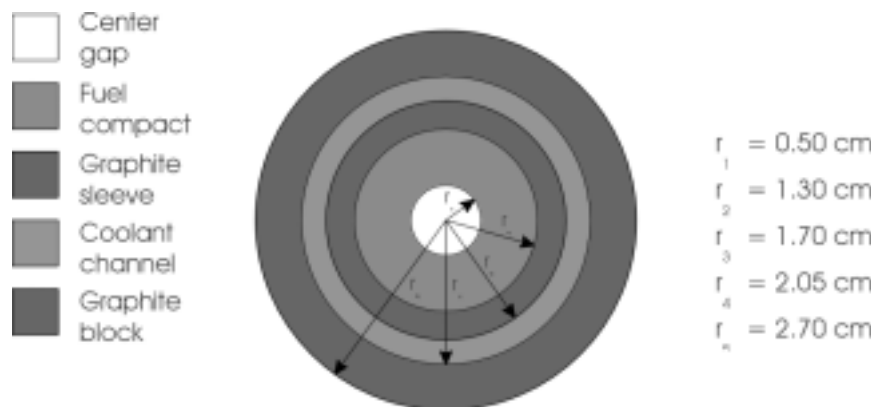
1-d cylindrical model of the fuel cell for TOTMOS

p = 5.15
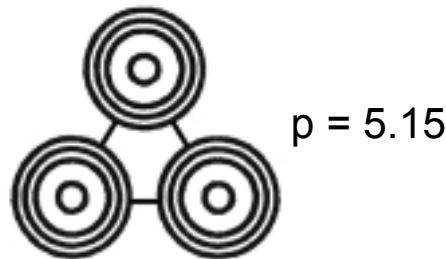
Dimension of the Fuel Lattice Used as Basis
in the New Fuel Cell Model

FIG. 2.59. Post-Test 1-d Cylinder Model of the Fuel Cell.

New 2-d BP Cell Model

In the pre-test prediction, the axial self-shielding of the BP was taken into account by a reduction of the B^{10} concentration in the 1-d TOTMOS cell calculations. Now, in the post-test calculations the axial self-shielding was considered by another method: it was provided that the absorption rate in the BP-regions of the whole core diffusion calculation is the same as in the detailed 2-d DORT-cell calculation for these regions.

Thus, the axial self-shielding of the BP was taken into account by a more accurate method compared to the method of reducing the B^{10} concentration. This reduction overestimated the efficiency of the BP compared to the use of group constants obtained in a 2-d DORT-cell calculation by about $\Delta k \approx 0.0065\text{-}0.0077$.

The revised 2-d cell model used in the DORT calculations is shown in Fig 2.60. This BP unit cell consists of three radial zones: the BP rod, surrounded by a graphite zone, corresponding to the area of 2/24 block, and a third radial zone representing the remaining fuel block. The group constants in this third radial zone are the cell-averaged group constants resulting from the fuel cell calculation. The first radial zone, the BP rod, is divided axially into five zones, representing the BP pellets, the graphite disks, and the upper and lower plugs of the graphite block. In the 2-d cell calculation the group constants are homogenized over the two inner radial zones and over the five axial zones of the BP rod and condensed to 26 energy groups. These 26 zone-weighted group constants obtained by the 2-d DORT cell calculation are used in the two BP-regions of each fuel block in the whole core diffusion computation.

The cross section of this BP cell corresponds to the cross section of the fuel block divided by the number of BP rods.
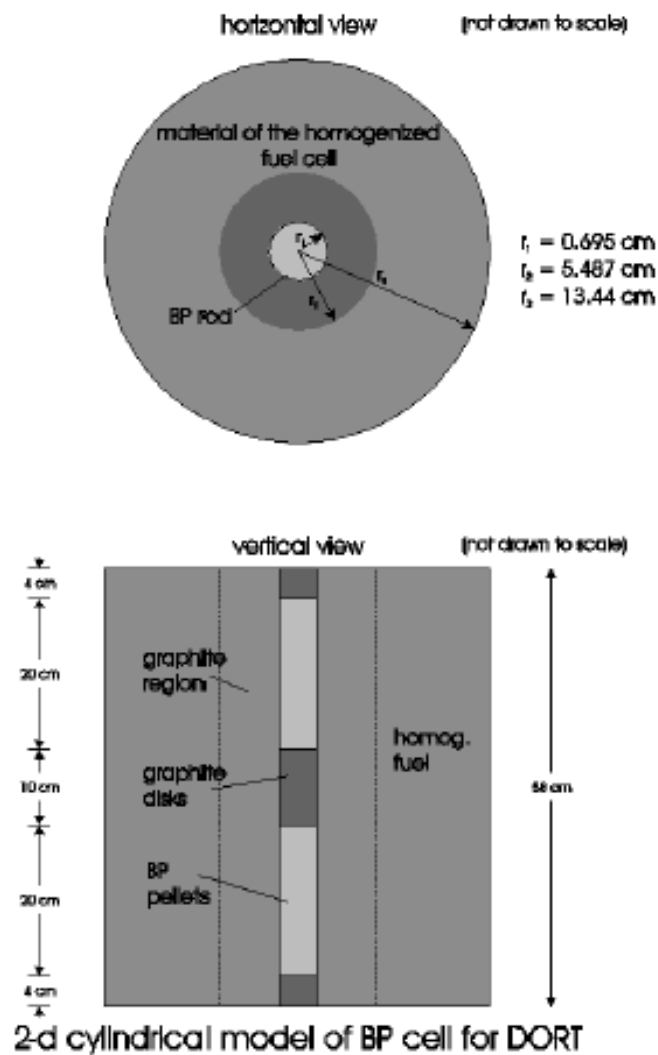

FIG. 2.60. Post-Test 2-d Cyl. Model of the BP Cell for DORT

New graphite cell model

The 26 group constants used in the third region of the HTTR fuel block are the zone-weighted cross sections supplied by the 1-d "empty" BP unit cell calculation. This "empty BP" cell has the same area as the cross section of the fuel block. It consists of three zones: the inner hole filled with helium instead of BP, surrounded by a graphite zone, corresponding to the area of 2/24 block, and a third zone, in which the cross sections of the homogenized fuel cell and of the homogenized replaceable reflector cell RB-2 are taken into account, because all empty BP holes in the 18 fuel columns assembly are situated at the outer surface of the annular core. Thus, the neutron spectrum in this "empty BP" unit cell is determined by the outer reflector and the corresponding fuel block.

In the "empty" BP cell calculation, the group constants are homogenized over the two inner zones and condensed to 26 energy groups. The k_∞-values obtained by the three different cell calculations are given on Table 2-46.

Table 2-46. Post-Test Results of the three Different Cell Calculations

Case	Enr. (wt.%)	k_∞-Values of the		
		New Fuel Cell 1-d TOTMOS	New BP Cell 2-d DORT	Empty BP Cell 1-d TOTMOS
343320	3.4	1.2808	1.1598	1.4955
393320	3.9	1.3075	1.2068	1.5419
673320	6.7	1.3814	1.3464	1.6900
793320	7.9	1.3943	1.3782	1.6983
433120	4.3	1.3230	1.2415	1.5693
483120	4.8	1.3374	1.2728	1.5987
943120	9.4	1.4140	1.4216	1.7288
993120	9.9	1.4157	1.4297	1.7356
433325	4.3	1.3230	1.2181	1.5707
523325	5.2	1.3490	1.2677	1.6164
633325	6.3	1.3742	1.3143	1.6581
593125	5.9	1.3665	1.3083	1.6477
633125	6.3	1.3742	1.3217	1.6594
723125	7.2	1.3893	1.3529	1.6808
793125	7.9	1.3943	1.3712	1.7011

Modified streaming correction

In the course of the pre-test calculations, it turned out: the streaming effect calculated by the CITATION code using anisotropic diffusion coefficients determined by the MARCOPOLO code [2-41] was about 33% smaller than the effect calculated by the Monte

Carlo code MVP of JAERI [2-22], in the case of 18 fuel columns in the core. In the case of the fully loaded core, the streaming effect was smaller and the difference between the diffusion and Monte Carlo calculation was reduced to about 15%, as can be seen on Table 2-47.

Table 2-47. Streaming Effects in Pre-Test and Post-Test Calculations

No. of Fuel Col.	Streaming Effect [% Δk/k]				
	Monte Carlo Code MVP[a] for:	Pre-Test Diffusion Code with Stream. Corr. for:	Post-Test Diffusion Code with **Modified** Stream. Corr. for:	Pre-Test Diffusion Code with Stream. Corr. for:	Post-Test Diffusion Code with **Modified** Stream. Corr. for:
	CR Guide Columns Irrad. Columns			all Coolant Channels and Holes of Core and Reflector	
18	2.30	1.53	2.32	1.69	2.46
24	—	1.27	1.92	1.38	2.02
30	1.30	1.10	1.68	1.18	1.75

[a] Results of JAERI-HTTR, presented at the 1st RCM of the CRP-5.

One possibility of getting more accurate diffusion constants is to compare the corresponding streaming effects obtained by diffusion and by Monte Carlo calculations and to adapt the anisotropic diffusion coefficients to the results of the Monte Carlo calculations.

Therefore, the neutron streaming coefficients calculated with the MARCOPOLO code had to be modified. When increasing the neutron streaming correction factors of the CR-guide and irradiation columns by about 20% (in r- and in z-direction) the streaming effect calculated by the diffusion code was the same as the reactivity effect resulting from the Monte Carlo calculation, as can be seen on Table 2-47.

For the control rod guide blocks CB-1 and CB-2, and the irradiation block IB-1 the ratios of the anisotropic diffusion coefficients to the homogeneous diffusion coefficients are given in Table 2-48 together with the modified streaming correction factors. They are listed in the 4 group structure. But in the core calculation 26 group constants were used, which were interpolated from the 4 group values.

Thus, in the recalculation of the first criticality and of the excess reactivities, these modified anisotropic diffusion coefficients for all CR-guide and irradiation columns were used. The anisotropic diffusion constants of the upper and lower replacable reflector, of the fuel and the dummy fuel blocks remained unchanged because there was no comparable Monte Carlo calculation.

Table 2-48. Streaming Correction Factors Obtained by the MARCOPOLO Code together with the Modified Factors Deduced from MVP Monte Carlo Calculations

Group	CR Guide Block CB-1		CR Guide Block CB-3		Irrad. Block IB-1	
	D_r/D_{hom}	D_z/D_{hom}	D_r/D_{hom}	D_z/D_{hom}	D_r/D_{hom}	D_z/D_{hom}
	Streaming Correction Factors (Pre-Test)					
1	1.140	1.574	1.156	1.632	1.139	1.567
2	1.176	1.933	1.196	2.036	1.175	1.923
3	1.181	1.950	1.202	2.054	1.180	1.939
4	1.188	2.024	1.209	2.137	1.186	2.013
	Modified Streaming Correction Factors (Post-Test)					
1	1.368	1.889	1.387	1.958	1.367	1.880
2	1.411	2.320	1.435	2.443	1.410	2.308
3	1.417	2.340	1.442	2.465	1.416	2.327
4	1.424	2.429	1.451	2.564	1.423	2.416

Table 2-49. Streaming Effects in the Pre-Test and Post-Test Detailed Core Calculations

No. of Fuel Columns	Pre-Test **Benoist** Stream.Correction Δk_{eff}	Post-Test **Modified** Stream.Correction Δk_{eff}
9	-0.0203	-0.0301
12	-0.0194	-0.0284
15	-0.0187	-0.0275
16	-0.0185	-0.0264
17	-0.0181	-0.0257
18	-0.0176	-0.0253
19	-0.0175	-0.0249
24	-0.0166	-0.0245
27	-0.0159	-0.0237
30	-0.0153	-0.0229

The use of the modified anisotropic diffusion constants decreased the k_{eff}-values in the whole core diffusion calculations by about $\Delta k \approx 0.01$-0.007 compared to the pre-test results, as can be seen on the Table 2-49.

Whole reactor calculations

In the post-test calculations the whole core was modelled with the CITATION diffusion code using the **26** group cross sections from the cell calculations. A 3-dimensional triangular-z model was chosen, as in the pre-test-prediction, but each block was divided vertically into 4 meshes and horizontally into **24** meshes, in order to arrange the BP rods and the empty BP-hole at their exact positions in the fuel block.

As in the pre-test calculations, four series of diffusion calculations were performed in order to show the influence of the modified streaming correction and of the axial BP heterogeneity on the k_{eff}-values. Both effects are augmented compared to the pre-test prediction, as can be noticed on Tables 2-49 and 2-50. The modified streaming correction reduces the multiplication constants by about $\Delta k = 0.03$ at 9 fuel columns loading to $\Delta k = 0.023$ at 30 fuel columns in the core. On the other hand, the more accurate treatment of the axial heterogeneity of the BP increases the multiplication factor by about $\Delta k = 0.024$ at 9 fuel columns in the core and by about $\Delta k = 0.034$ at fully loaded core. This stronger effect of the BP when using the more accurate treatment of the axial heterogeneity is mainly due to the fact, that the Σ_{abs}-values obtained by the 2-d cell calculation are significantly smaller in the thermal energy range than those macroscopic absorption cross sections obtained by the 1-d cell calculation with B^{10} reduction, as can be seen from Fig 2.61.
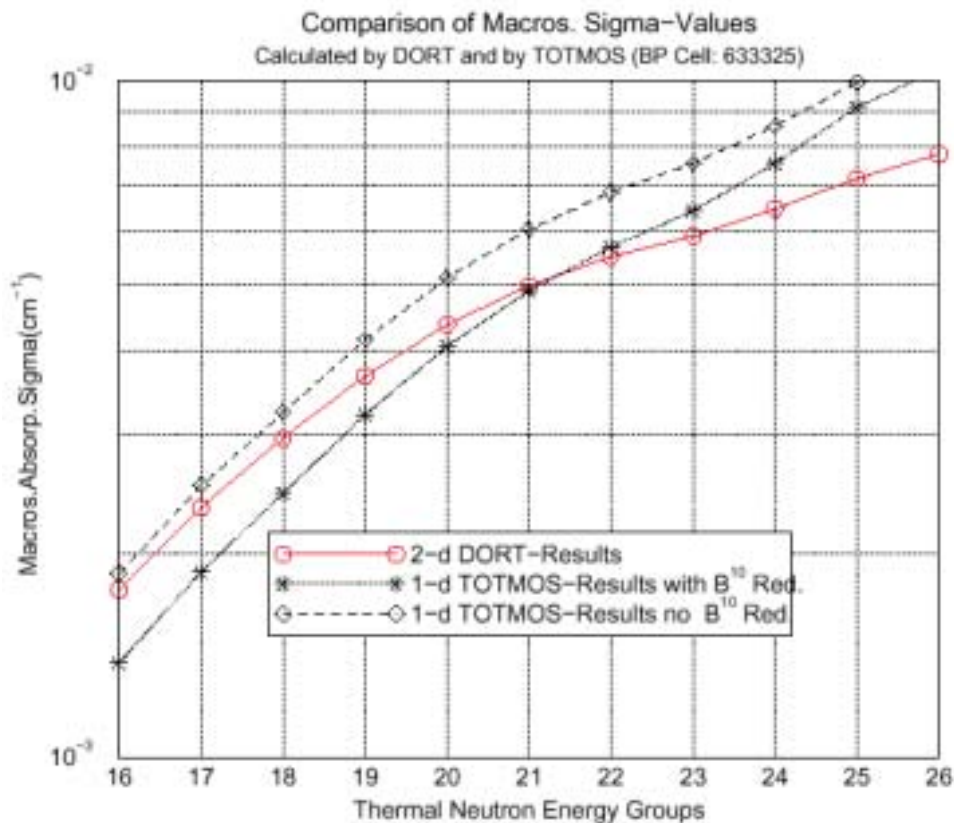

FIG. 2.61. Comparison of Macroscopic Absorption Cross Sections Obtained by Different Methods.

Table 2-50. Axial Self-Shielding Effect of the BP in the Detailed Core Calculations Obtained by Different Methods

No. of Fuel Columns	Pre-Test **B¹⁰-Reduction** Δk_{eff}	Post-Test **2-d BP Cell Calculation** Δk_{eff}
9	+0.0189	+0.0245
12	+0.0196	+0.0255
15	+0.0200	+0.0257
16	+0.0201	+0.0265
17	+0.0203	+0.0269
18	+0.0207	+0.0273
19	+0.0213	+0.0281
24	+0.0242	+0.0314
27	+0.0252	+0.0333
30	+0.0263	+0.0336

Table 2-51. Results of the Post-Test Diffusion Calculations together with the Experimental Results

No. of Fuel Columns	k_{eff} Calc.	k_{eff} Exper.	Δk Calc.-Exp.	ρ [% $\Delta k/k$] Calc.	ρ [% $\Delta k/k$] Exper.
9	0.9408	0.9282	0.0126	-6.30	-7.7[a]
12	0.9642	0.9481	0.0161	-3.70	-5.5[a]
15	0.9811	0.9652	0.0159	-1.90	-3.6[a]
16	0.9866	0.9701	0.0165	-1.40	-3.1[a]
17	0.9959	0.9785	0.0174	-0.41	-2.2[a]
18	1.0080	0.9913	0.0167	0.79	-1.0[a]
19	1.0263	1.0152	**0.0111**	2.60	1.5
21	1.0556	1.0417	0.0139	5.30	4.0±1.1[b]
24	1.0944	1.0834	0.0110	8.60	7.7±2.1[b]
27	1.1261	1.1198	0.0063	11.20	10.7±3.0[b]
30	1.1336	1.1346	−0.0010	11.80	12.0±3.3[b]

 (CR Insertion and Al in the Neutron Detector Holders considered: Δk=0.004+0.002)
[a] from 1/M Measurement [2-43]
[b] from IK Method

Table 2-52. Post-Test Effective Multiplication Factor and Excess Reactivity at the First Criticality

No. of Fuel Columns	k_{eff}	ρ [%Δk/k]
17	0.9959	-0.41
18	1.0080	+0.79

Table 2-53. Post-Test Effective Multiplication Factor and Excess Reactivity at 18, 24, and 30 Fuel Columns Loading

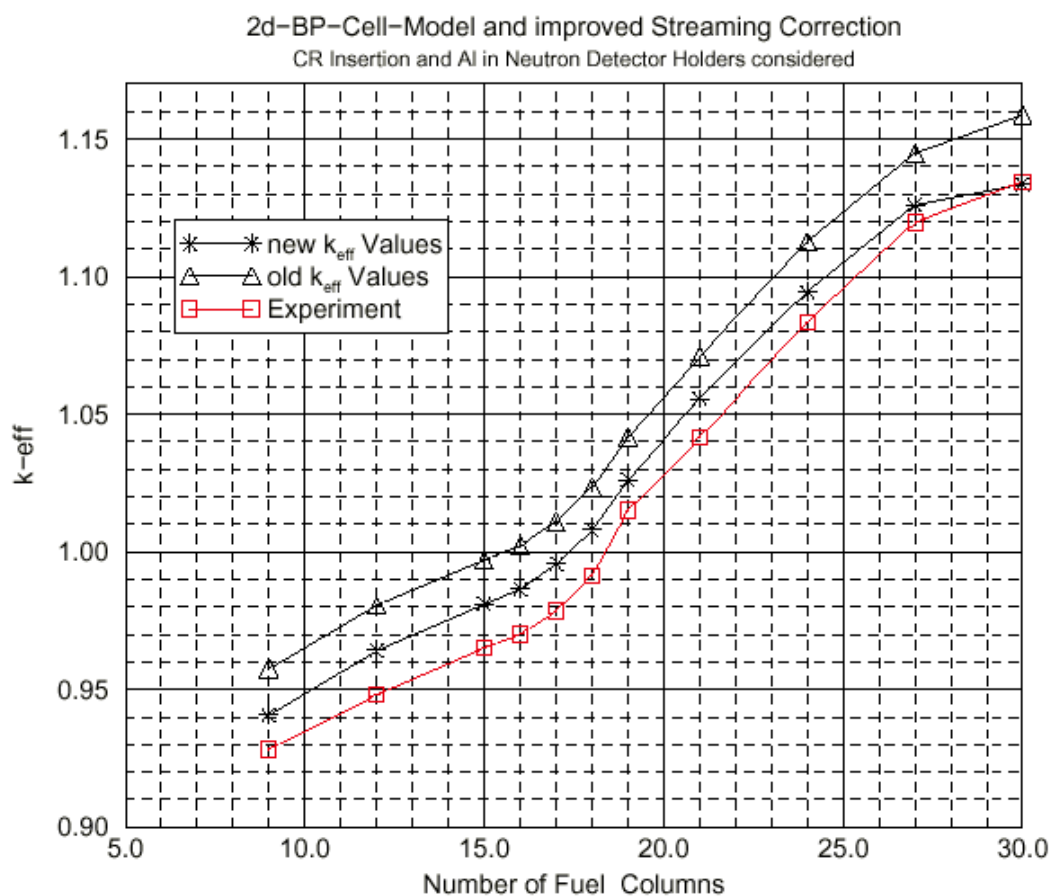| No. of Fuel Columns	k_{eff}	ρ [%Δk/k]
18	1.0080	0.79
24	1.0944	8.60
30	1.1336	11.80

FIG. 2.62. New and Old k_{eff}-Values of the Diffusion Calculations in Comparison with the Experimental Results.

When taking into account the modified neutron streaming in the big holes of the core, the neutron axial self-shielding in the BP rods by the more accurate method, and when not only the reactivity of the CR insertion of Δk=0.0040, but also the reactivity of the aluminium in the temporary neutron detector holders of Δk=0.0020 is subtracted, the first criticality will now be achieved at 18 fuel columns loading. The excess reactivity amounts to Δk/k=0.79%. The excess reactivity of the thin, thick, and the fully loaded core is 0.79%, 8.63%, and 11.80%, respectively. The results of the post-test calculations are given on Tables 2-51 to 2-53. In Figure 2.62 the new and the old k_{eff}-values of the diffusion calculations are presented together with the experimental results.

Discussion of the post-test results

When summing up all post-test studies, the intermediate calculations using simplified whole core models and the final calculations for the detailed core, the analysis yields the following effects at 18/19 fuel columns in the core compared to the pre-test results:

- when considering the detailed structure of the HTTR fuel block in the whole core calculation, the multiplication factor decreases by about $\Delta k \approx 0.043$,
- the description of the detailed energy-dependence of the neutron flux adequately by a fine energy group structure increases the k_{eff}-value by about $\Delta k \approx 0.035$,
- when taking into account the residual air in the graphite pores, the higher boron impurity in some dummy fuel blocks, and the reactivity effect of the aluminium in the neutron detector holders, the multiplication factor is reduced by about $\Delta k \approx 0.009$,
- when considering the axial heterogeneity of the BP by 2-d cell calculations, k_{eff} of the whole core calculation increases by about $\Delta k \approx 0.0068$,
- and when treating the neutron streaming effect by modified diffusion constants on the basis of the Japanese Monte Carlo results, k_{eff} is reduced by about $\Delta k \approx 0.0075$.

The number of fuel columns to achieve first criticality increases by about 2 fuel columns in comparison to the pre-test results presented at the 1.RCM [2-22]. Now, the discrepancy between measurement and FZJ diffusion calculation amounts to Δk=0.0111 at the first criticality (i.e. at 19 fuel columns), as can be seen on Table 2-51.

2.2.3.5. Conclusion

Altogether it turns out that the following procedures seem to be necessary for a better approach to the experimental results:

- detailed heterogeneity of the BP- and fuel-region in the whole core calculation,
- use of fine group constants or of broad group constants including detailed leakage information in the diffusion calculations of the whole core in order to describe the core/reflector coupling accurately,
- treatment of the axial self-shielding in the BP rods by 2-d cell calculations,
- consideration of an enhanced neutron streaming, brought about here by an adaption of the diffusion constants to results of Monte Carlo calculations.

When applying these improvements and regarding the actual boron impurity in some dummy fuel blocks together with air in the graphite pores the first criticality was recalculated for 18 fuel columns in the case of fuel loading from the core periphery. This corresponds to a

critical mass of 33.1 kg U^{235}. Moreover, it turned out that a 26 energy group structure in the whole core diffusion calculation seems already to be sufficient to get reliable results when no detailed leakage information is used in generating the group constants for the whole core diffusion calculations.

2.2.3.6. Acknowledgement

2.2.4. Indonesia [2-45]

Initial fuel loading and first criticality of the HTTR was accomplished in an annular core configuration. This core type was chosen because of high inherent safety characteristics for loss of coolant accidents [2-46]. The vessel cooling system (VCS) surrounding the reactor pressure vessel is designed to maintain the fuel temperature at less than the limit of 1600°C in a loss of coolant accident. The decay heat will be transferred radially through the regions of fuel, side removable and permanent reflector blocks and reactor pressure vessel to the cooling panel of the VCS through heat conduction, radiation and convection without any necessity for active cooling. Introduction of the annular core type is expected to enhance the heat removal mechanism, because the heat transfer pass is shortened by thinning of the fuel region.

In the fuel loading for the start up core physics experiment, three different types of core were considered; a thin and thick annular core with 18 and 24 fuel columns, respectively, and a fully loaded core that consists of 30 fuel columns. The core size of the HTTR is about half the size of a commercial HTGR. The high excess reactivity in HTTR is similar to that of HTGR, which is needed to compensate for the effects of temperature, xenon, burn up, etc. during power operations.

Data for the core physics calculation is applied by JAERI [2-47]. The data include specifications for core and its internal components, such as fuel, replaceable reflectors, permanent reflectors, control rods and dummy fuel elements. Also provided are HTTR details (see Section 2.1.1) including specifications of the fuel rods, fuel compacts and coated fuel particles. Generation of cell cross-sections in this study was performed using CELL Module of the SRAC-EWS Code system [2-48], while the whole core calculation was performed using CITATION Module of the SRAC-EWS.

The purpose of this study was to examine when the first criticality can be achieved by using annular thin core loading mechanism. In this loading type, fuel columns are loaded in the outermost fuel region (18 columns, i.e. annular thin core). Upon completion of the initial 18 columns, fuel loading continued with another 6 fuel columns in the inner fuel region (24 columns, i.e. thick annular core). Finally, loading continued with another 6 fuel columns in the innermost fuel region, so that the full core of 30 fuel columns was achieved.

2.2.4.1. Calculation Model and Procedures

Calculation for the start up benchmark test was developed and all calculations were performed for a core temperature of 300K and helium pressure of 1 atm. Figure 2.63 depicts the flow diagram of the benchmark calculation.

The SRAC-EWS Code system [2-48] was applied throughout the calculations, and the nuclear data in 107 groups were obtained mainly from JENDL-2 and ENDF/B-V. The ULIBMAKE module of SRAC-EWS was applied to generate the user library files from the public library, and to collapse these files into 54 energy groups. The CELL module was then applied to further condense these into 6 groups (i.e. 3 groups in the fast region and 3 groups in the thermal region), and to perform the cell calculation in collision probability method. In order to save computing time, the cell calculations were performed by using the equivalent cylindrical geometry (i.e. Wigner-Seitz's approximation) with white boundary conditions, rather than the more exact hexagonal geometry, because the effect on k_∞ was minimal, as pointed out by Jeong et al.[2-49]. The CITATION module was applied for the whole core diffusion calculations.
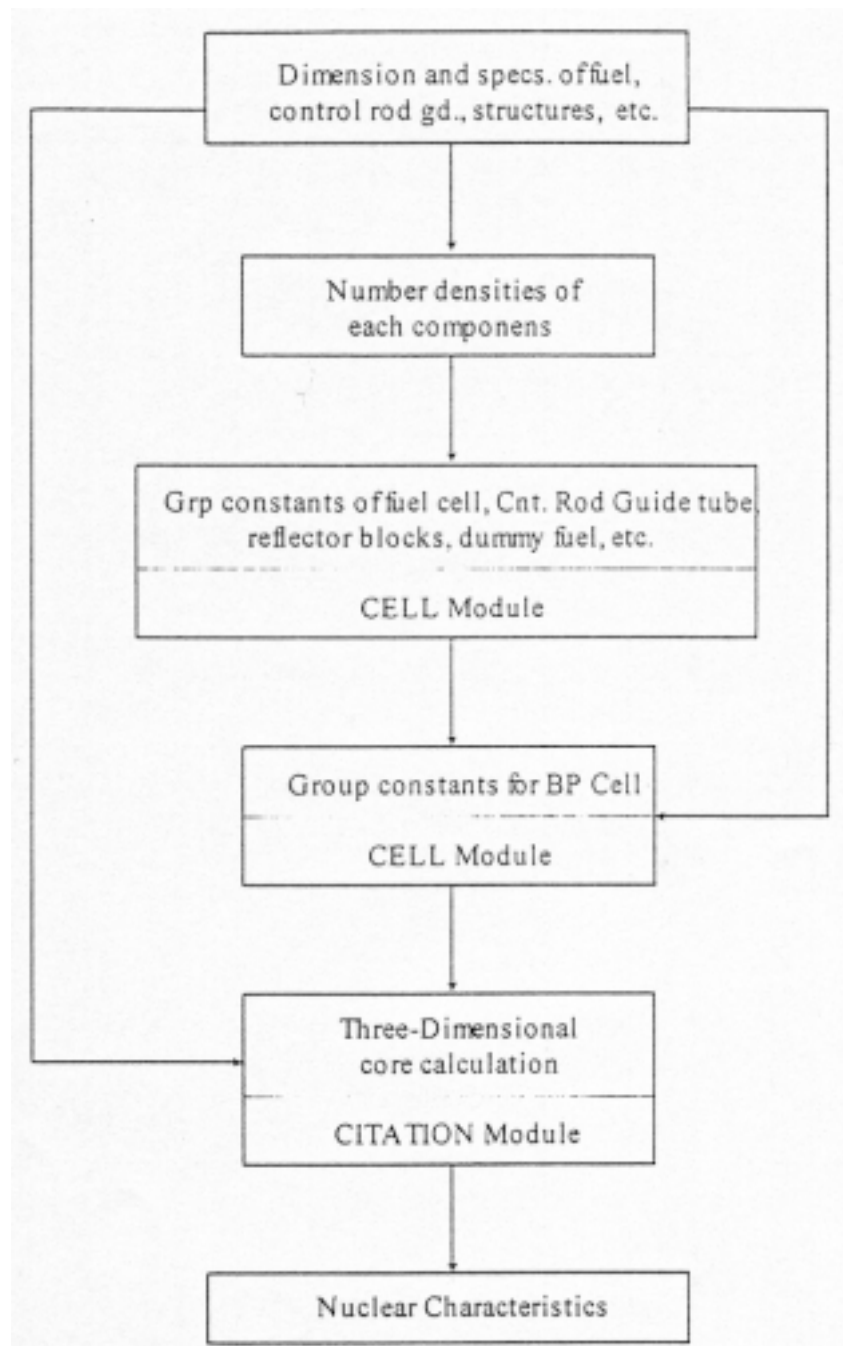
FIG. 2.63. Flow diagram of cell and core calculation for the HTTR benchmark test.

Cell Module was used to generate group constants of fuel and graphite blocks for succeeding core calculations. In the fuel region, the double-heterogeneity effects originating from the structure of fuel rods, in which the coated fuel particles are dispersed within fuel compacts, is considered by the use of collision probability method. The outer radius R for 33 pin block was 3.249 cm, and for 31 pin fuel block was 3.352 cm.

For the control rod guide tube with three large holes, the collision probability method was also utilized. Radial and axial directional diffusion coefficients for the unit cell were calculated by Benoist's formula. Similar to a coolant channel in fuel block, the content of the holes was helium gas at 1 atm at 300K. An isotropic (white) reflection boundary condition

was applied in the outer boundary of the unit cell. The unit cell in the control rod guide consists of a void region and a graphite region. The inner and outer radius of this region was 6.15 and 10.91 cm, respectively.

Average group constants of the fuel rods were calculated by using a one-dimensional cylindrical fuel cell model as depicted in Figure 2.64. The neutron flux was calculated by the collision probability method, which was used to average the group constants in the fuel cell geometry. The average group constants of the fuel block with BPs were also calculated in one-dimensional cylindrical BP cell model shown in Figure 2.64. The outer radius of the BP region was 0.7 cm, while the homogenized fuel region outer radius was 13.44 cm. Variation in axial composition of material was taken into consideration by averaging the number density in the axial region, taking into account their volume ratio. Table 2-54 shows the infinite multiplication factor (k_∞) for each fuel cell and its corresponding BP cell.

The whole core calculation was performed using CITATION Module of SRAC-EWS in θ-R-Z geometry. The angular distribution was made such that there were nine angular-divisions in one-sixth of the horizontal cross-section of the core.
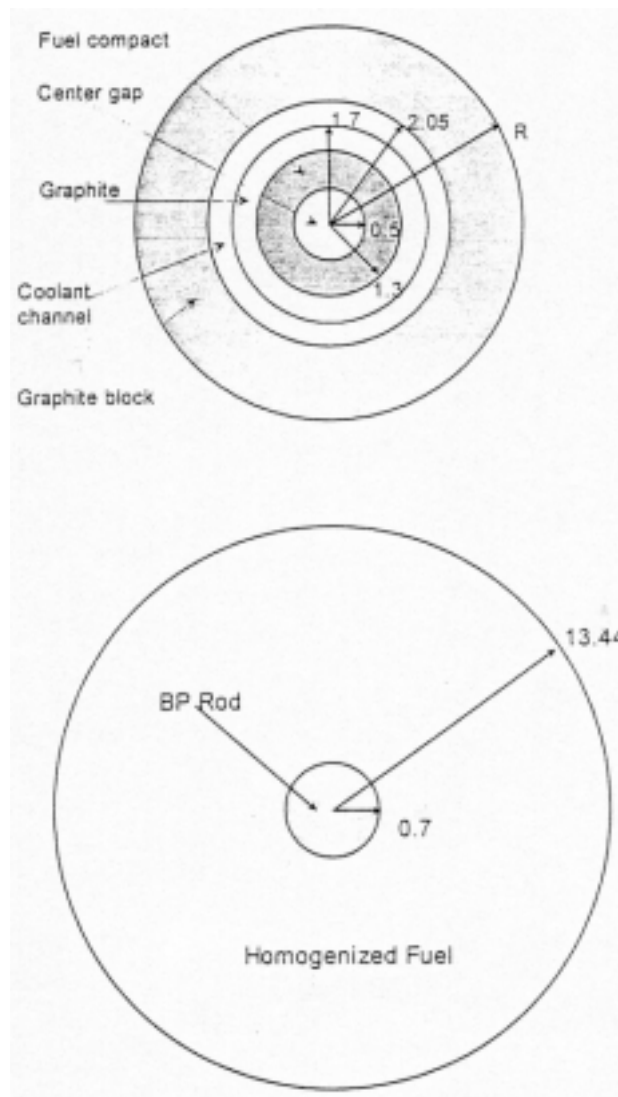

FIG. 2.64. Fuel and BP Cell model for the SRAC code calculation (all units in cm.).

Table 2-54. Calculated infinite multiplication factors (k_∞)
for Fuel Cell and BP Cells

Fuel Layer	Fuel block ID	Infinite mult. factor (k_∞)	
		Fuel Cell	BP Cell
1st layer	f673320	1.5446	1.3519
	f793320	1.5594	1.3872
	f943120	1.5996	1.4309
	f993120	1.6013	1.4397
2nd layer	f523325	1.5082	1.2566
	f633325	1.5375	1.3092
	f723125	1.5721	1.3469
	f793125	1.5782	1.3674
3rd layer	f433325	1.4786	1.2012
	f523325	1.5082	1.2566
	f593125	1.5470	1.2966
	f633125	1.5553	1.3116
4th and 5th layer	f343320	1.4259	1.1491
	f393320	1.4593	1.1979
	f433120	1.4932	1.2340
	f483120	1.5129	1.2653

2.2.4.2. Results of HTTR-FC Calculations

Multiplication factors (k_{eff}) and excess reactivity ρ for first criticality where all control rods are assumed to be fully withdrawn, are provided in Table 2-55. It indicates that the first criticality is to be achieved when 18 columns of fuel are inserted. The excess reactivity at first criticality was determined be 0.577 % Δk/k. At 17 columns, the k_{eff} was determined to be exactly one with zero excess reactivity, therefore the first criticality was estimated at 18th column.

Table 2-55. Effective multiplication factor and excess reactivity at first criticality.

Number of fuel column	Effective mult. factor [k_{eff}]	ρ [% Δk/k]
16	0.9979	-0.002
17	1.0000	0.000
18	1.0058	0.577

2.2.4.3. Results of HTTR-EX Calculation

Multiplication factors (k_{eff}) and excess reactivity ρ for 30 column, 24 column and 18 columns of fuel loaded into the core are shown in Table 2-56. The control rods were assumed to be in the fully withdrawn condition for all calculations.

Table 2-56. Effective multiplication factor and excess reactivity at 18, 24 and 30 column loaded in the core.

Number of fuel column	Effective mult. factor [k_{eff}]	ρ [% Δk/k]
18	1.0058	0.577
24	1.0692	6.472
30	1.0931	8.517

2.2.5. Netherlands

Both NRG and IRI are taking part in the benchmark of start-up core physics of the HTTR. To compare the performance of the SCALE based IRI code package with that of the WIMS/PANTHER code package of NRG, a calculational intercomparison has been performed. This report first describes the NRG and IRI efforts in the first Benchmark (Phase 1) using the Monte Carlo code KENO Va (3-D) and the diffusion theory codes BOLD VENTURE (2-D) and PANTER (3-D). In the second phase of the Benchmark, only KENO calculations are performed, for the scram reactivities of the core and reflector control rods and the isothermal temperature coefficients are given for phase 2. NRG/IRI also participated in the start-up measurement of reactivity and reactor noise measurements.

2.2.5.1. Computational Methods and Associated Data

The computational tools used at IRI for the cross section generation have been described previously [2-51]. In short it contains, as a branch, the SCALE-4 code system with master libraries produced by NJOY from the JEF-2.2 basic nuclear data files. The used reactor codes for this study are: KENO-Va and BOLD VENTURE. At ECN, the WIMS-7B code system has been used for this study which has libraries also based on JEF-2.2. The reactor code used at ECN is PANTHER-5.0.

Cross sections for use in KENO [2-50]

In KENO, only the coated fuel particles (CFP's) in the fuel compacts are homogenised with the graphite matrix of the fuel compacts; all other reactor components can be modelled explicitly. As the fuel also contains the only two resonant nuclides (^{235}U and ^{238}U) present in the core model, the only problem is the generation of cross sections for the homogenised fuel compacts. The general CFP and compact data are given in Table 2-57.

Table 2-57. General CFP and Compact Data

	radius (μm)	density (g/cm^3)	material
fuel kernel	298.5	10.79	UO$_2$
1st coating	358.5	1.14	PyC (low dens.)*
2nd coating	389.5	1.89	PyC
3rd coating	418.5	3.20	SiC
4th coating	464.5	1.87	PyC

*PyC: Pyrolitic graphite
Compact dimensions: i/o diameter = 1.00/2.60 cm, height = 3.91 cm.

Since the problem is similar to the generation of cross sections for the fuel pebbles of a pebble-bed type HTR, the following scheme was adopted from the analysis work for HTR-PROTEUS [2-51]:

1. First only the coated fuel particles inside a fuel rod are considered. An infinite close-packed hexagonal CFP lattice is calculated by BONAMI, NITAWL and XSDRNPM. XSDRNPM is run in spherical geometry for a white boundary elementary cell of the CFP lattice. This elementary cell contains two regions: a sphere of 0.0597 cm diameter which contains the fuel kernel of UO$_2$ surrounded by the homogenised mixture of the

coating layers and graphite matrix in the fuel compact. The matrix graphite contains some natural boron to represent impurities in the graphite. A cell-averaged weighted library, WGH(1), is produced which takes the self-shielding of the fuel in the Caps into account.

2. An infinite fuel-rod lattice is treated by BONAMI and NITAWL to obtain working library WRK(1). The unit cell with cylinder geometry has three regions. The innermost region is a channel filled with helium (0.5 cm radius). This region is surrounded by a cylinder of 1.3 cm radius with the fuel. The outermost region surrounding the fuel contains fuel block graphite (r = 3.29 cm). A triangular lattice is assumed with a pitch of 6.2668 cm, consistent with 1/33rd block for the 33-rods fuel block. This step is required because it provides the unweighted data for the materials outside the fuel region. The overall Dancoff factor for the core has been deduced from the Dancoff factors for a lattice of CFP's in a fuel compact and for a lattice of fuel rods in a fuel block [2-51].

3. The library WRK(1) cannot be used for the fuel-rod lattice cell calculation as it would not take into account the self-shielding in the CFP's. Therefore the WGH(1) and WRK(1) libraries are merged. All fuel-region materials are taken from the weighted library WGH(1), the other materials from WRK(1). The resulting library is called WRK(2).

4. XSDRNPM is run with working library WRK(2) for the unit cell of the infinite fuel-rod lattice. This unit cell of cylindrical geometry has five radial zones: 1. Channel with helium (r ≤ 0.5 cm). 2. Fuel zone (r ≤ 1.3 cm). 3. Graphite sleeve of fuel rod (r ≤ 1.7 cm). 4. Fuel hole in fuel block filled with helium (r ≤ 2.05 cm). 5. Fuel block graphite with reduced density to take the fuel handling hole into account. The radius is of this zone is 3.2903 cm (1/33rd fuel block). If no axial dimensions are used, this run yields the k_∞ of the fuel rod lattice. XSDRNPM is run with a buckling search option to get a critical system (by the addition of a leakage term in the form of $DB^2\phi$). The weighted library WGH(2) with zone-averaged cross sections is produced.

5. In order to obtain a working library for KENO, WGH(2) and WRK(1) are merged. The cross sections for the nuclides inside the fuel compact are taken from WGH(2), and the cross sections for all nuclides in the other components (He, C, ^{10}B, and ^{11}B) are taken from WRK(1). The resulting library is denoted as WRK(3).

No group collapsing is done in any of these steps. All libraries contain cross section data for 172 energy groups! A simpler scheme would have been possible if no comparison had to be made for two-groups cross sections.

Two-group cross sections

In total, five two-group cross-section libraries have been generated for comparison purposes:

1. GRLAT2GR: XSDRNPM output of step 1 but with condensation
2. RODLAT_K: output of XSDRNPM k-calculation using WRK(1) as input (step 2)
3. HTTR_K: output of step 4 XSDRNPM, k-calculation and using WRK(2) as input
4. HTTR_B2: output of step 4 XSDRNPM, buckling search using WRK(2) as input

5. RODLAT_B2: output of XSDRNPM, buckling search and using WRK(1) as input (step 2)

The order of the numbers in Tables 2-58 and 2-59 correspond to this order. These five sets enable the assessment of the effects of step 1, the separate treatment for the coated particles, and of the spectrum used for weighing (buckling search versus k-calculation). Table 2-58 lists the microscopic total (MT = 1), absorption (MT = 27), and transport (MT = 1000) cross section for the nuclides in the fuel compact. For the uranium isotopes ^{235}U and ^{238}U also the total number of fission neutrons (MT = 452), and the fission (MT = 18) and capture (MT = 101) cross-section are specified in Table 2-59.

Table 2-58. Two-group cross sections for nuclides in the fuel compact (5.2 w% enrichment)

nuclide	σ_{tot} (b)		σ_{abs} (b)		σ_{tr} (b)	
	group 1	group 2	group 1	group 2	group 1	group 2
^{10}B	26.86	1132.4	24.49	1130.3	39.62	1446.0
	47.49	2147.2	45.16	2145.0	34.45	3074.8
	49.40	2157.8	47.07	2155.6	29.67	3080.0
	45.26	2095.3	42.92	2093.2	34.56	2214.5
	44.19	2096.0	41.85	2093.8	34.59	2246.6
^{11}B	4.239	4.871	6.414 E-5	1.620 E-3	2.796	3.970
	4.267	4.941	8.961 E-5	3.073 E-3	2.686	4.757
	4.274	4.945	9.209 E-5	3.088 E-3	2.608	4.762
	4.223	4.941	8.706 E-5	2.999 E-3	3.441	4.666
	4.225	4.937	8.562 E-5	3.000 E-3	3.436	4.666
C	4.128	4.752	1.295 E-4	1.000 E-3	2.808	3.988
	4.157	4.805	1.567 E-4	1.891 E-3	2.693	4.857
	4.164	4.808	1.576 E-4	1.900 E-3	2.617	4.862
	4.114	4.805	1.673 E-4	1.845 E-3	3.373	4.727
	4.116	4.803	1.647 E-4	1.846 E-3	3.369	4.729
O	3.754	3.889	1.231 E-3	5.561 E-5	7.760	9.647
	3.752	3.943	1.293 E-3	1.062 E-4	2.701	3.840
	3.751	3.912	1.295 E-3	1.054 E-4	2.654	3.794
	3.736	3.910	1.437 E-3	1.023 E-4	3.189	3.757
	3.740	2.941	1.407 E-3	1.036 E-4	3.185	3.790
Si	2.669	2.113	2.644 E-3	5.057 E-2	2.050	1.807
	2.612	2.176	3.548 E-3	9.593 E-2	2.382	2.187
	2.605	2.178	3.621 E-3	9.640 E-2	2.399	2.190
	2.652	2.174	3.570 E-3	9.361 E-2	2.356	2.133
	2.651	2.173	3.511 E-3	9.363 E-2	2.353	2.134
^{235}U	22.93	177.5	12.52	163.2	88.03	733.5
	28.80	366.3	18.20	351.5	22.22	543.2
	29.00	363.6	18.39	349.0	19.18	534.0
	27.53	352.2	17.08	337.6	21.45	374.3
	27.60	356.8	17.12	342.1	21.96	385.8
^{238}U	14.77	10.08	1.775	0.853	64.94	26.97
	17.71	10.87	3.779	1.545	22.11	11.52
	15.86	10.79	2.879	1.534	14.31	11.38
	15.47	10.75	2.670	1.492	12.65	10.79
	17.27	10.84	3.541	1.510	15.24	10.92

Table 2-59. Total fission neutrons and fission and capture cross section of uranium isotopes

|	ν		σ_{fis} (b)		σ_{capt} (b)	
nuclide	group 1	group 2	group 1	group 2	group 1	group 2
^{235}U	2.440	2.439	8.457	137.8	4.066	25.42
	2.437	2.438	11.82	299.9	6.378	51.63
	2.437	2.438	11.92	297.7	6.462	51.25
	2.438	2.438	11.12	288.0	5.962	49.67
	2.438	2.438	11.16	291.8	5.967	50.31
^{238}U	2.736	2.489	4.581 E-2	3.577 E-6	1.729	0.853
	2.740	2.489	4.628 E-2	6.640 E-6	3.732	1.545
	2.741	2.489	4.610 E-2	6.591 E-6	2.833	1.534
	2.742	2.489	5.093 E-2	6.407 E-6	2.619	1.492
	2.741	2.489	5.023 E-2	6.486 E-6	3.491	1.510
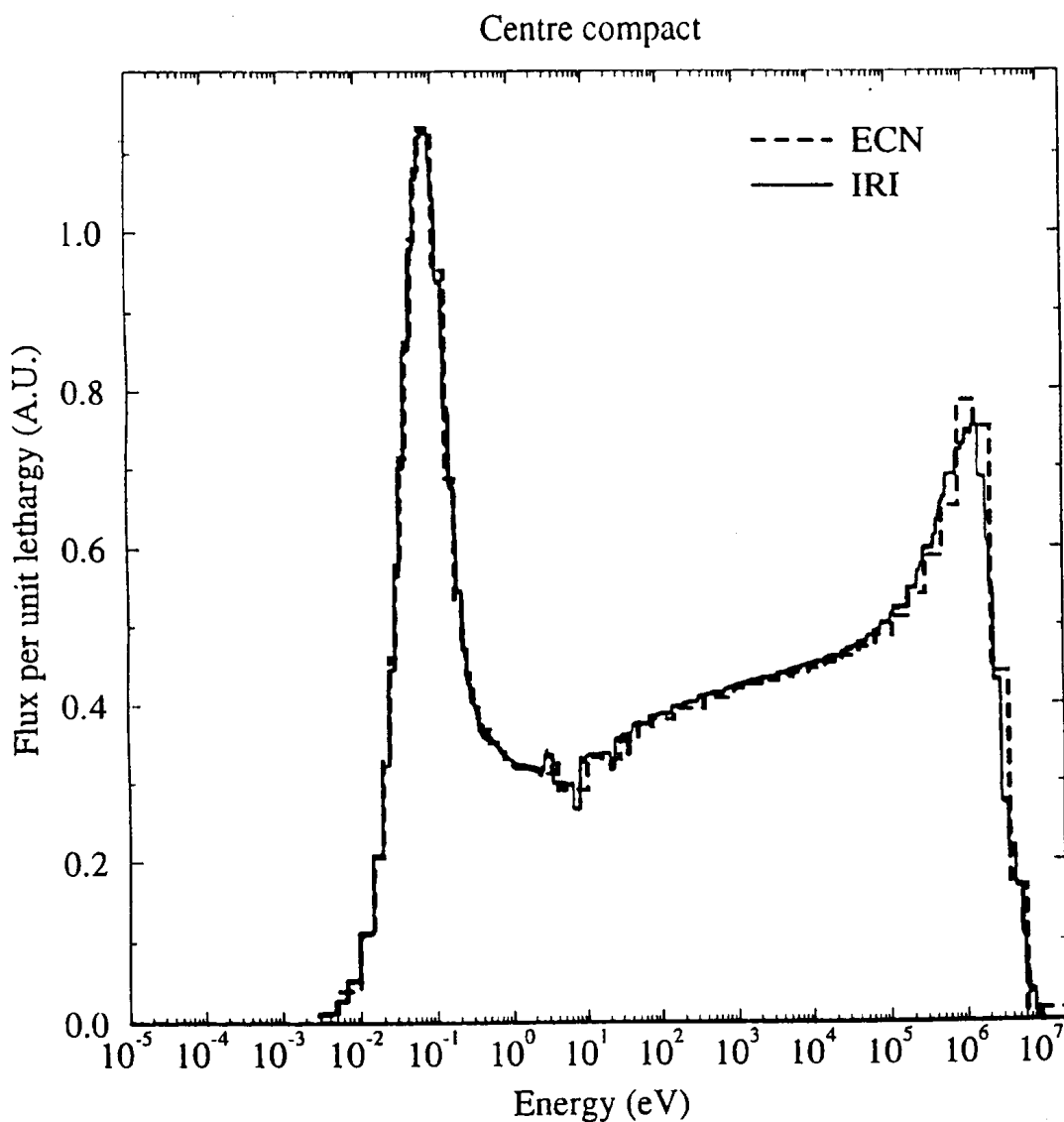
FIG. 2.65. Neutron spectrum in the centre of the compact

The spectrum in the grain lattice is much harder than in the fuel-rod lattice, which explains the lower values of the cross sections. The extra leakage term in the buckling search is seen to slightly reduce the cross sections, because of the greater leakage of low energy neutrons compared to high energy neutrons. Figure 2.65 shows the spectrum in the centre of the fuel-rod lattice, as calculated with step 4 of the cross-section generation procedure.

Cross sections for BOLD-VENTURE [2-50]

In BOLD VENTURE the core region is represented by five rings, containing the A, B, C, D, and E labelled columns, respectively. The material in each ring is completely homogenised. In order to maintain the reaction rates, the cross-section generation procedure for KENO was extended.

The first three steps are identical to the procedure for KENO. The fourth step is similar, but now a cell weighting is performed instead of a zone weighting. Subsequent steps are new.

4. XSDRNPM is run with working library WRK(2) for the unit cell of the infinite fuel-rod lattice. This unit cell of cylindrical geometry has five radial zones: 1. Channel with helium ($r \leq 0.5$ cm). 2. Fuel zone ($r \leq 1.3$ cm). 3. Graphite sleeve of fuel rod ($r \leq 1.7$ cm). 4. Fuel hole in fuel block filled with helium ($r \leq 2.05$ cm). 5. Fuel block graphite with reduced density to take the fuel handling hole into account. The burnable poison rods are not taken into account. The radius of this zone is 3.2903 cm (1/33rd fuel block). XSDRNPM is run with a buckling search option to get a critical system (by the addition of a leakage term in the from of $DB^2\phi$). The weighted library WGH(2) with cell-averaged cross sections is produced.

5. Unweighted cross sections for the materials outside the fuel blocks (i.e. inside the control rod guide blocks and reflector) have to be added to WGH(2). These unweighted cross sections of C, ^{10}B, and ^{11}B, were taken from WRK(1). The resulting library is called WRK(3).

6. XSDRNPM is run with library WRK(3) for a 1D-model of the reactor. This model contains six radial zones. The first five represent the five rings of the core region, the outermost zone represents the permanent reflector. The radii of the zones were calculated to be 19.0064 cm, 50.2861 cm, 82.8468 cm, 115.6112 cm, 148.4444 cm, and 214.9814 cm. With these radii, the area of the rings is identical to the true area of the columns (the pitch in the core region is taken to be 18.1 cm, hence the space between the blocks is taken into account). The material within each zone is completely homogenised. The atomic densities in the homogenised zones can be found in the appendix. Note that the burnable poison rods are not taken into account. XSDRNPM is run with a buckling search option and with zone weighting, producing weighted library WGH(3). For the homogenised KENO model the 172 groups were not condensed, for BOLD VENTURE the groups were condensed to 13 broad groups, like for HTR-PROTEUS [2-52].

Two-group cross sections

Two-group cross section data is obtained by condensing the 172 fine groups to 2 broad groups in step 6 of the procedure in section 2.2.1. The results are summarised in Tables 2-60 thru 2-63.

Table 2-60. Two-group cross sections for the uranium isotopes in the fuel compact (5.2 w% enrichment) in the radial zones B, C, and D.

nuclide		σ_{tot} (b)		σ_{abs} (b)		σ_{tr} (b)	
		group 1	group 2	group 1	group 2	group 1	group 2
^{235}U	B	27.79	368.3	17.18	354.2	21.30	372.4
	C	29.13	378.6	18.39	364.5	23.47	372.8
	D	27.34	380.8	16.78	366.7	21.04	385.3
^{238}U	B	15.71	10.47	2.716	1.544	12.34	10.45
	C	16.08	10.50	2.929	1.581	12.11	10.45
	D	15.59	10.50	2.651	1.589	12.26	10.48

Table 2-61. Two-group cross sections for the uranium isotopes in the fuel compact (5.2 w% enrichment) in the radial zones B, C, and D.

nuclide		ν		σ_{fis} (b)		σ_{capt} (b)	
		group 1	group 2	group 1	group 2	group 1	group 2
^{235}U	B	2.438	2.438	11.18	302.3	6.000	51.94
	C	2.438	2.438	11.92	311.1	6.469	53.44
	D	2.439	2.438	10.93	313.0	5.846	53.72
^{238}U	B	2.742	2.489	5.486 E-2	6.640 E-6	2.661	1.544
	C	2.741	2.489	4.884 E-2	6.805 E-6	2.880	1.581
	D	2.742	2.489	5.667 E-2	6.841 E-6	2.595	1.589

Table 2-62. Two-group cross sections for the non-fissionable nuclides in the fuel compact (5.2 w% enrichment) in radial zones B, C, and D.

nuclide		σ_{tot} (b)		σ_{abs} (b)		σ_{fis} (b)	
		group 1	group 2	group 1	group 2	group 1	group 2
O	B	3.807	3.775	1.543 E-3	1.063 E-4	3.350	3.620
	C	3.814	3.773	1.371 E-3	1.090 E-4	3.394	3.620
	D	3.805	3.773	1.590 E-3	1.096 E-4	3.351	3.619
Si	B	2.730	2.106	3.694 E-3	9.728 E-2	2.500	2.059
	C	2.672	2.108	3.707 E-3	9.978 E-2	2.455	2.059
	D	2.749	2.108	3.683 E-3	1.003 E-1	2.501	2.061
C	B	4.177	4.639	1.779 E-4	1.917 E-3	3.515	4.566
	C	4.220	4.636	1.647 E-4	1.966 E-3	3.609	4.568
	D	4.163	4.635	1.813 E-4	1.977 E-3	3.510	4.564
^{10}B	B	45.86	2177.5	43.47	2175.3	34.01	2199.1
	C	49.71	2233.4	47.33	2231.3	39.40	2201.1
	D	44.63	2245.6	42.23	2243.5	33.07	2266.9
^{11}B	B	4.287	4.778	8.849 E-5	3.116 E-3	3.593	4.498
	C	4.332	4.778	9.315 E-5	3.197 E-3	3.690	4.497
	D	4.273	4.778	8.700 E-5	3.214 E-3	3.589	4.501

Table 2-63. Two-group cross sections for the nuclides in the graphite of the blocks in all radial zones

nuclide		σ_{tot} (b)		σ_{abs} (b)		σ_{fis} (b)	
		group 1	group 2	group 1	group 2	group 1	group 2
C	A	4.290	4.810	1.178 E-4	2.185 E-3	3.442	4.772
	B	4.130	4.844	1.440 E-4	2.039 E-3	3.418	4.774
	C	4.183	4.846	1.351 E-4	2.095 E-3	3.528	4.776
	D	4.113	4.847	1.463 E-4	2.106 E-3	3.412	4.779
	E	4.347	4.815	1.161 E-4	2.580 E-3	3.500	4.786
reflector		4.524	4.818	1.274 E-4	2.858 E-3	3.971	4.838
^{10}B	A	57,31	2483.0	54.99	2480.7	38.79	2600.2
	B	46.77	2316.6	44.43	2314.4	34.60	2344.3
	C	50.72	2380.7	48.40	2378.5	40.15	2345.5
	D	45.50	2393.3	43.16	2391.1	33.63	2424.5
	E	65.21	2933.7	62.91	2931.5	38.77	2788.0
reflector		97.35	3251.3	95.12	3249.1	79.34	3168.6
^{11}B	A	4.404	4.976	1.017 E-4	3.554 E-3	3.515	4.701
	B	4.239	4.995	8.824 E-5	3.316 E-3	3.495	4.705
	C	4.294	5.003	9.325 E-5	3.407 E-3	3.609	4.705
	D	4.221	5.004	8.666 E-5	3.425 E-3	3.490	4.718
	E	4.462	5.020	1.116 E-4	4.199 E-3	3.583	4.721
reflector		4.640	5.052	1.519 E-4	4.654 E-3	4.066	4.755

Cross sections for PANTHER

Cross sections for the reactor code PANTHER have been generated by means of the code suite WIMS-7B. Apart from service modules for group condensing and material homogenisation, two collision probability modules were used to calculate the flux weighted cross sections of the fuel cell (PROCOL) and for the fuel blocks or assemblies, control guide blocks and reflector blocks (PIJ).

In order to avoid much extra work, densities, impurities and sizes of graphites, CFPs and coatings, weighted means of these parameters where appropriate, have been derived to be used all over the reactor. This leads to the following standardised parameters for the CFPs (Table 2-64).

Table 2-64. Parameters for CFPs

	radius (μm)	density (g/cm^3)	material
fuel kernel	297.95	10.774	UO_2
1st coating	358.80	1.127	PyC (low density)
2nd coating	389.45	1.896	PyC
3rd coating	418.35	3.225	SiC
4th coating	464.20	1.866	PyC

Compact dimensions: i/o diameter = 1.00/2.60 cm, height = 3.91 cm.

Table 2-65. Parameters for Graphites

	density (g/cm^3)	impurity (ppm B$_{nat}$)
matrix	1.690	0.82
sleeve	1.770	0.37
fuel / control block	1.770	0.40
repl. reflector	1.760	0.37
perm. reflector	1.732	1.91

PROCOL [2-50]

In the WIMS-suite a cell module PROCOL, based on collision probabilities, exists to calculate fluxes in systems with spherical grains packed in a matrix with an annular geometry.

A cell radius of 3.29 cm has been used, consistent with a lattice of a 1/33rd part of a fuel block or assembly, in which explicitly modelled: the inner gas channel (r = 0.50 cm), the compact (r = 1.30 cm), the gas gap (r = 1.3125 cm), sleeve (r = 1.70 cm) and the fuel hole drilling in the fuel block (r = 2.05 cm). Using this model, flux weighted cross sections are obtained for homogenised CFP's + matrix + gas gap, to form the compact material with cross sections in the 69 neutron energy groups structure of the library.

The spectrum in the centre of the inner gas channel in the compact with 5.2 w% enrichment is shown in Figure 2.65. Comparison with the spectrum as obtained with the KENO cross sections is very good. Differences are only due to the resolution of the spectrum with the number of energy groups used in the calculations (KENO: 172 vs. WIMS: 69).

Accordingly obtained cross sections were condensed to 16 neutron energy groups for subsequent use in the WIMS assembly module PIJ, which calculates collision probabilities in multi-pin assembly systems.

For comparison purposes microscopic cross sections for the nuclei present in the compacts were condensed to two group cross sections. In WIMS only microscopic absorption and fission cross sections are easily available, but for some elements transport and total cross sections could be deduced from macroscopic cross sections. Values for an enrichment of 5.2 w% are given in the Tables 2-66 and 2-67 and can be compared with those values given in Tables 2-58 and 2-59. Agreement is in general rather good which can be confirmed by the spectrum comparison of Figure 2.65 and the calculated neutron multiplication factors: k_{inf} = 1.499 for the 'KENO'-cell and k_{inf} = 1.493 for the 'PROCOL'-cell.

Table 2-66. Comparative two group cross-sections (5.2 w% enrichment)

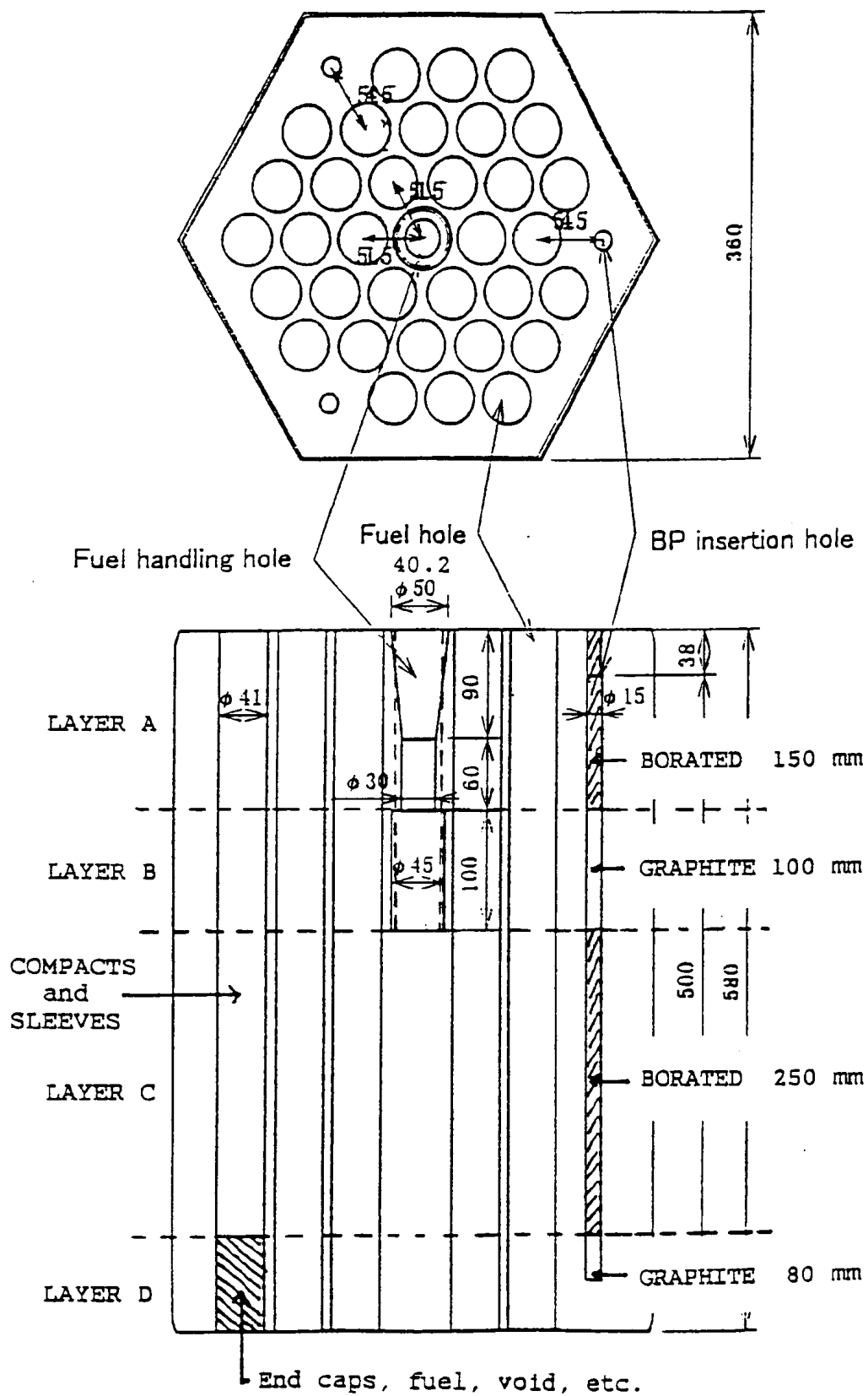| nuclide	σ_{tot}(b) group 1	group 2	σ_{abs}(b) group 1	group 2	σ_{tr}(b) group 1	group 2
^{10}B			42.20	2095		
C	4.086	4.805	1.882E-4	1.856E-3	3.348	4.702
O			1.527E-3	1.029E-4		
Si			3.623E-3	9.397E-2		
^{235}U			1.692E+1	3.397E+2		
^{238}U			2.747	1.499		

FIG. 2.66. Axial composition of the fuel block in PIJ.

Table 2-67. Uranium isotope fission neutrons and fission and capture cross-sections (5.2 w% enrichment)

	ν		σ_{fis}(b)		σ_{capt}(b)	
	group 1	group 2	group 1	group 2	group 1	group 2
^{235}U	2.438	2.438	1.096E+1	2.897E+2	5.968	49.91
^{238}U	2.742	2.489	5.768E-2	6.437E-6	2.689	1.499

PIJ [2-50]

For modelling in PIJ the fuel assembly has been adapted in the following way:

1. The stack of compacts has been moved to the top such that the upper rim of the upper compact is flush with the fuel block,
2. The upper graphite plug and buffer plate has been moved to the bottom,
3. The stack with the burnable poison (BP) pellets and graphite disks has been moved to the top as in 1, while the length of the upper section of the BP stack has been changed from 20 cm to 15 cm and the lower section to 25 cm
4. The fuel handling hole has been simplified by taking an effective diameter of 4.017 cm and a length of 25.0 cm.

This way four layers in the assembly can be created (See Figure 2.66):

1. First layer of 15 cm height with compacts, fuel handling hole (FHH) and BP pellets,
2. Second layer of 10 cm with compacts, FHH and graphite disks,
3. Third layer of 25 cm with compacts, graphite for FHH and with BP pellets,
4. Fourth layer of remaining 8 cm with a mix of 4.75 cm of compact, 2.35 cm of graphite and 0.9 cm of void at the fuel positions and graphite at the FHH and BP positions.

The void has been modelled in the empty BP insertion leg.

For each layer a model of the fuel assembly has been laid out in which the hexagonal perimeter has been replaced by an equivalent circle (radius 19.01 cm). Within this circle the fuel positions (comprising: inner gas space, compact, sleeve and outer gas space), FHH and BP insertion holes are modelled at the exact positions and filled with the materials in conformance. This circle in turn is surrounded by another circle (radius 38.01 cm), divided into 12 segments, to accommodate the matching surrounding materials for the fuel assembly under study (Figure 2.67). It makes a total of 206 material regions per assembly layer.

The coolant bearing reflector blocks in the 1st, 2nd and 8th reactor layer are modelled in the same way but with empty fuel holes and of reduced diameter.

To reduce the number of materials, the PIJ model is finally divided into seven regions: one central region comprising the FHH position and the six inner fuel positions, and the six surrounding segments (Figure 2.67). Materials within a region are homogenised or smeared to one material. Finally the seven materials for the four layers are smeared, according to their height, to seven final materials for one assembly having flux weighted cross sections in 16 neutron energy groups.
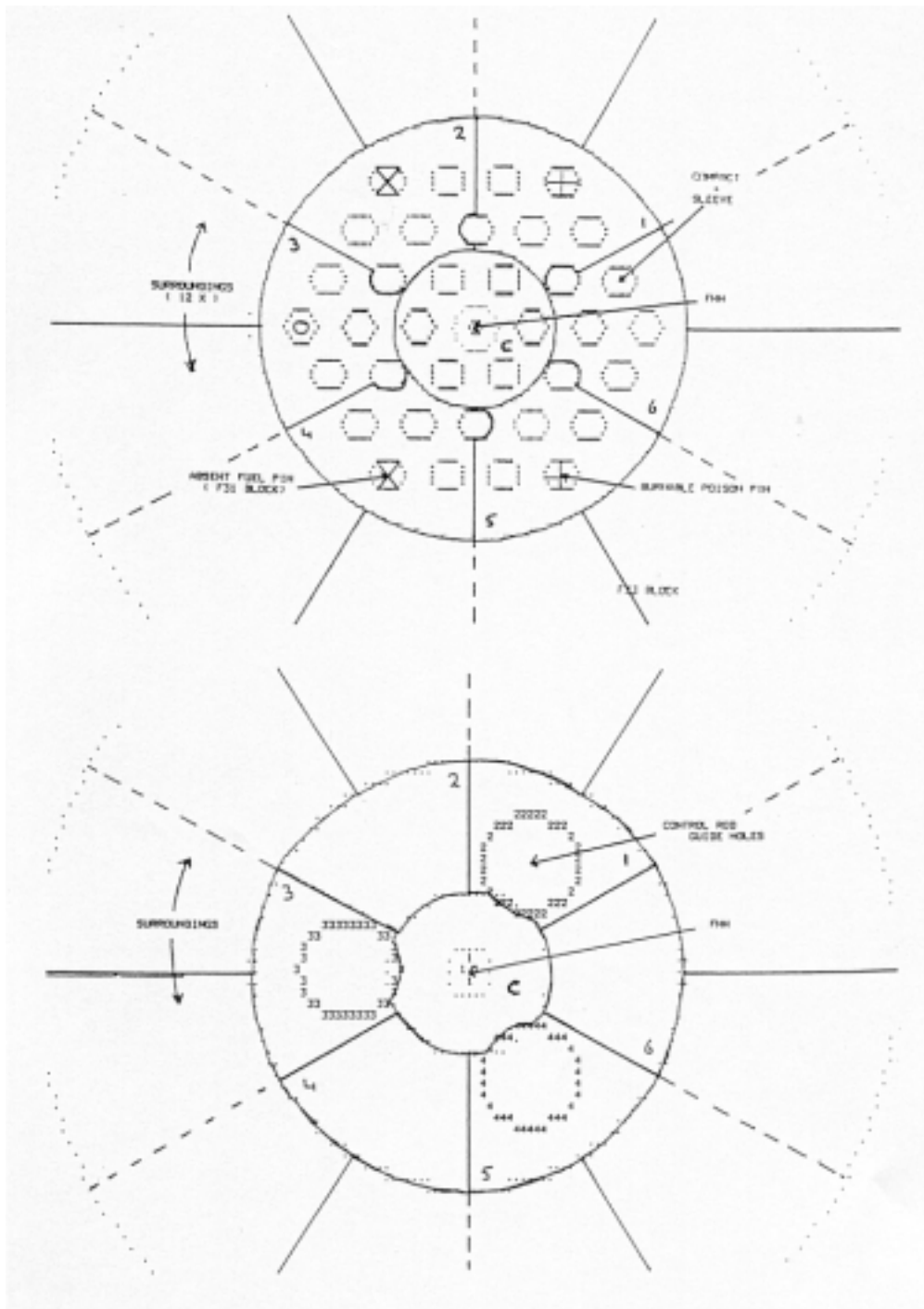
FIG. 2.67. Radial composition of the fuel and control guide block in PIJ.

The procedure for the control guide blocks (Figure 2.67) and reflector blocks is similar; also divided into seven regions but with only two layers, with and without FHH.

The advantage of the sub-division in seven regions is that the anomalies in a block, like BP stacks, absent fuel pins, control guide holes, control rods, etc. are confined to only one region a piece and are not smeared over the entire block. This allows for more pronounced local absorption and/or streaming, which form major problems for modelling this kind of reactor cores.

For all 48 different block configurations (enrichments, block types, surroundings, etc.) two runs with PIJ were done; first a run without control rods (unrodded) and a second run with control rod material modelled in the control guide holes and using rodded material in that sector of the surrounding where present (rodded). Afterward all cross sections were condensed to two energy groups ($E_{th} = 2.1$ eV) and organised in such a way that it can be used in the reactor code PANTHER, leading to 336 different materials in as well a rodded state as an unrodded state.

By making use of the modules PROCOL and PIJ the double heterogeneity formed by the CFP's and the fuel rods has been modelled explicitly and therefore no Dancoff factor has to be introduced.

2.2.5.2. Results of HTTR first criticality (Phase 1) [2-53]

The KENO model is a very detailed model of the HTTR in which practically all components are modelled explicitly, with the following exceptions:

1 As mentioned before, the coated fuel particles were homogenised with the graphite matrix of the fuel compacts.
2 It is not possible to model hexagonal blocks in KENO-Va. Therefore, the permanent reflector was approximated by a cylinder of 214.98 cm radius which preserves the volume of the actual reflector. Furthermore, the hexagonal blocks in the core and in the replaceable reflector were represented by cylinders of 36 cm diameter (the distance between the parallel faces of the blocks). These cylinders (which contain all fuel rods and the two burnable poison rods or all coolant channels) were placed in a large cylinder of graphite with a radius of 162.9 cm (Figure 2.68).

In the BOLD VENTURE model the HTTR is represented by an R-Z model. It contains six zones in the radial direction, and nine in the axial direction, one for each layer. The six radial zones are the:

1. Central control rod guide column (column A)
2. First fuel zone (the six B columns)
3. Second fuel zone (the 12 C columns: 6 fuel columns and 6 control rod columns)
4. Third and fourth fuel zone (the 18 D columns)
5. Replaceable reflector (the 24 E columns)
6. Permanent reflector
    The height of each layer is 58 cm, except layer 9 (42.9 cm). The radii of the zones are: 19.01, 50.29, 82.85, 115.61, 148.44 and 214.98 cm. Calculations were performed with a 2 cm mesh, both in axial as radial direction and the BP rods were simulated by adding boron to the radial zones B, C and D to such an extend that a reactivity change, as determined by auxilary KENO calculations, was reached.

For PANTHER a 3-D model has been developed in a hexagonal representation, taking a cluster of seven sub hexes (size: 13.68 cm flat-to-flat) per hexagonal reactor assembly position in the radial direction and 5 layers per assembly in the axial direction. This leads to 937 radial reactor channels with an equivalent radius of 220 cm and 45 axial layers of 11.6 cm.
Control rods, those left partially inserted in the E-column ring, reached only till the bottom level of the upper block (464 cm level).
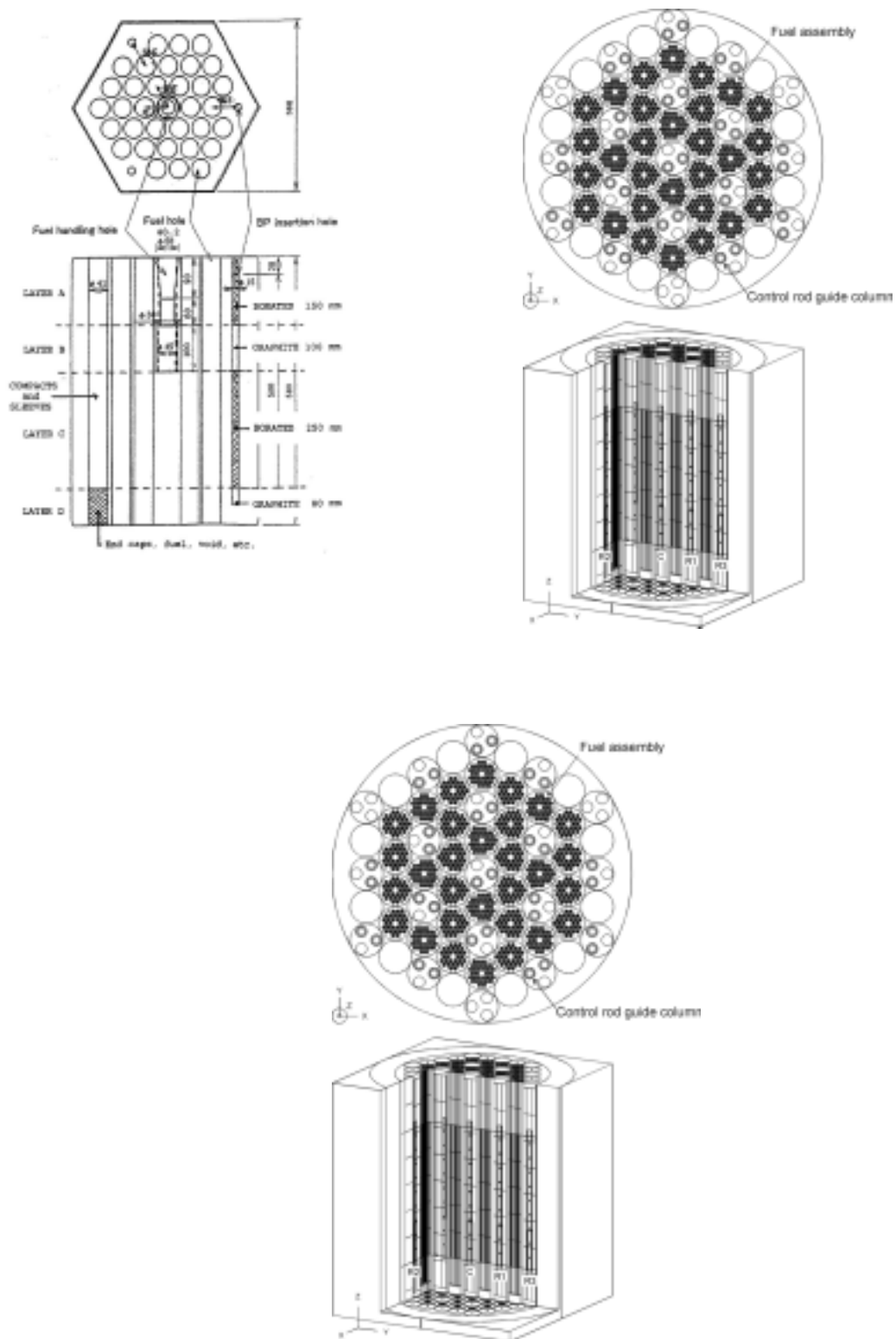
FIG. 2.68. Fuel assembly (upper left), the KENO model for the critical reactor (upper right, and the KENO model for scram with all control rods (C, R1, R2 and R3) (lower).

Materials defined and prepared in the WIMS data generation phase has been laid down according to proper compositions and orientations of the reactor assembly blocks in the reactor. For the simple core all enrichments were set at 5.2 w%.

In PANTHER the assemblies which carry control rods are represented by two sets of nuclear data: one set for the part where is no control rod inserted (unrodded) and a set for the rodded part. The control rod insertion depth for a certain control rod bank determines whether PANTHER uses the set for the rodded material or for the unrodded material in a particular mesh, thus enabling to drive a control rod.

The results of the calculations by the different codes are presented in Table 2-68. Good agreement can be found between the KENO and PANTHER results, the higher k_{eff} values for BOLD VENTURE can be attributed to neutron streaming in the control rod guiding holes
.

Table 2-68. Comparison of the results

	KENO	BOLD-VENTURE	PANTHER	Measured
k_{eff} simple core	1.1278 ± 0.0005	1.1592	1.1251	
k_{eff} fully loaded core				
- rods withdrawn	1.1584 ± 0.0005	1.1974	1.1595	
- rods inserted	0.6983 ± 0.0005		0.7510	0.685 ± 0.010
critical insertion				
- above bottom core	170.5 cm		161.5 cm	178.9 cm

2.2.5.3. Results HTTR-CR and HTTR-TC for Phase 2 [2-53]

The second benchmark of the HTTR core physics (Phase 2), defined by JAERI (Yamashita et.al.,1999b), were also calculated by using the Monte-Carlo code KENO-Va (V4.3) for a fully loaded core with 30 fuel elements and are presented in the Working Material of the IAEA meeting (CRP-5, 1999 and Türkcan et.al.,1999).

In Phase 2 the following answers were requested by the organisers:

- Scram reactivities (control rod worth) for the control rods at critical position and after a scram of the reflector control rods (HTTR-SR) and after a scram with all the control rods (HTTR-SA), both at a temperature of 300K.
- Isothermal temperature coefficients for a fully loaded core from 280K to 480K in six temperature steps (HTTR-TC). Where the control rod settings (C, R1 and R2) have slightly different settings due to a temperature elevation and the critical insertion of the control rods C, R1 and R2, (R3 stays fully out) at 480K.

For the new benchmark calculations, new cross-sections were prepared for seven different temperatures using the aforementioned procedure. The resulting cross section libraries contain data for 172 neutron energy groups. The geometry input for KENO is revised to be able to calculate the questions of the benchmark. The KENO model for a critical reactor and with all control-rods inserted is shown in Figure 2.69. The results of the benchmark-phase 2 will be summarised.

The scram reactivity of control rods ($\Delta k/k$) is defined by:

$$\rho_R = \frac{k_{Crit} - k_{RCR-in}}{k_{Crit}.k_{RCR-in}}$$

With: $k_{Crit.}$: Effective multiplication factor at critical CR position
and k_{RCR-in}: Effective multiplication factor at CR position after scram.

Table 2-69 provides the scram reactivity for two different scram conditions. Also given are the calculated and measured scram reactivities (Fujimoto et.al.,1999).

Table 2-69. Scram Reactivities (Using KENO)

CR Group	Critical position (mm) HTTR-Crit	Position after scram (mm) HTTR-SR	Position after scram (mm) HTTR-SA
C	1789	1789	-41
R1	1789	1789	-41
R2	1789	-41	-41
R3	Full out	-41	-41
k_{eff} (average)	1.0093 ± 0.000	0.9178 ± 0.0005	0.6809 ± 0.0005
ρ_{calc}		0.0988 ± 0.0007	0.4778 ± 0.0007
ρ_{meas}		0.120 ± 0.012	0.46 ± 0.04

The results using PANTHER calculations include the following:

K_{eff} at critical position = 1.0088; K_{eff} after scram HTTR-SA = 0.7317; ρ = 0.375

This scram reactivity is too low but can be explained by neutron streaming in the control rod holes and is to be recalculated by means of anisotropic cross section

In the second question of the benchmark, the isothermal temperature coefficients (HTTR-TC) for a fully loaded core between temperatures 280K to 480K (in six steps) were asked, where the control rods C, R1, and R2 have slightly different settings due to temperature elevation (13 mm).

The effective multiplication factors should be calculated for the following temperatures: 280, 300, 340, 380, 420, 460 and 480 Kelvin and the isothermal temperature coefficients should be calculated at: 290, 320, 360, 400, 440 and 470 Kelvin. The insertion depth of C, R1, R2 is the same at level =1776 mm and R3 again is fully withdrawn. Also the critical position for those control rods at 480K, with R3 fully out, is requested for the benchmark.

The following relation should evaluate the isothermal temperature coefficients for a fully loaded core from the effective multiplication factors:

$$\rho_n = \frac{k_{n+1} - k_n}{k_{n+1}.k_n}.\frac{1}{(T_{n+1} - T_n)}$$

ρ_n : Temperature coefficient between T_n and T_{n+1} ($\Delta k/k/K$)
T_n : Core temperature at n^{th} measurement (K)
T_{n+1} : Core temperature at $n+1^{th}$ measurement (K)
k_n : Effective multiplication factor at T_n
k_{n+1} : Effective multiplication factor at T_{n+1}.

Results of the calculations are shown in Figure 2-69. The calculated isothermal temperature coefficient (average between 320K and 440K) is −14.7 (pcm/°C), while the measured value equals −14.2 (pcm/°C) on the average. The calculated critical control rod position at 480K is 1879 mm, while for the measurements at T= 395K; 1873 mm and at T= 418K; 1903 mm are found.

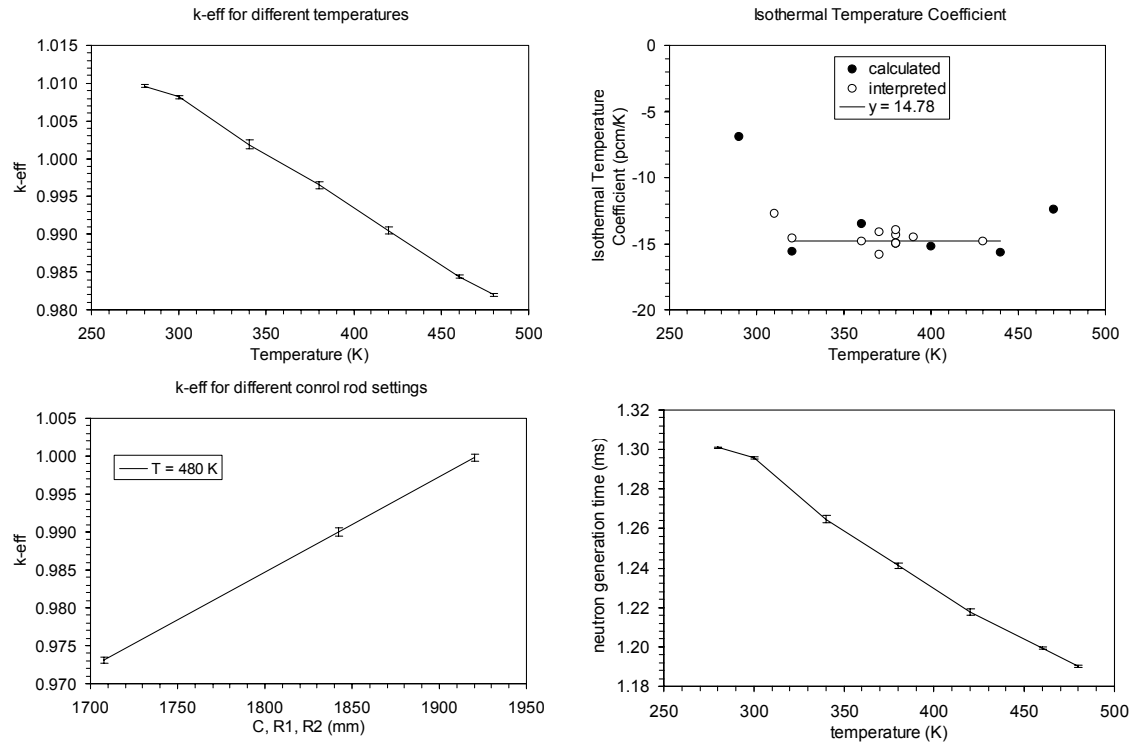The PANTHER value for ρ_{iso} = −15.2 (pcm/K), and the control rod position at 480K is calculated as 1934 mm.

Figure 2-69. The effective multiplication factor (upper left) and isothermal temperature coefficient at different core temperatures, the multiplication factor for the different control rod settings of C, R1, R2 while R3 fully out (lower left) and the neutron generation time versus core temperatures (lower right).

2.2.5.4. Reactivity and reactor noise measurements of the HTTR during the start-up Cores [2-53]

During the start-up phase of the HTTR at different core configurations, reactivity and the reactor noise measurements were carried out in parallel with measurements of the HTTR Physics group. For these measurements two temporary compensated ionization chambers CIC-A and B were used. Figure 2.70 shows the horizontal cross-section of the core and the positions of the detectors. Measurements were carried out by using the signal processing system DSA-2 (Türkcan, 1993) in real-time. During the on-line reactivity experiments, the measured DC signals were digitised and the reactivity is calculated by using the Inverse Kinetics Method (IK).

During the first critical approach after the loading of the 19th fuel assembly, the source criticality at very low power is achieved. For criticality, first the neutron source is removed and then by moving the central control rod (C) to compensate for the reactivity until the first criticality of the reactor is reached on Nov. 10 1998. Figure 2.71 shows the result of reactivity measurements during this approach to criticality.
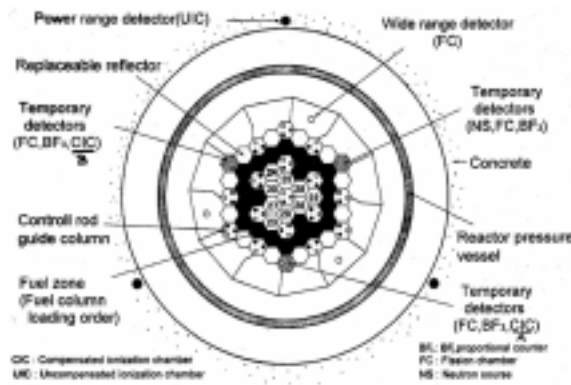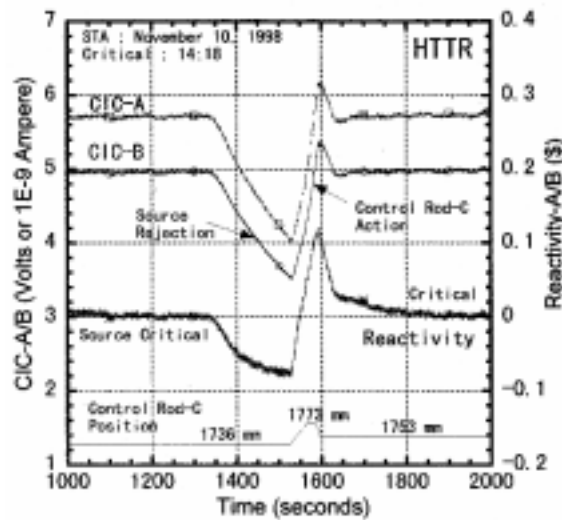
FIG. 2.70. HTTR horizontal neutron detector positions.

FIG. 2.71. Approach to criticality.

After each new few fuel loading, the reactivity value of the control rods were measured successively with the IK-method by the HTTR physics group and by DSA-2 system. As an illustration the experimental result is given in Figure 2.72 for full core with 30 fuel assemblies. By the move of a control rod with a small step, the neutron flux is increased while the reactor power is kept in the same power range by compensating the reactivity effect by another control rod. For each action where the reactivity is constant over about 80 seconds the calculated reactivity is averaged. This way the average reactivity worth of the control rod is determined for this stepwise change.
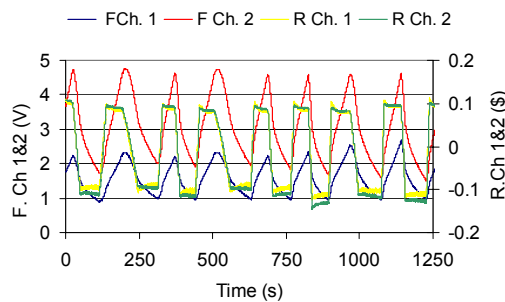

Fig. 2.72. Measured reactivity at HTTR full core. Two measured signals of Ch1 (A) and Ch2 (B) and the computed reactivity (blocks match each other, scale on right).

114

For the reactor noise measurements, the same neutron detector signals were used and the reactor at very low power is kept as stable as possible especially for this measurement. Signals were conditioned for the noise measurements by using high- and low-pass filters with a gain amplifier.

Inherent to this type of reactor, the neutron generation time is long and was calculated to be: 1.173±0.001 ms. The prompt neutron decay constant is quite close to the decay of the fastest delayed neutrons, therefore no intermediate plateau can be recognized in the measured spectral functions such as the Normalized Auto and Cross Power Spectral Density (NAPSD and CPSD).

Figure 2.73 is an example of the measurements on the 21 fuel element critical core at very low power. Our investigations indicated a shortcoming of the bandwidth of the used current amplifiers due to the large cable capacity of about 100-m of cable between the detectors and the amplifiers. This situation was not possible to change during the measurements.
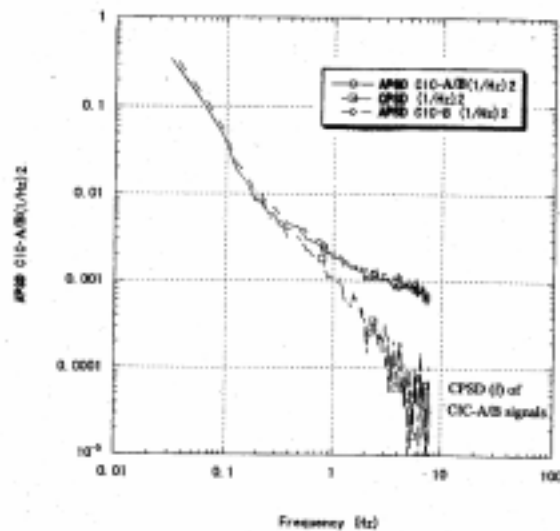

FIG. 2.73. The NAPSD(f) and the NCPSD(f) functions measured 21st fuel loading. The cross spectra do not give clear break frequency.
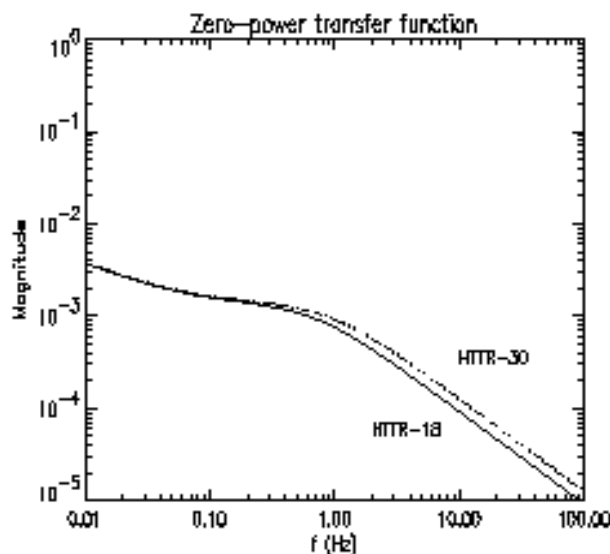

FIG. 2.74. Calculated Transfer functions for 18 and 30 fuel elements loading.

The measured coherence between the two neutron detector signals was 0.8 at 0.1 Hz and gradually decreased to 0.2 at 1 Hz and the phase between them practically zero. The calculation of the zero-power transfer function (Figure 2.74) for different number of fuel loading, the transfer function shape did not changed considerably.

2.2.5.5. Summary of results [2-53]

On the level of cell calculations a good agreement has been obtained between the cross sections and the spectra as prepared by the SCALE-system and as prepared by WIMS. Calculations with detailed geometry converged to very good agreement between the results of PANTER and the results of KENO with an exact geometrical model. In the second phase, KENO results gave very well the measured values of the scram reactivities as well as the estimation of the isothermal temperature coefficient within the requested temperature interval. Therefore, we can conclude that the Benchmark calculations of the start-up physics calculations were successful and that the results of the reactivity measurements and the reactor noise analysis done at the HTTR, using the DSA-2 system, resulted with a good agreement with the results of the HTTR Physics Group.

2.2.6 Russian Federation

2.2.6.1. General analysis method and model description

For benchmark calculations in the diffusion approximation, the computer codes WIMS-D/4 and JAR [2-54, 2-55] were used. MCU [2-56] and MCNP [2-57] codes, implementing the Monte Carlo method were used as reference.

WIMS-D/4 code [2-54] has been used for computation of few-group constants for fuel and the reflector blocks. The code is provided by 69 groups system of nuclear constants in neutrons retardation and thermalization range on the basis of estimated nuclear data in ENDF/B6 format. The characteristic feature of WIMS is a two-stage approach to solution of a task on spatial-energy neutron distribution in a reactor cell. In the first place, a detailed spectrum in 69 groups for every zone, typical for the cell is calculated: fuel, shell, coolant and moderator. Then cross-sections are convoluted to a specified few-group approximation, where detailed distribution of neutrons in geometric zones of the unit cell is calculated. The S_4-method was used in the first and second stages of the calculation. In calculations of spatial resonance screening the equivalence theorem is employed, with the help of which the heterogeneous problem comes to an effective homogeneous. Detailed matrices of scattering cross-sections for main moderators are employed in the neutron thermalization calculations.

For calculating of fuel cells with double heterogeneity of fuel allocation at the fuel particles and fuel compacts level in the cell, containing burnable poison rods, Segev algorithm [2-57] was used to calculate macro-sections for a cell, associated with a fuel compact. When using the Segev formalism to calculate parameters of fuel compact cell containing fuel particles, it is necessary to carry out calculation of three cell variants in cluster PIJ or PIJ-PERSEUS option:

a) a cell associated with fuel particle is calculated, whereby a kernel is represented as a rod with radius $r_c = 9/16\, r_{sph}$, on which matrix moderator and shells, related to one kernel is "spread". Radii of the rod and cell are chosen so that collision probability for neutron, born in fuel, would be the same in cylindrical of module and spherical geometry. At cell calculation by WIMS at the given stage a value of Dankoff factor for inner region of the cell (γ) is found;

b) a cell associated with annular fuel compact, in which the fuel and the compact matrix graphite are homogenized, is calculated. Panniculus equivalent of serves the shell from graphite, taking into account of gas, related to one compact, serves a layer of external moderator. At this stage, a value of Dankoff factor for outer region of the cell (Γ) is determined;

c) then γ_{input} is calculated:
$$\gamma_{input} = \cfrac{1}{1 + (1/\gamma - 1) \cdot \cfrac{Vm \cdot \Sigma m}{Vm \cdot \Sigma m + \cfrac{1/L}{1/A + 1/\Gamma - 1}}} \quad (1)$$

where V_m - volumetric fraction;
Σ_m - moderator scattering cross-section;
$L = M^{1/3} \cdot l_{cell}$; $\qquad\qquad\qquad\qquad\qquad\qquad\qquad\qquad (2)$
M - number of fuel particles;
l_{cell} - mean chord;
A - Bell factor.

The value of γ_{input} is set in WIMS and calculation as per point "b" is repeated. Resulting from the last calculation macroscopic cross sections and multiplication factor for a fuel compact cell with double heterogeneity are acquired. It is worth noting that value of γ_{input} weakly depends on fuel temperature and isotopic content in case of fixed geometrical parameters of a cell.

Basic results of diffusion calculations were obtained in two-group approximation with thermal and epithermal neutrons cut-off energy of 0.625 eV, selected from the condition of obtaining values of cross-sections for transition to higher energy close to zero, that is defined by the calculation model of scattering in the reactor code, that takes account of energy transitions only in direction with energy decrease.

In the case of the cell with burnable poison rods calculation, the same option of WIMS code was used, but poison rods in the cell was surrounded by effective fuel composition accounting shielding factors.

The macro-constants received at WIMS calculation stage were then accepted as input data for reactor calculations by JAR code. The JAR code [2-55] is based on the nodalization method and makes it possible to carry out three-dimensional analysis of reactor in few-group diffusion approximation. The reactor core and the reflectors in a calculations model are represented as hexagonal prisms, broken down on triangles and divided into axial zones.

For the diffusion calculations the effect of nonuniformity of poison in burnable rods through its height was not accounted. Burnable pellets and graphite pellets were homogenized in the vertical direction. The construction of control rods absorber through its height is considered as uninterrupted.

The MCU code [2-56] based on Monte-Carlo methodology employs a combination of DLC/MCUDAT-1 data libraries. MCU is used to compute a continuous spectrum of neutrons moderation within energy range 10^{-5} eV to 20 MeV, and to solve the neutron transport problem with an external source or criticality problems. To describe cross-sections in the field of unresolved resonance the subgroup dividing method is used, while for resolved resonance range the detailed description of cross-sections is possible on the basis of special data libraries.

MCNP code (Version 4A) [2-57] has been used to check results of the diffusion calculations. Nowadays the MCNP code is one of the most efficient computer codes, which employ the Monte Carlo methodology for analysis of high temperature gas-cooled nuclear reactors. Possibility of the MCNP code application for analysis of HTGRs with double heterogeneity of fuel allocation on the basis of comparison with other codes, was studied before. The heterogeneous model by MCNP was described so that each coated fuel particle was located in unit lattice by lattice geometry in fuel compact (not randomly).

Among essential features of MCNP, a capability to compute continuous spectrum of neutrons moderation within energy interval 0 to 20 MeV in approximation of point-by-point representation of nuclear data, should be pointed out. Point cross sections of neutrons interaction with nucleus were prepared by using of NJOY code in ENDF /B6 format. In criticality analysis a multiplication factor k_{eff} was estimated by three ways for larger reliability: viz.: estimation on collisions (col), estimation on absorption (abs), estimation on free track length (trk). Moreover, a combined estimation of k_{eff} based on the first three estimates was made.

For the Monte-Carlo calculations the detailed geometry was taken into account, but the presence of spacers on the fuel rod surface was not into account. Beside in the MCNP-4A code version the location of coated particles in graphite matrix is described in the form of cubic lattice.

Design model of the reactor (Figure 2.75) consists of nine layers of hexagonal fuel blocks and graphite blocks of reflector, divided into four subzones each. The reactor core includes reactivity compensation rods viz.: control rods and channels for the reserve shutdown system. It is supposed in the analysis, that the poison in the reactivity compensation rods is distributed axially without gaps, which actually are available in the rods and are about 6.45 % from the overall length of rod.

To calculate few-group cross sections and multiplication factor, the fuel block is modeled by an annular cell, area of which corresponds to 1/3 area of a fuel block; a burnable poison rod, a hole for it or a graphite disk are set in the center and surrounded by fuel, medium content of which corresponds to 1/3 of the block. The fuel content of the surrounding zone is homogenized taking into account a double heterogeneity of fuel arrangement and from condition to preserve multiplication factor value and migration parameters in the zone compared with a cell of the annular fuel compact (Figure 2.76).

Macro-cross sections of graphite reflector cells, including absorber rods or gas cavities for their location, were also calculated using the WIMS code. A calculation model of the cell is the following: in the center of the cell a cavity or an absorber rod (with detailed description of its geometry) is set, which is surrounded by a graphite ring with outer of radius, determined from the condition of surrounding graphite volume conservation. A layer, containing homogenized fuel content is used as an outer layer of the cell (for shaping spectrum).

Information about the codes, calculation models and nuclear data are summarized in Tables 2-70, 2-71 and 2-72.

Table 2-70. Codes, model and library of nuclear data for Diffusion calculations

Items	Name of Country	Russia
	Name of Institute	OKBM
Nuc. data file	ENDF/B6	
Fuel cell code	WIMS-D/4	
Theory	S4	
Model	Cylindrical cell	
Cut - off energy	0,625 eV	
No. of groups	69	
BP cell code	WIMS-D/4	
Theory	S4	
Model	Cylindrical cell	
No. of groups	69	
Control rod cell cal.	WIMS-D/4	
The theory	S4	
Model	Cylindrical cell with the central absorbing zone	
Number of groups	69	
Core cal. Code	JAR-3D	
Model	Triangular lattice (6 points / blocks)	
No. of groups (Fast + Thermal)	1+1	

Cavity for reserve
shutdown system

Control rods

Fuel block with
burnable poison rods

Fuel blocks with
different enrichment on
uranium-235

Bottom reflector block

a) reactor in plan

b) fuel column along height
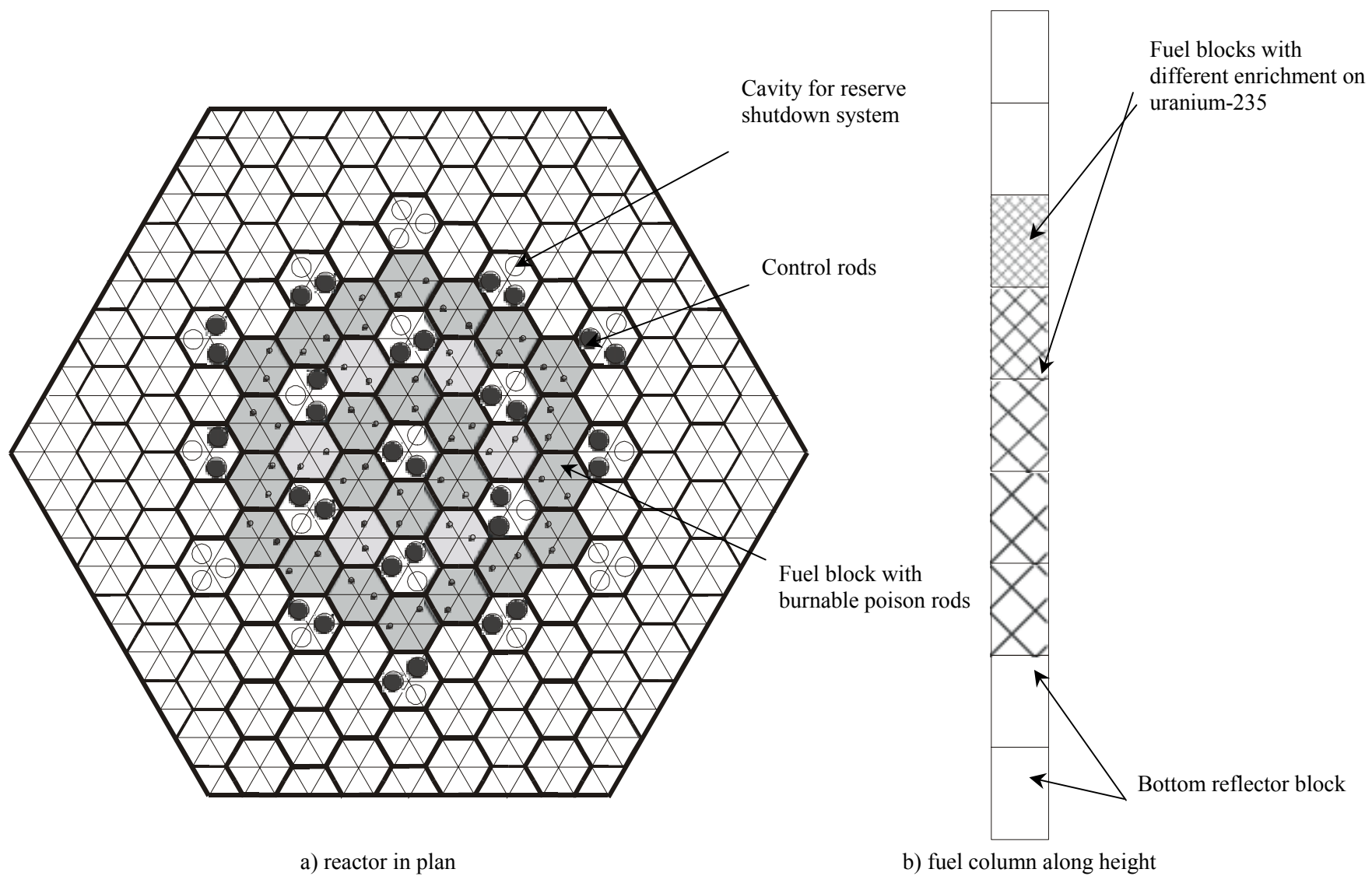
FIG. 2.75. Reactor calculation model.

Fuel kernel
(UO$_2$)

Multilayer
coating

Fuel matrix
graphite related to
one fuel particle

Annular fuel compact

Graphite sleeve

Gas gap and graphite spacing ribs

Fuel block graphite related to a fuel compact

Graphite
disks

BP pellets

Burnable poison rod

Homogenized fuel

a) plan view   b) axial view

Fuel particle   Fuel compact   Fuel cell with burnable poison rod
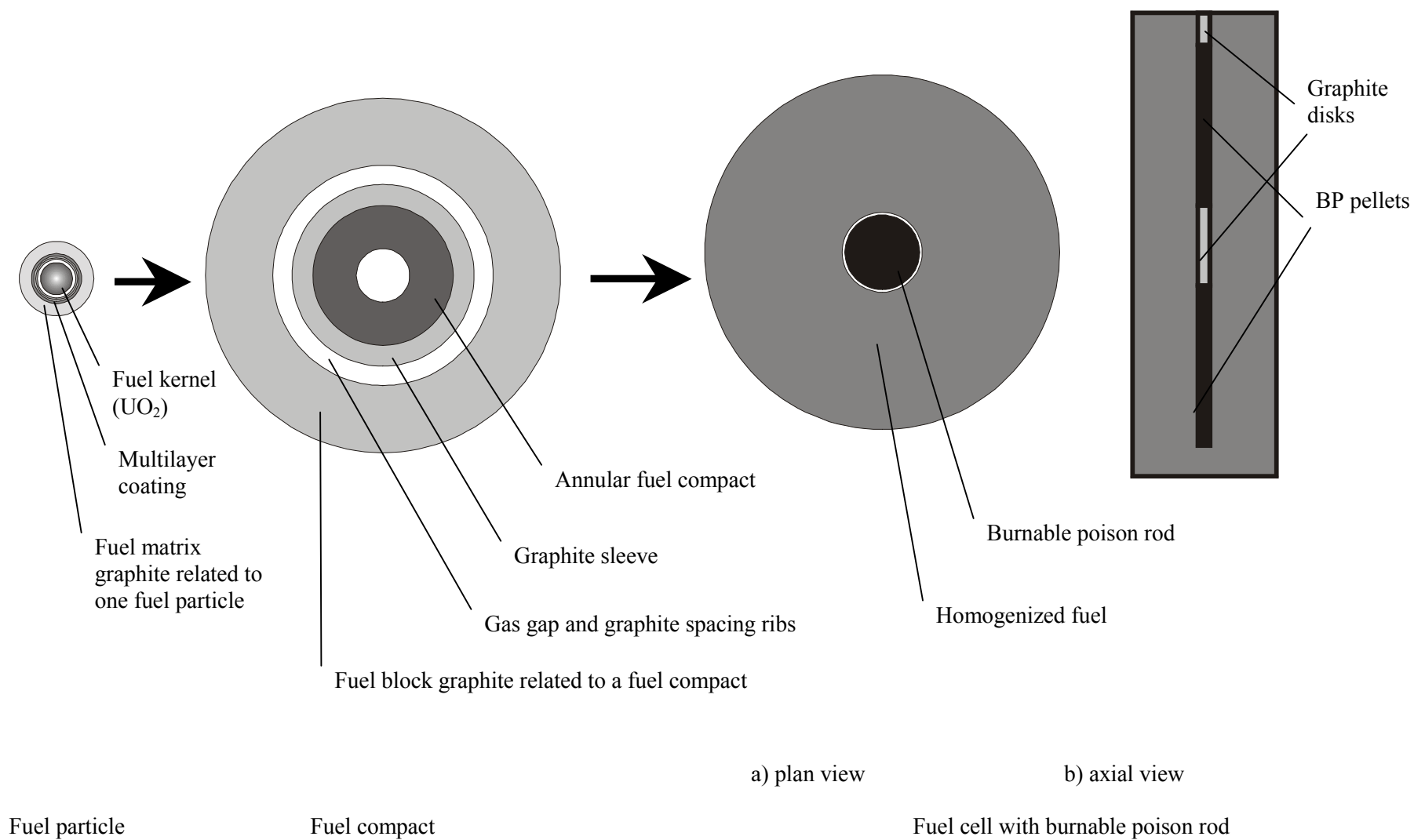
FIG. 2.76. Fuel cell calculation mode.

Table 2-71. Codes, models and nuclear data library for Monte-Carlo calculations

Items	Name of Country: Russia	Name of Country: Russia
	Name of Institute: RRC KI	Name of Institute: IBRAE
Code	MCU	MCNP 4A
Nuc. data file	DLC/MCUDAT-1.0	ENDF/B6 NJOY
Energy structure	Continuous	Continuous
Coated fuel particles	Fuel kernels are not smeared	Detailed account
History	200	2000 (up to 16000)
Batches	5000	1000
Skipped batches	1	10

Table 2-72. Methodical errors

Items	Calculation refining	Taking into account	
		Monte-Carlo calculation (MCNP)	Diffusion calculation
Forms and dimensions			
1 Graphite sleeve	Detailed description of spacer of sleeve	homogenized	homogenized
	Detailed description of gaps between sleeve and fuel compact	+	+
2 Graphite block	Detailed description of coolant holes, gaps between dowel pin and dowel socket, chamfering and spot facing	+	homogenized
3 Handling hole of graphite block	Detailed description of handling hole in all types of blocks	+	-
4 Position of burnable absorber	Horizontal locations of burnable absorbers are displaced on 3 mm to outside in fuel blocks	+	+
5 Shock absorber of control rod (CR)	Detailed description of shock absorber	+	-
6 Heterogeneity of coated fuel particle (CFP)	Statistical treatment of CFP location in fuel compact	cubic cell	determined location
Composition and density			
7 Fuel compact	Fuel compact load drift from nominal	-	-
8 Air in graphite block	Residual air in graphite block	-	-
9 Impurity in dummy block	Impurity revising from 2,5ppm to 3,lppm	+	+
10 Partial insertion of R2-CR	Partial insertion of R2-CR	+	+
11 Composition of graphite block	Different composition of a part of permanent reflector and dummy block	+	+

2.2.6.2. First Criticality [HTTR-FC]

Analysis of k_{eff} dependence on sequence of fuel columns loading was conducted, the results of which are depicted in Figure 2.77. In connection with this a consecutive loading, considered accordingly the specification JAERI-memo 10-005 and symmetrical loading, is illustrated in Figures 2.78, 2.79 and 2.80. First results of HTTR-FC calculations were presented at IAEA Research Coordination Meeting [2-59]. The results on phase 2 of Benchmark Problems of HTTR were presented at IAEA CRP-5 meeting in China, October 18-22, 1999 [2-60, 2-61].

Characteristic	Value		
	Diffusion calculations	Monte Carlo calculations	
Organization	OKBM	IBRAE	RRC KI
Number of fuel columns	16	16	17
k_{eff}	1.005	1.006±0.0016	1.004±0.0012
Reactivity excess, %Δk/k	0.498	0.596	0.398

In the annular reactor core of small diameter with high neutron leakage value of multiplication factor is very sensitive to disposition of fuel columns, and to ensure a power distribution symmetry, while control rods in upper most position it makes sense to load the fuel columns symmetrically throughout the core.
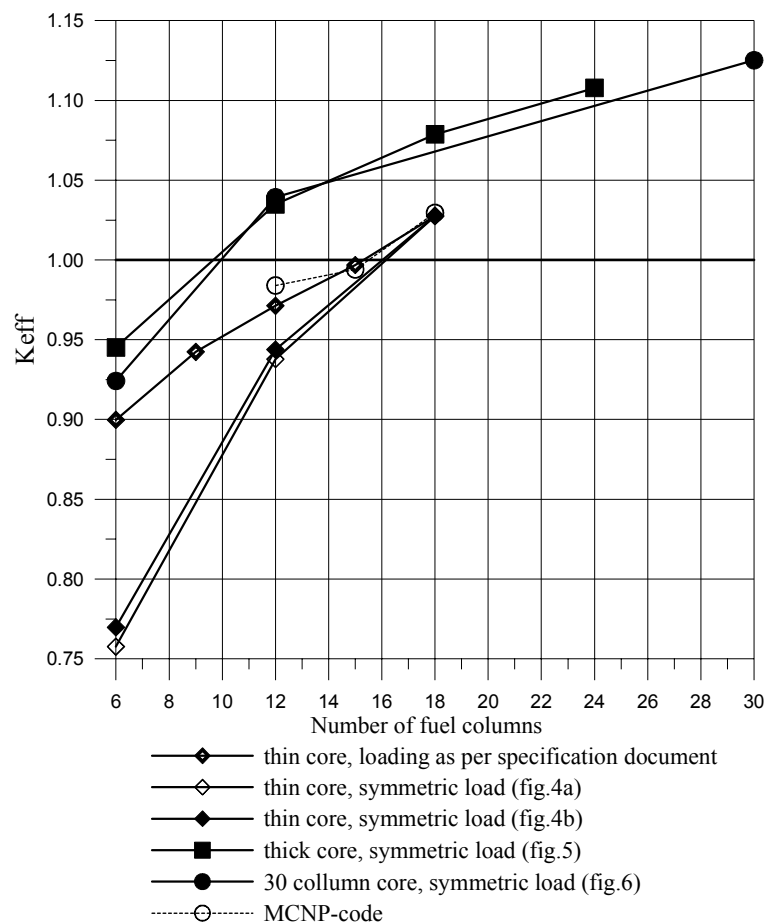

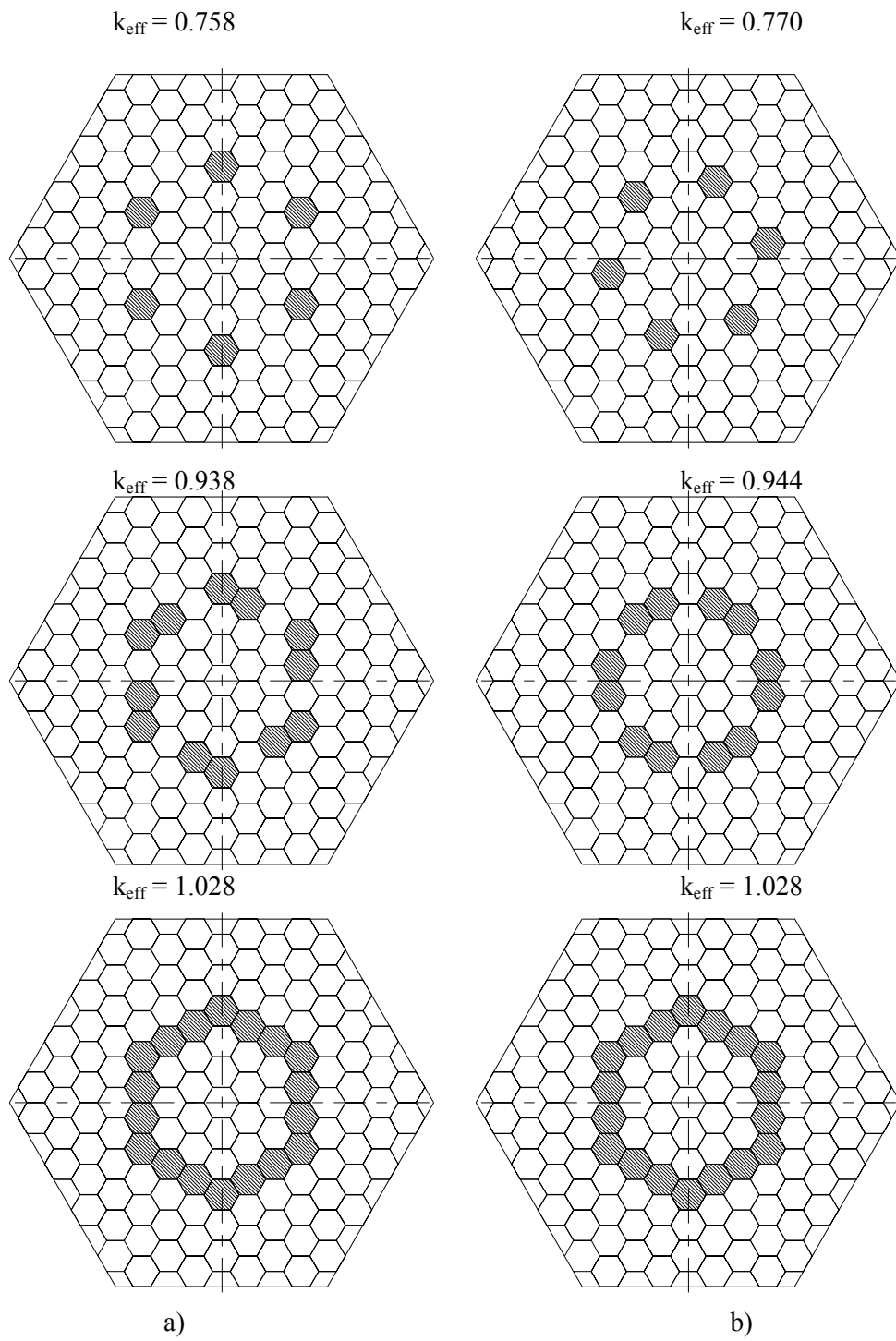FIG. 2.77. k_{eff} versus number and arrangement of fuel columns.

k_eff = 0.758   k_eff = 0.770

k_eff = 0.938   k_eff = 0.944

k_eff = 1.028   k_eff = 1.028

a)   b)

FIG. 2.78. k_eff versus fuel columns arrangement (thin annular core – 18 fuel columns).

k_eff = 0.945

k_eff = 1.038

k_eff = 1.035

k_eff = 1.079

k_eff = 1.108
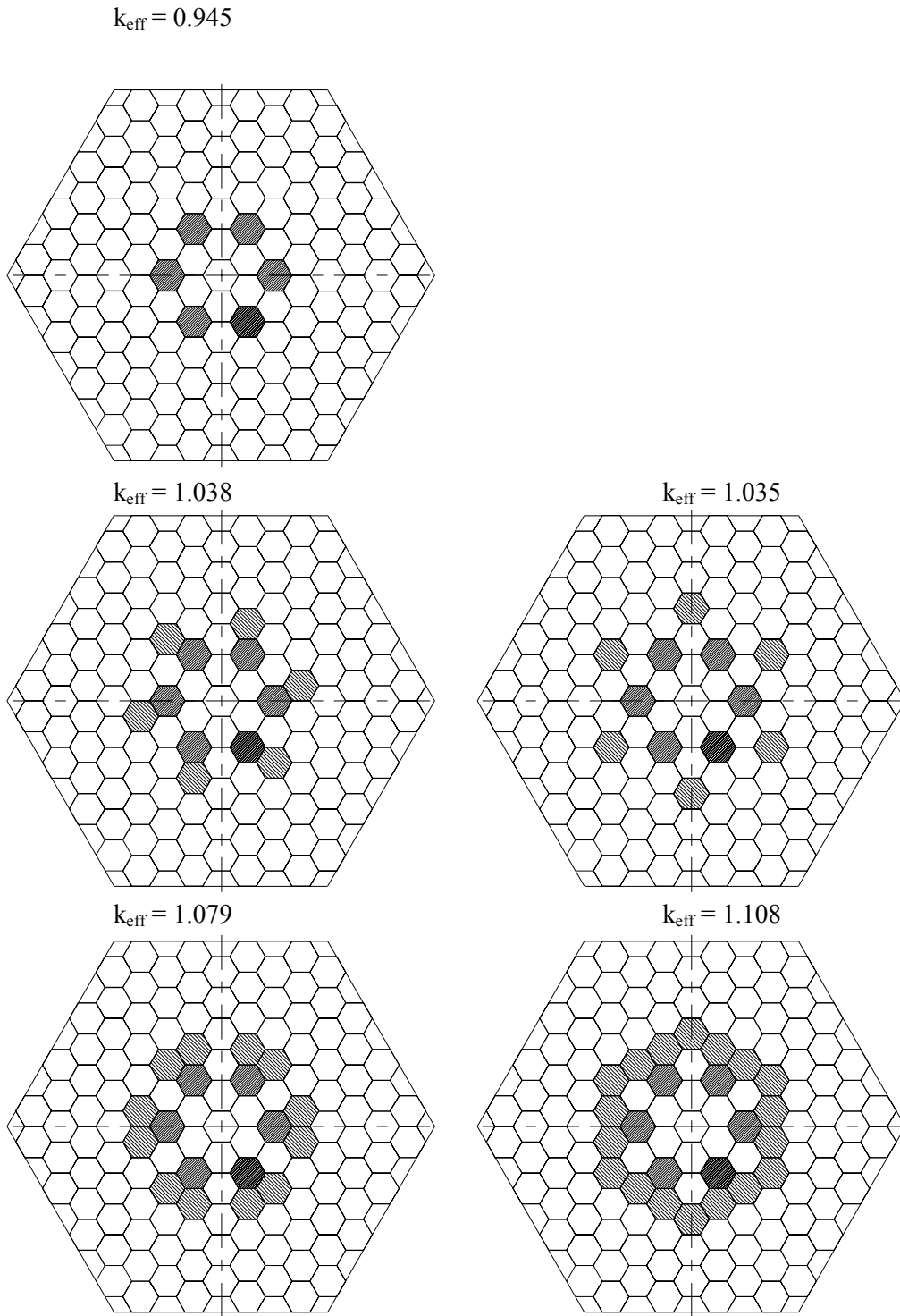
FIG. 2.79. k_eff versus fuel columns arrangement (thick annular core – 24 fuel columns).

$k_{eff} = 0.924$

$k_{eff} = 1.039$

$k_{eff} = 1.125$
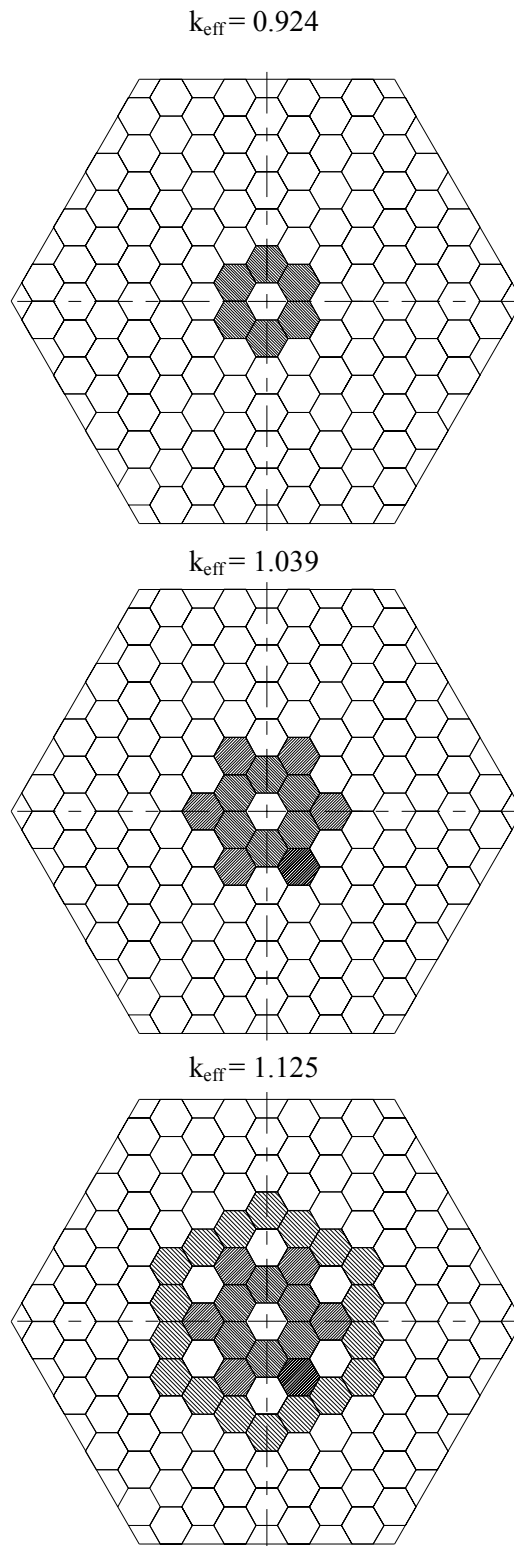
FIG. 2.80. k_{eff} versus fuel columns arrangement (completely loaded core – 30 fuel columns).

The Diffusion and Monte-Carlo calculations for the benchmarks HTTR-CR, HTTR-EX, HTTR-SC and HTTR-TC are provided in Tables 2-73, 2-74, 2-75 and 2-76, respectively.

2.2.6.3. Control Rod Position at Criticality [HTTR-CR]

Table 2-73. Results of Diffusion and Monte-Carlo Calculations for the HTTR-CR Benchmark Problem

Characteristic	Value		
	Diffusion calculations	Monte Carlo calculations	
Organization	OKBM	IBRAE	RRC KI
Depth of control rods insertion, cm			
18 columns	271	259	306
24 columns	196	195	201
30 columns	166	170	154

2.2.6.4. Excess Reactivity [HTTR-EX]

Table 2-74. Results of Diffusion and Monte-Carlo Calculations for the HTTR-EX Benchmark Problem

Characteristic	Value		
	Diffusion calculations	Monte Carlo calculations	
Organization	OKBM	IBRAE	RRC KI
Reactivity excess, %$\Delta k/k$			
18 columns	2.68	2.70	1.70
24 columns	9.73	10.83	9.80
30 columns	11.14	13.55	13.40

2.2.6.5. Scram Reactivity [HTTR-SC]

Table 2-75. Results of Diffusion and Monte-Carlo Calculations for the HTTR-SC Benchmark Problem

Characteristic	Value		
	Diffusion calculations	Monte Carlo calculations	
Organization	OKBM	IBRAE	RRC KI [b]
Worth of reflector rods			
$k_{eff}^{krit\ [a]}$	1.0023	1.0098±0.0015	1.0265±0.0010
$k_{eff}^{after\ drop}$	0.9242	0.9205±0.0017	0.9349±0.0010
ρ ($\Delta k/k$)	0.0843	0.0961±0.0020	0,0955±0.0014
Worth of all rods			
k_{eff}^{krit}	1.0023	1.0098±0.0015	1.0265±0.0010
$k_{eff}^{after\ drop}$	0.6573	0.7172±0.0015	0.6746±0.0010
ρ ($\Delta k/k$)	0.5237	0.4040±0.0019	0.5081±0.0014

[a] Calculated value at critical position of rods obtained by experiment.

[b] Results were obtained accordingly the JAERI-memo 10-005 including graphite impurity data.

2.6.6.6. Isothermal Temperature Coefficient [HTTR-TC]

Table 2-76. Results of Diffusion and Monte-Carlo Calculations for the HTTR-TC Benchmark Problem

Characteristic	Value		
	Diffusion calculations	Monte Carlo calculations	
Organization	OKBM	IBRAE	RRC KI
Multiplication factor of reactor for design temperatures			
k_{280}	-	-	-
k_{300}	1.0023	1.0032±0.0002	1.0279±0.0010
k_{340}	0.9930	0.9954±0.0002	1.0232±0.0010
k_{380}	0.9844	0.9886±0.0002	1.0160±0.0010
k_{420}	0.9768	0.9822±0.0002	1.0124±0.0010
k_{460}	0.9699	0.9754±0.0004	1.0052±0.0010
k_{480}	0.9665	0.9726±0.0002	1.0026±0.0010
Temperature coefficients ($\Delta k/k/K$)			
ρ_{290}	-	-	-
ρ_{320}	$- (2.33 \cdot 10^{-4})$	$- (1.95 \pm 0.10) \cdot 10^{-4}$	$-(1.1 \pm 0,4) 10^{-4}$
ρ_{360}	$- (2.19 \cdot 10^{-4})$	$- (1.73 \pm 0.10) \cdot 10^{-4}$	$-(1.7 \pm 0,4) 10^{-4}$
ρ_{400}	$- (1.97 \cdot 10^{-4})$	$- (1.65 \pm 0.10) \cdot 10^{-4}$	$-(0.9 \pm 0,4) 10^{-4}$
ρ_{440}	$- (1.82 \cdot 10^{-4})$	$- (1.77 \pm 0.16) \cdot 10^{-4}$	$-(1.8 \pm 0,4) 10^{-4}$
ρ_{470}	$- (1.81 \cdot 10^{-4})$	$- (1.48 \pm 0.32) \cdot 10^{-4}$	$-(1.3 \pm 0,7) 10^{-4}$

2.6.6.7 Accuracy analysis

The accuracy analysis of obtained results is presented as follows:

Table 2-77. Excess reactivity [HTTR-EX]

	18 columns	24 columns	30 columns
Diffusion calculations			
Average value (in accordance with RCM4 results), %$\Delta k/k$	1.6	8.8	12.4
Average calculated value / experimental value, %	[a)]	+ 14	+ 3.3
WIMS-JAR value / average calculated value, %	+ 67	+ 10	- 10
WIMS-JAR value / experimental value, %	[a)]	+ 26	- 7
Monte - Carlo calculations			
Average value (in accordance with RCM4 results), %$\Delta k/k$	1.87	10.1	13.0
Average calculated value / experimental value, %	[a)]	+ 31	+ 8.3
MCNP value / average calculated value, %	+ 44	+ 7	+ 4.2
MCU value / average calculated value, %	- 9	- 3	+ 3
MCNP value / experimental value, %	[a)]	+ 40	+ 13
MCU value / experimental value, %	[a)]	- 27	+ 12

[a)] Experimental result is absent.

Table 2-78. Control rods worth [HTTR-SC]

	Reflector control rods	All control rods
Diffusion calculations		
Average value (in accordance with RCM4 results), %Δk/k	9.2	48.0
Average calculated value / experimental value, %	- 23	+ 4.3
WIMS-JAR value / average calculated value, %	- 8	+ 9
WIMS-JAR value / experimental value, %	- 30	+ 14
Monte - Carlo calculations		
Average value (in accordance with RCM4 results), %Δk/k	9.2	44.8
Average calculated value / experimental value, %	- 23	-2.6
MCNP value / average calculated value, %	+ 4.4	- 10
MCU value / average calculated value, %	+ 3.8	+ 13
MCNP value / experimental value, %	- 20	- 12
MCU value / experimental value, %	- 20	+ 10

Table 2-79. Isothermal Temperature Coefficient at the temperature range 345 – 407 K [HTTR-TC]

Diffusion calculations	
Average value (in accordance with RCM4 results), %Δk/k·K	- 1.63·10⁻⁴
Average calculated value / experimental value, %	+ 21
WIMS-JAR value / average calculated value, %	+ 28
WIMS-JAR value / experimental value, %	+ 54
Monte - Carlo calculations	
Average value (in accordance with RCM4 results), %Δk/k·K	- 1.32·10⁻⁴
Average calculated value / experimental value, %	- 2
MCNP value / average calculated value, %	+ 28
MCU value / average calculated value, %	- 4
MCNP value / experimental value, %	+ 25
MCU value / experimental value, %	- 4

Calculated accuracy analysis, presented above, demonstrates that 2-groups diffusion approximation gives significant error at the excess reactivity calculation for annular core with one ring of fuel assemblies. Multigroups approximation is necessary for calculation of this type core.

Large spread in excess reactivity values, obtained by MCNP and MCU, from average calculated and experimental values demonstrates the necessity to revise calculational initial data (it may be moisture content in graphite), on the one side, and also to verify nuclei data library, on the other side.

Errors analysis of control rods worth estimation shows the necessity to use multigroups diffusion approximation for calculations of the side reflector control rods worth that is estimated with the most errors. Deviation of Monte-Carlo calculated control rods worth from experimental one in the range about 20 % should be also referred to the effect of initial data because deviation in calculated values is not large.

To estimate reactivity temperature coefficients, it is necessary additional analysis characterized by accurate modeling of geometry and fuel particle distribution, detail modeling of burnable poison position by Monte-Carlo method, and for diffusion calculations it is necessary to model axial distribution of burnable poison, neutrons streaming for adequate accounting of leakage and to use multigroups approximation.

Significant dependence of the results versus chosen nuclei data libraries and its compiled programs defines the necessity to choice basic library for HTGRs calculation especially for description of thermalization effects.

2.2.7 Turkey [2-63]

2.2.7.1 Introduction

This study was performed by the Nuclear Engineering Department of Haceettepe University as a contribution to the IAEA CRP on Evaluation of HTGR Performance. MCNP-4B has been utilized throughout this study. This is a multi-purpose Monte Carlo n-particle (neutron, photon, and electron) transport code. This code also performs criticality analysis.

Reactor configuration

The HTTR core consists of vertically arranged prismatic hexagonal blocks with a height of 580 mm and a width of 360 mm accross flats. Active core height and effective diameter are 390 cm and 230 cm, respectively. Reactor core is made of 30 fuel colums and 7 control rod guide columns. The core is enveloped by 24 prismatic hexagonal reflector blocks. Among them, there are 9 control rod guide columns, 12 replaceable reflector columns, and 3 irradiation colums. The whole structure is surrounded by a permanent graphite side reflector.

Each fuel column consists of 2 top reflector blocks, 5 fuel assemblies, and 2 bottom reflector blocks. There are two types of fuel assemblies; containing 31 and 33 fuel rods. Each fuel block contains three burnable poison (BP) insertion holes, but only two of them are filled with B_4C-C BP materials (containing 2.22 or 2.74 wt. %.natural boron). Fuel rods contain 14 annular fuel compacts. These compacts are manufactured with inner and outer diameters of are 10 and 26 mm, respectively, and a height of 39 mm. UO_2 coated particles are embedded into graphite matrix to form the fuel compact.

Each assembly contains only one type of fuel. However, there are 12 different fuel types with enrichments between 3 to10 wt. % of U-235.

Control rods are made of B_4C pellets sorrounded by a 3.5 mm thick sleeve of Alloy 800H. The total height of control rods is 3094 mm. Inner and outer diameters are 65 mm and 113 mm, respectively. The detailed geometry and composition of all components are provided by a JAERI report [2-5].

MCNP-4B model and simulations

MCNP-4B is a very versatile computer code for particle transport simulation purposes [2-62]. It has extended features in geometrical modeling in three dimensional space. Every single geometrical detail is defined to generate full HTTR core model. The complexity of the reactor core structure makes this detailed modeling necessary. Horizontal cross sectional views of the HTTR core model with MCNP-4B are given in Figures 2.81 and 2.82.

The primitive element of the model is a coated particle. It is generated with five concentric spherical volumes. Then, these coated particles are uniformly distributed into a hexagonal prismatic lattice which is enclosed by an annular cylindirical graphite. Thus, a fuel compact model containing 13 000 CFP's is obtained. 14 fuel compacts are then stacked into a structre made of graphite. Hence, a fuel assembly is constructed by placing this structure in a hexagonal lattice. Two types of fuel assemblies with 31 and 33 fuel rods are generated in the model as mentioned earlier.
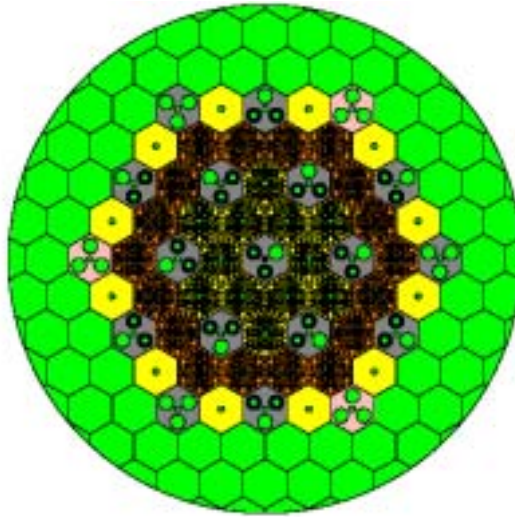
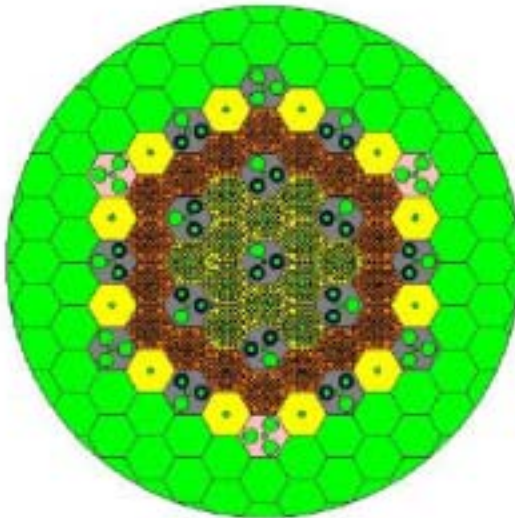*Figure 2.81. Top cross sectional view of HHTR core in MCNP model.*

Figure 2.82. Cross sectional view of HTTR core in MCNP model with fuel and control assemblies.

Control rod guide colums are also modeled by leaving appropriate space for two control rod locations and a location for reserve shut down rod system.

MCNP provides a facility to visualize the geometry described in the model. Hence, the model is geometrically verified by taking views from different vertical and horizontal cross sections.

Criticality calculations are performed with 5 000 source particles generated in each cycle. 150 cycles are considered in each run. ENDF/B-VI cross section library with continuous energy is utilized throughout the calculations. Cross sections are evaluated at respective temperatures as necessary for graphite provided by thermal neutron libraries TMCCS.
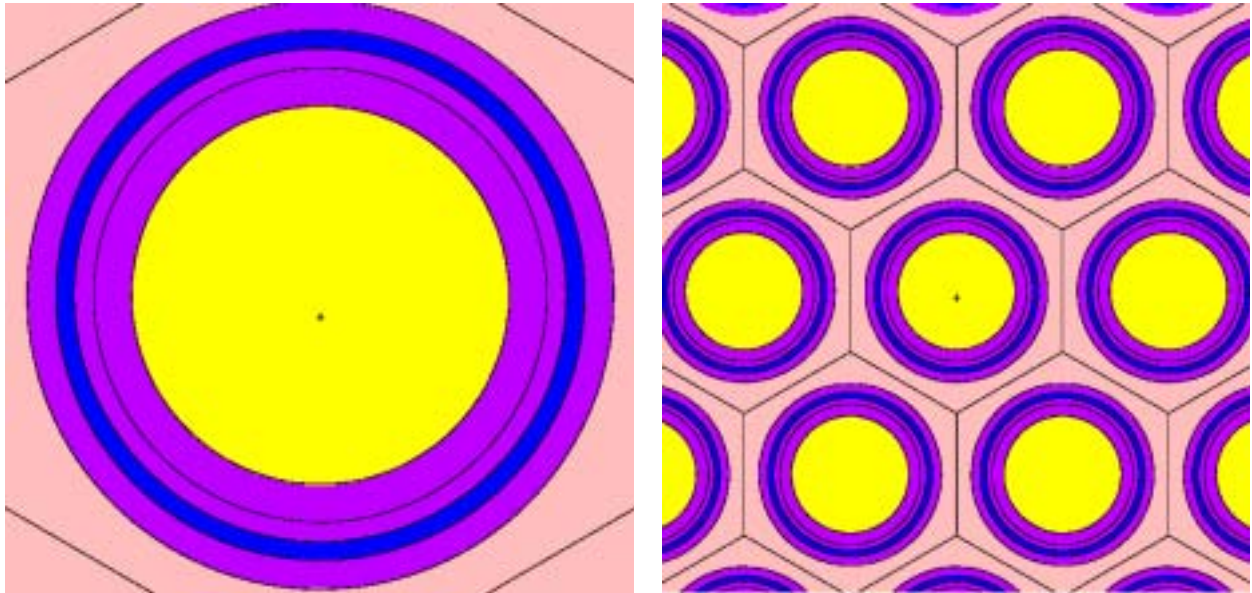
Figure 2.83. MCNP model for Coated Fuel Particles and their arrangement in fuel compact.

2.2.7.2. Results of benchmark problems

In this work, all benchmark problems expect HTTR-FC (Phase 2) are studied.

Benchmark Problem I: HTTR-FC (Phase 1)

The number of fuel columns necessary to make the reactor critical is calculated in this problem. Results of criticality calculations with different number of fuel colums are shown in Table 2-80. The reactor is estimated to be critical with 15 fuel colums.

Table 2-80. Variation of effective multiplication factor with loaded fuel colums

Fuel Colums	k-eff	Error
12	0.98703	0.00102
13	0.99252	0.00102
14	0.99923	0,00103
15	**1.00503**	**0.00108**
16	1.01226	0.00103
17	1.02079	0.00105
18	1.03073	0.00097
19	1.04698	0.00091

Benchmark Problem 2:   HTTR-CR

Control rod insertion depths for three different core loading configurations are evaluated for criticality condition. Control rod positions are evaluated from the top of the 8th layer (the top of the bottom reflector).

Table 2-81. Control rod depths for criticality and calculated k-eff

Fuel Columns	Control Rod Depth (cm)	k-eff	Error
18	285	0.99859	0.0016
24	210	1.00864	0.0013
30	164	0.99901	0.00152

Benchmark Problem 3: HTTR-EX

Excess reactivities are calculated for three different cases mentioned in Benchmark Problem 2 assuming 300K for moderator and fuel temperatures.

Table 2-82. Excess reactivities for three different fuel l oading conditions

Fuel Columns	k-eff	Error	Excess Reactivity (%)
18	1.03073	0.00097	2.981
24	1.11969	0.00109	10.689
30	1.15641	0.00095	13.525

Benchmark Problem 4: HTTR-SC

There are two cases defined in this problem for evaluating scram reactivity. The first one is specified with all reflector control rods are inserted when the reactor is critical. The second one is evaluaeted with all control rods, reflector and core, are inserted again with the critical configuration for fully loaded core.

Table 2-83. Scram reactivities with two different cases

	Scram Reactivity (%)
All reflector CRs in	-7.75
All reflector & core CRs in	-37.96

Benchmark Problem 5: HTTR-TC

Isothermal temperature coefficients are calculated for fully loaded core at the critical condition. Critical control position is also evaluated at a temperature of 480K to be 190 cm..

Table 2-84. Critical control rod position at 480K and corresponding k-eff

CR Position (cm)	k-eff	Error
190	0.99838	0.00220

As mentioned earlier cross sections for graphite at different temperatures are evaluated by means of thermal neutron libraries TMCCS. There are only 4 sets of data at temperatures of 300K, 600K, 800K, and 1200K available in our institution. Therefore, k-eff evaluations are performed for these temperatures and the results are shown in Figure 2.84. As it can be seen from the figure, the slope of the curve change with temperature. Therefore, it is rather difficult to make an accurate prediction of isothermal temperature coefficient. However, it is estimated for the first two datum points to be 1.20 10^{-4} 1/K around the midpoint of 450K.
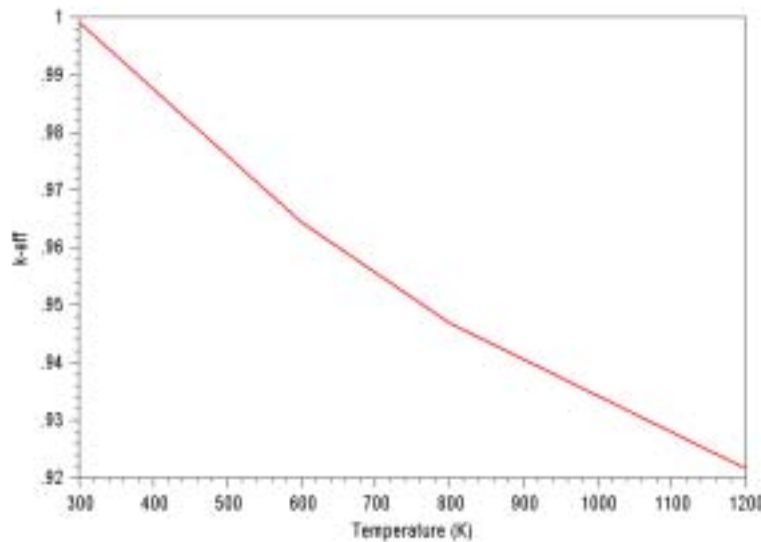
Figure 2.84. Effective multiplication factor as a function of temperature.

2.2.7.3 Conclusions

Results of HTTR start-up core physics benchmark problems are presented. Calculations are performed by MCNP-4B code and with continuous energy cross sections. Phase 2 of the first problem (HTTR-FC) is not taken into consideration. Therefore, all problems are performed with the original data. Geometrical modeling is done such a way that geometrical details are considered as much as possible. Isothermal reactivity calculation presented in this study is not very reliable due to the lack of relevant cross section data at rather close temperatures.

2.2.8. United States of America

2.2.8.1. Computational Methodology [2-64]

The Monte Carlo code MCNP4a was used because the geometry of the coated fuel particles, fuel compacts, burnable poisons, fuel element and reflector blocks, and the control rods and guide blocks can be modeled explicitly without any approximations.

MCNP4a uses nuclear data from the ENDF/IBV Version 0 cross-section library. The thermal neutron scattering matrix for the graphite is based on $S(\alpha,\beta)$ of ENDF/BV. A core temperature of 300 K is assumed. MCNP4a uses track length, collision and analog estimators in determining the most probable value of k_{eff}. The number of histories per batch is 10,000. The number of batches is 30 with the first 5 batches being discarded for statistical reasons.

The core is modeled with hexagonal lattices consisting of control rod guide blocks, fuel blocks, and permanent reflector blocks. The fuel rods and the burnable poison rods are modeled using cylindrical body descriptions. The fuel block consists of several smaller hexagonal lattices containing one fuel rod or burnable poison rod. This is shown in Figure 2.85. In the geometry description, all hexagonal lattices were assigned to a universe number. The universe numbers were then input into an array to describe the location of the hexagonal blocks in the reactor core. The cross sectional model of the 30 column reactor core is shown in Figure 2.86. The outer boundary of the permanent reflector was modeled as a cylinder.

The fuel compacts are modeled with cylinders and the coated fuel particles (CFPS) are modeled with spherical body descriptions. In the control rod insertion heterogeneous excess reactivity calculations all five layers of the CFP are modeled. There are about 13,000 fuel particles defined for each fuel compact corresponding to a packing density of 30 percent with each fuel rod containing 14 fuel compacts. Therefore, for plotting simplicity the fuel particles are not shown in the cross sectional view of the fuel hexagonal lattice. The fuel particle representation is smeared in the homogeneous excess reactivity calculation.

The burnable poison rods are modeled as two different types. The geometry does not change but the material composition of the burnable poison changes. There are graphite disks that separate the upper and lower parts of the burnable poison rods. There are only two of the three burnable poison rod positions filled for each fuel hexagonal lattice. The third hole contains helium coolant. The configurations of the burnable poison rods change throughout the reactor core and are shown in Figure 2.86.

There are three pairs of control rods in the outer ring that are not used in the approach to criticality. All other control rod insertion depths change as one bank. The control rods in the outer ring can only be removed to 72.5 cm from the top of the active core because a sufficient negative reactivity addition rate must be available for reactor scrams. The control rods in the inner rings can be fully withdrawn. Therefore, in the excess reactivity model, the control rod holes contain coolant in the inner rings.
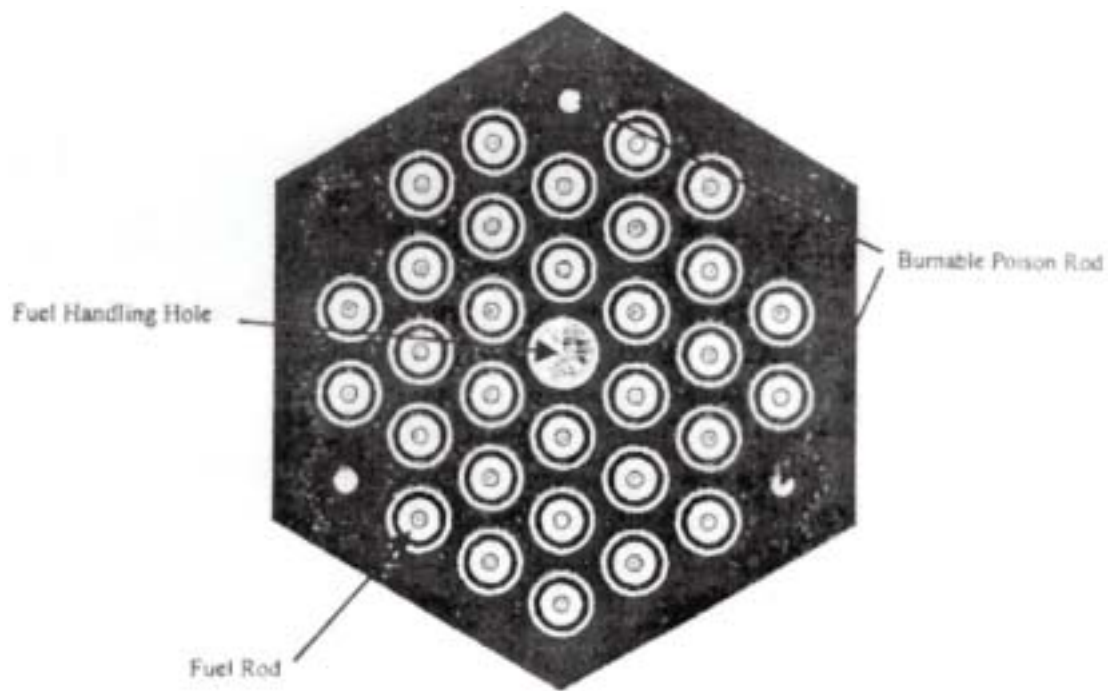
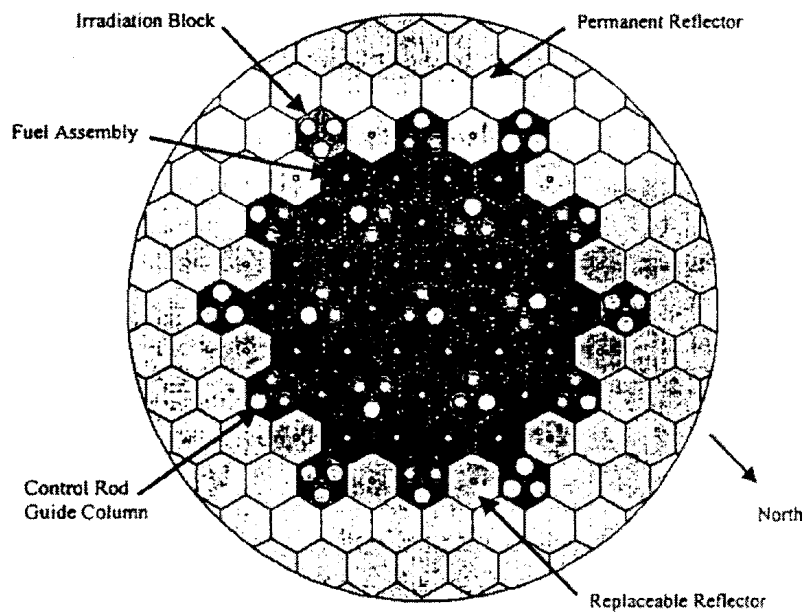FIG. 2.85. Cross section of fuel assembly.

FIG. 2.86. Cross section of fully loaded core.

2.2.8.2. Results [2-65]

Monte Carlo methodology was used by the US in the initial HTTR criticality benchmark problem (MCNP-4a), and the calculations were limited to the case of the full core (30 elements loaded). The calculations made for the initial problem consisted of k-effective calculations vs. control rod (C/R) position in cm from the bottom of the active core, evaluated at two different uniform core temperatures (300K and 800K), and are shown in Figure 2.87 and detailed in Table 2.85.
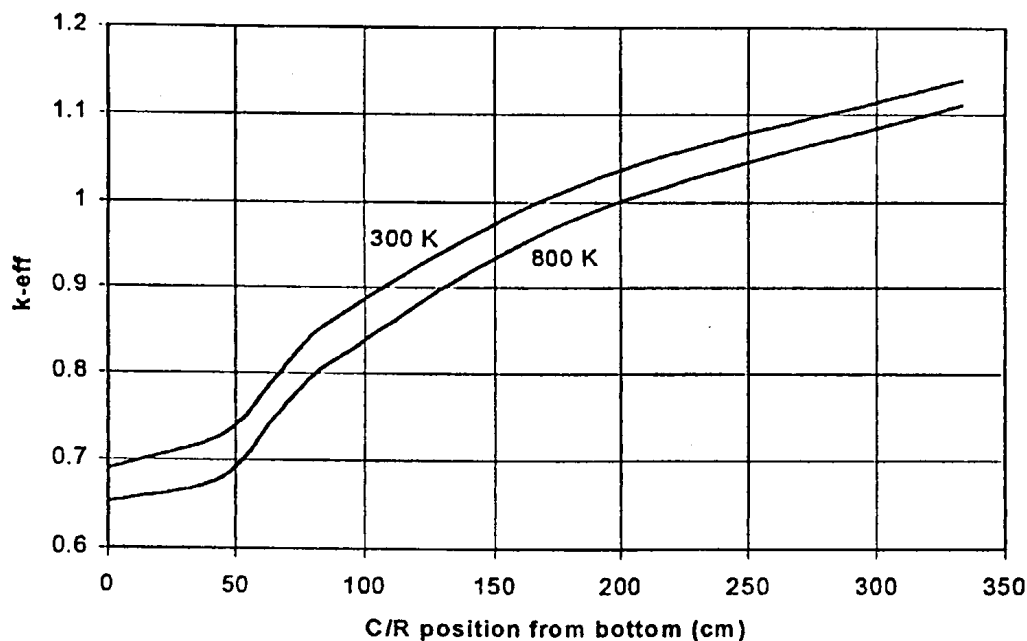

FIG. 2.87: HTTR K-eff at 300 and 800K.

Table 2-85. MCNP4a Summary of results

Core Temperature, K	Critical Rod Position (cm)*	K-eff, (Rods Full In)	K-eff, (Rods Full Out)	Homogeneous Model, K-eff, (Rods Full Out)
300	159	0.6899 (0.005)	1.1400 (0.004)	1.1336 (0.005)
800	194	0.6525 (0.006)	1.1118 (0.005)	1.10598 (0.004)

* Distance withdrawn (from bottom of the active core)

As specified in JAERI's initial benchmark problem description, the outer ring of reflector C/Rs were modeled as fully withdrawn, and all other rods were moved in tandem, and their position with respect to the bottom of the active core denoted as "C/R position."

There were no additional MCNP calculations done for Part 2 of the benchmark; hence only simplified and approximate versions of the new benchmark problem calculations were done using the original MCNP results. Hence for the scram reactivity estimates, "scram from critical" results are for the case of all but the outer ring reflector rods inserting, rather than the configurations specified in the new benchmark. The calculations of temperature coefficient of reactivity also use just the original k-effective calculations at 300K and 800K rather than the more detailed calculations specified in the new benchmark.

HTTR-SC

For the HTTR-SC benchmark problem, the scram reactivity from critical was calculated from the expression noted in the benchmark definition (difference between k-effective at critical [1.0] and k-effective with rods fully inserted divided by the product of the two k-effective values). The results are shown in Figure 2.88 as a function of core temperature (curve labeled "Scram from Critical."). Hence the scram reactivity for the core temperature specified in the benchmark (300K) is 0.45. The scram reactivity for the case where all rods drop would be somewhat greater. Note that at higher temperatures, the scram reactivity would be greater, as expected. Figure 2.88 shows a scram reactivity of 0.53 for a uniform core temperature of 800K. Also shown in Figure 2.88 is the reactivity worth of the rods (again excluding those rods in the outermost outer reflector ring) for full travel.
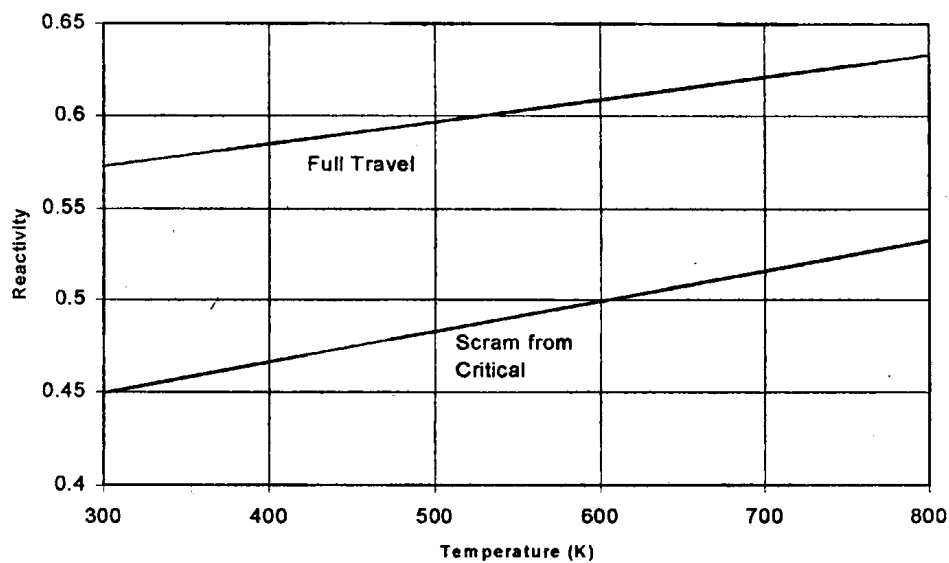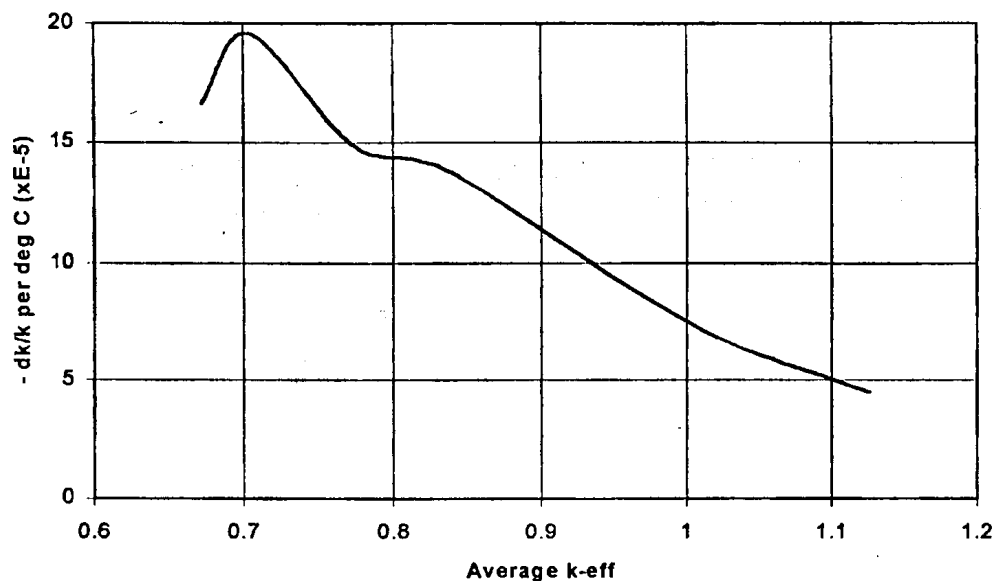
FIG. 2.88. Scram reactivity

FIG. 2.89. Temperature coefficient of reactivity vs. k-eff

HTTR-TC

The calculated temperature coefficient of reactivity (for uniform core temperatures) is plotted vs. average k-effective in Figure 2.89. The point at which the curve intersects k-eff = 1.0 is taken as the value of interest. That value is –7.5E-5 dk/k per degree C, evaluated at the average of the two temperatures at which k-eff was calculated (300K and 800K), i.e. 550K. It is interesting to note that Figure 2.89 shows that the coefficient becomes considerably more negative at smaller values of k-eff. One interpretation of this result would suggest that if the shutdown reactivity is calculated using the conventional estimated temperature coefficient of reactivity (at k-eff = 1.0), a non-conservative (low) value of shutdown reactivity would result.

REFERENCES TO CHAPTER 2

[2.1.] JAPAN ATOMIC ENERGY RESEARCH INSTITUTE, "Present Status of HTGR Research and Development", JAERI, Oarai, Japan, 1996.

[2.2.] YAMASHITA, K., "A new HTR concept concerning a modular system with block-type fuel elements and its comparison with a pebble-bed-type HTR", Jül-1842, Kernforschungsanlage Jülich GmbH, 1983, (in German).

[2.3.] KUNITOMI, K., et. al., "Development of New Type of HTGR", (Proc. 73rd JSME Fall Annual Meeting), JSME, Japan, 1995.

[2.4.] NEYLAN, A.J., SILADY, F.A., and BAXTER, A.M., "Gas Turbine Module Helium Reactor (GT-MHR): A Multipurpose Passively Safe Next Generation Reactor", Proceedings of The ASME/JASME 3rd International Conference on Nuclear Engineering, ASME, 1995.

[2.5.] JAPAN ATOMIC ENERGY RESEARCH INSTITUTE, "Benchmark Problem's Data for The HTTR's Start-up Core Physics Experiments" JAERI-memo 10-005, Oarai, Japan, 1998.

[2.6.] BREY, H.L., (Ed), "Current Status and Future Development of Modular High Temperature Gas Cooled Reactor Technology", IAEA-TECDOC-1198, Vienna, 2001

[2.7.] WEISBRODT, I.A., "Status of Gas-Cooled Reactor Technology", Private communication, Vienna, March 1997.

[2.8.] INTERNATIONAL ATOMIC ENERGY AGENCY, "Design and Evaluation of Heat Utilization Systems for the High Temperature Engineering Test Reactor", IAEA-TECDOC-1236, Vienna, August 2001.

[2.9.] FUJIMOTO, N., YAMASHITA, K., "JAERI's Benchmark Calculation of HTTR Core Physics-Phase 2", JAERI, (Proc. Second RCM of CRP on Evaluation of HTGR Performance, held at Beijing), IAEA, Vienna, 1999

[2.10.] FUJIMOTO, N., et. al., "JAERI's Benchmark Calculation of Start-up Core Physics with HTTR Nuclear Characteristics Evaluation Code System", JAERI memo 11-030, Oarai, Japan, pp. 80-106, 1999.

[2.11.] YAMASHITA, K., et. al., "Nuclear design of the High-Temperature Engineering Test Reactor (HTTR)", Nucl. Sci. Eng. pp.122, 212-228, 1996.

[2.12.] SHINDO, R., YAMASHITA, K. and MUARTA, I., "DELIGHT-7; One-dimensional fuel cell burnup analysis code for High Temperature Gas-cooled Reactors (HTGRs)", JAERI-M 90-048, 1990, (in Japanese).

[2.13.] LATHROP, K. D. and BRINKLEY, F. W., "TWOTRAN-II: and interfaced exportable version of the TWOTRAN code for two-dimensional transport", LA-4848-MS, Los Alamos, USA, 1973.

[2.14.] HARADA, H. and YAMASHITA, K., "The reactor core analysis code CITATION-1000VP for High Temperature Engineering Test Reactor", JAERI-M 89-135, 1989, (in Japanese).

[2.15.] FOWLER, T. B., VONDY, D. R. and CUNNINGHAM, G. W., "Nuclear reactor core analysis code, CITATION", ORNL-TM-2496, Oak Ridge, USA, 1971.

[2.16.] MORI, T. and NAKAGAWA, M., "MVP/GMVP:General Purpose Monte Carlo Codes for Neutron and Photon Transport Calculations based on Continuous Energy and Multi-Group Methods", JAERI-Data/Code 94-007, 1994.

[2.17.] MORI, T., NAKAGAWA, M. and SASAKI, M., "Vectorization of Continuous Energy Monte Carlo Method for Neutron Transport Calculation", J. Nucl. Sci. Technol., 29 [4], pp. 325, 1992.

[2.18.] SHIBATA, K., et al.: Japanese Evaluated Nuclear Data Library, Version-3, JAERI-1319, 1990.

[2.19.] OKUMURA, K., et al., SRAC95; "General Purpose Neutronics Code System," JAERI-Data/Code 96-015, Japan Atomic Energy Research Institute, 1996.

[2.20.] MURATA, I., MORI, T. and NAKAGAWA, M., "Continuous Energy Monte Carlo Calculations of Randomly Distributed Spherical fuels in High-Temperature Gas-Cooled Reactors Based on a Statistical Geometry Model", NSE, 123, pp. 96-109, 1996.

[2.21.] N. NOJIRI, M. NAKANO, N. FUJIMOTO, K. YAMASHITA, M. TATEUCHI, S.FUJISAKI, S. YOSHIMUTA, K. SAWA, M. SATO, M. ISHIHARA, T. IYOKU, H. SAWAHATA, "Benchmark problem's data for the HTTR's start-up core physics experiments", JAERI, Oarai, Japan, January, 1998

[2.22.] K. YAMASHITA, N. FUJIMOTO, M. NAKANO, U. OHLIG, "IAEA Benchmark calculation results of the HTTR's start-up core physics tests", Japan Atomic Energy Research Institute memo 11-030, 1999

[2.23.] R. SANCHEZ, A. HEBERT, Z. STANKOVSKI, M. COSTE, S. LOUBIERE, C VAN DER GUCHT and I. ZMIJAREVIC, "APOLLO2 Twelve Years Later", Mathematics and Computation, Reactor Physics and Environmental Analysis in Nuclear Applications, Madrid, September, 1999

[2.24.] J.J. LAUTARD, S. LOUBIERE, C. MAGNAUD, "CRONOS, A Modular Computational System for Neutronic Core Calculations", (Proc. IAEA Specialists Meeting), France, September, 1990

[2.25.] J.P. BOTH, Y. PENELIAU, "The Monte Carlo code TRIPOLI4 and its first benchmark interpretations", International Conference PHYSOR 96, Mito, Ibaraki, Japan, September, 1996

[2.26.] INTERNATIONAL ATOMIC ENERGY AGENCY, "Report of Second RCM of CRP on Evaluation of HTGR Performance" (held in Beijing, October 18-22, 1999), IAEA, Vienna, 1999

[2.27.] N. FUJIMOTO, "Data for re-calculation of HTTR-FC", Japan Atomic Energy Research Institute, November, 2000

[2.28.] F. MOREAU, R. SANCHEZ, S. SANTANDREA, "Contribution to the NEA C5G7 MOX benchmark", International Conference PHYSOR 2002, Seoul, South Korea, October, 2002

[2.29.] PETROVIC, P. BENOIST, "B_N Theory: Advances and New Models for Neutron Leakage Calculation", Advances in Nuclear Science and Technology, Plenum Publishing Corporation, New York, vol. 24, 1996

[2.30.] P. BENOIST, J. MONDOT, I. PETROVIC, "Calculational and experimental investigations of void effect. A new model for leakage treatment of heterogeneous assemblies", Nuclear Science and Engineering, 118, 197, 1994.

[2.31.] N. NOJIRI, N. FUJIMOTO, K. YAMASHITA, "HTTR's Benchmark Calculation of Start-up Core Physics Tests", JAERI, Japan, 1998.

[2.32.] N. FUJIMOTO, K. YAMASHITA, M. NAKANO, M. TATEUCHI, S.FUJISAKI, "Experimental Results of HTTR's Start-up Core Physics Tests", JAERI, (Proc. Second RCM of CRP on Evaluation of HTGR Performance, Beijing, October 2000), IAEA, Vienna, 2000.

[2.33.] N. FUJIMOTO et al., "Control Rod Position and Temperature Coefficients in HTTR Power-Rise Test", JAERI Tech 2000-091 (2000).

[2.34.] NOJIRI, N., et al., Private Communication, JAERI, Japan, (Jan. 1998)

[2.35.] PHILIPPEN, P., Private Communication, (1994)

[2.36.] GREENE, N.M., et al., AMPX-77: A Modular Code System for Generating Coupled Multigroup Neutron-Gamma Cross-Section Libraries from ENDF/B-IV and/or ENDF/B-V, Oak Ridge National Laboratory, ORNL/CSD/TM-283, (Oct. 1992)

[2.37.] TEUCHERT, E., HAAS, K.A., ZUT-DGL-V.S.O.P.:Programmzyklus für die Resonanzabsorption in heterogenen Anordnungen, FZ-Jülich, Interner Bericht IRE-70-1, (1970)

[2.38.] BROCKMANN, H., „TOTMOS: An Integral Transport Code for Spectrum Calculations," FZ-Jülich, ISR, Germany, (Dec. 1995)

[2.39.] RHOADES, W.A., et. al., „DORT-TORT, Two- and Three-Dimensional Discrete Ordinates Transport Code, „ Version 5.13.14, ORNL CCC-543, Oak Ridge, USA, (Jan. 1992)

[2.40.] FOWLER, T.B., et al., „Nuclear Reactor Core Analysis Code: CITATION", ORNL-TM-2496, Oak Ridge, USA, Rev.2, (July 1971)

[2.41.] YANG, CH., BENOIST, P., „Scattering anisotropy and neutron leakage in reactor lattices", Nucl. Sci. Eng., 86, pp. 47-62, (1984)

[2.42.] FUJIMOTO, N., Private Communication, JAERI, Japan,(Nov. 2000)

[2.43.] FUJIMOTO, N., Private Communication, JAERI, Japan, (March 2001)

[2.44.] BROCKMANN, H., OHLIG, U., „Calculational Results for the Benchmark Problems of the HTTR Start-up Core Physics Experiments", ISR, FZJ Research Centre-Jülich, Germany, October 15, 2001.

[2.45.] AZIA, F., LASMAN, A. N., and BAKRI, A., "Results of Benchmark Calculation on Start-up Core Physics of High Temperature Engineering Test Reactor", (Presented at the First RCM of CRP on Evaluation of HTGR Performance, Vienna, August 1998), BATAN, Indonesia, 1998.

[2.46.] RONEN, Y., LEIBSON, M. J., Nuclear Technology, 80, pp. 216-224, 1988.

[2.47.] NOJIRI, N., et al., "Benchmark Problems Data for the HTTR Start-up Core Physics Experiments", JAERI Memo 10-005, 1998.

[2.48.] KUGO, T., TSUCHIHASHI, K., TAKANO, H. and AKIE, H., "An EWS Version of SRAC-Code: SRAC-EWS", JAERI, 1994.

[2.49.] JEONG, C. J., OKUMURA, K., ISHIGURO, Y. and TANAKA, K., "Accuracy of Cell Calculation Methods Used for Analysis of High Conversion Light Water Reactor Lattice" Journal Nuclear Science & Technology, 27, pp. 515-523, 1990.

[2.50.] DE HAAS, J.B.M., WALLERBOS, E.J.M., "Analysis of the HTTR with Monte-Carlo and Diffusion Theory, An IRI, ECN Intercomparison", ECN-I-98-056, the Netherlands, September 1998.

[2.51.] WALLERBOS, E.J.M., HOOGENBOOM, J.E., "IRI Results for the benchmark problems of start-up core physics of the high temperature engineering test reactor (HTTR)", IRI-131-98-007, Interfaculty Reactor Institute, Delft, 1998.

[2.52.] WALLERBOS, E.J.M., HOOGENBOOM, J.E., and VAN DAM, H., "IRI results for LEU HTR-PROTEUS cores 5, 7, 9 and 10", IRI-131-97-005, Interfaculty Reactor Institute, Delft, 1997

[2.53.] DE HAAS, J.B.M, TURKCAN, E., "HTTR Criticality, Physical Parameters Calculations and Experimental Results", NRG/IRI, the Netherlands, Presented at the ICENES-2000 Meeting, 2000.

[2.54.] ASKEW, J.R., et.al., WIMS-D/4, A general description of the lattice code WIMS - code for unit cell calculation and preparation of few energy group macrosections. ENDF/B6 nuclear cross sections library is used. JBWES, pp. 564, Oct. 1966.

[2.55.] ZIZIN, M., SHISHKOV, L., YAROSLAVTSEVA, L., JAR, Test neutron-physics calculations of nuclear reactors. - code for 3D reactor calculation in few energy group approximation , Moscow, Atomizdat, pp. 9, 1980.

[2.56.] LIMAN, G., MAYOROV, L., YUDKEVICH, M., MCU, Code package for solution of radiation problems in reactors by Monte Carlo method. Collected volume: Questions of Atomic Science and Technique, Series: Physics and Technique of Nuclear Reactors, Iss.7, p.27, 1985 - code for unit cell and 3D reactor calculations in multi energy group approximation. The original cross section data library collection is used: ABAGIAN, L., ALEKSEEV, N., BRYZGALOV, V., et al., MCU-PFFI A Software with DLC/MCUDAT-1.0 Nuclear Data Library. Certificate number of PC 61 of Russian Federal Agency for Supervisions and Radiation Safety, Moscow, 1996

[2.57.] MCNP, A General Monte Carlo Code for Neutron and Photon Transport, LA-7396-M, 1981 - code for 3D reactor calculations. Point by point interactions of isotopes with neutrons required by MCNP were prepared with the help of NJOY program package: JOY – Nuclear Data Processing System, LA-9303-M, 1982 - on the basis of ENDF/B6 format. MCNP- 4A option was used, Los Alamos, USA, 1981.

[2.58.] SEGEV, M., "An Equivalence Relation for Doubly Heterogeneous Lattice", Nucl. Sci. Eng. 81, pp.151-160, 1982.

[2.59.] KUZAVKOV, N., MAROVA, E., SUKHAREV, YU., (OKBM), MITENKOVA, E., NOVIKOV, N., (IBRAE), BRYZGALOV, V., GLUSHKOV, E., GOMIN, E., (RRC KI), HTTR's Start-up Core Benchmark Physics Calculation, JAERI-memo 11-030, March 1999

[2.60.] GLUSHKOV, E., GOMIN, E., BRYZGALOV, V., LOBYNTSEV, V., (RRC KI), "Benchmark Problems of HTTR Core Physics (Phase 2). Monte-Carlo Calculation Results", (Proc. Second RCM of CRP on Evaluation of HTGR Performance, Beijing, 1999), IAEA, Vienna, 1999.

[2.61.] KUZAVKOV, N., MAROVA, E., SUKHAREV, YU., (OKBM), MITENKOVA, E., NOVIKOV, N., (IBRAE), "Benchmark Problems of HTTR and HTR-10 Core Physics-Phase 2", (Proc. Second RCM of CRP on Evaluation of HTGR Performance, Beijing, 1999), IAEA, Vienna, 1999

[2.62.] LOS ALAMOS NATIONAL LIBRARY, "MCNP- A General Monte Carlo Particle Transport Code", LA-1265-M, Los Alamos, USA, 1997.

[2.63.] SEKER, V., COLAK, U., KADIROGLU, O.K., "Results of HTTR Start-up Core Physics Benchmark Problems", Hacettepe University, Ankara, Turkey, 2001

[2.64.] BENTZINGER, D. and BALL, S., "ORNL's Benchmark Calculation of the HTTR's Startup-Core Physics with Continuous Energy Monte Carlo Code MCNP4a", JAERI, Memo 11-030, ORNL, USA, March 1999

[2.65.] BENTZINGER, D. and BALL, S., "HTTR Benchmark – Part 2, Temperature Coefficient of Reactivity and Scram Reactivity Calculations", ORNL, USA, November, 1999.